CFD simulation of nuclear graphite oxidation

P Sukdeo

Student number: 21389136

Dissertation submitted in fulfillment for the requirements for the degree Master of Engineering Science at the Potchefstroom Campus of the North-West University

Supervisor: Prof. CG du Toit

Potchefstroom

South Africa

May 2010

Dedicated to my wife Shoma and son Yastiv for their support.

Acknowledgements

- I would like to thank Pebble Bed Modular Reactor (Pty) Ltd. for supplying the computer hardware, software, logistical and financial support. This research would not have been possible without these resources.

- Thank you to Walter Schmitz from Pebble Bed Modular Reactor (Pty) Ltd. for promoting this study and for his guidance and advice during the course of this work. A big thank you for the translation of the numerous German texts.

- I would also like to thank my managerial team at PBMR (PTY) Ltd. For their support: Mr. Reshendren Naidoo, Mr. Heinrich Stander and Mr. Willie Theron.

- By the conclusion of this study, PBMR (PTY) Ltd. was in a state of rationalization. I would like to wish my numerous friends and colleagues all the best with future endeavors.

- Finally, I would like to thank my family for their support and understanding.

Abstract

This study investigates the development of a strategy to simulate nuclear graphite oxidation with Computational Fluid Dynamics (CFD) to determine an estimate of graphite lost.

The task was achieved by comparing the results of the CFD approach with a number of different experiments. For molecular diffusion, simulated results were compared to analytical solutions. Mass flow rates under conditions of natural convection were sourced from the 2002 NACOK experiment. Experimental data from the KAIST facility were sourced for the basic oxidation of graphite in a controlled environment. Tests included the reactions of carbon with oxygen and with carbon dioxide.

Finally, the tests at NACOK from 2004 and 2005 were chosen for comparison for the simulation of oxidation. The 2005 test considered two reacting pebble bed regions at different temperatures. The 2004 test included multiple detailed structural graphite.

Comparison of results indicated that the phenomenon of diffusion can be correctly simulated. The general trends of the mass flow rates under conditions of natural convection were obtained. Surface reaction rates were defined with user functions in Fluent. Good comparisons of the simulated and the KAIST experimental results were obtained.

For the 2005 NACOK comparison, the pebble bed regions were simulated with a porous medium approach. Results showed that correct trends and areas of oxidation were estimated. The 2004 tests were with a combination of a porous medium and surface reaction approaches. More detailed oxidation experimental data would possibly improve the accuracy of the results.

This research has shown that the CFD approach developed in the present study can identify areas of maximum oxidation although the accuracy needs to be improved. Both the porous and detailed surface reaction approaches produced consistent results. The limitations of the approach were discussed. These included transient phenomena which were estimated with steady state simulations, and the effects of change in geometry were not considered.

Keywords

Oxidation, Graphite, CFD, High Temperature Reactor, Air Ingress.

TABLE OF CONTENTS

LIST OF FIGURES AND TABLES

List of Figures

List of Tables

NOMENCLATURE

List of Symbols

Symbols	Description	SI Unit
A	Constant	-
B	Burn-off	-
C	Carbon	-
$[C_A]$	Concentration of specie A	-
C_p	Specific Heat Capacity	J/kg.K
CH_4	Methane	-
CO	Carbon monoxide	-
CO_2	Carbon dioxide	-
D	Diameter	m
D_{A-B}	Diffusion co-efficient for mixture of species A and B	m^2/s
D_{eff}	Effective Diffusivity	m^2/s
$D_{i,m}$	Mass diffusion coefficient of species i	m^2/s
D_{ij}	Binary mass diffusion coefficient of spatial component i in component j	m^2/s
D_p	Diameter of pebble	m
E	Energy	J
E_a	Activation energy	kJ/mol
$f(B)$	Function of Burn-off	-
g	Gravity	m/s^2
h	Enthalpy	J/kg
Δh	Change in Enthalpy	J/mol

H_2	Hydrogen	-
He	Helium	-
H_2O	Water Vapor	-
ln	Natural logarithm	-
l	Length	m
J	Diffusion flux	kg/m^2.s
K	Pre-Exponent Factor in Arrhenius equation	-
k	Thermal Conductivity	W/m.K
MWe	Mega Watt Electric	W
MWt	Mega Watt Thermal	W
m	Mass Flow Rate	kg/s
$M_{w,A}$	Molecular weight of specie A	kmol
n	Order of reaction	-
N	Total number of species in a mixture	-
N_2	Nitrogen	-
O_2	Oxygen	-
P	Pressure	Pa
P_{O_2}	Partial Pressure of Oxygen	Pa
Pe	Peclet Number	-
PyC	Pyrolitic Carbon	-
Q_{air}	Quantity of air	kmol
$Q'_{graphite}$	Quantity of graphite lost	kg
r_I	Volumetric reaction rate in Regime I	mol/m^3.s
$R_{i,r}$	Nett rate of creation of specie i in reaction r	-
R_{C-O_2}	Surface reaction rate of carbon with oxygen	kg.mol/m^2.s

R_{UGC}	Universal Gas Constant	J/mol.K
Re	Reynolds number	-
S_m	Source term for mass equation	-
SiC	Silicon Carbide	-
T	Temperature	K
t	Time	s
V	Velocity	m/s
X	Mole fraction	-
Y	Mass fraction	-
y^+	Thickness of the laminar sub-layer	m

List of Greek Symbols

Symbols		SI Unit
α	Permeable loss coefficient in porous media	$1/m^2$
β	Temperature Exponent	-
ρ	Density	kg/m^3
ε	Porosity	-
ϕ	Inertial resistance factor in porous media	1/m
φ	Flattening coefficient of a sphere	-
μ	Viscosity	kg/m.s
ϖ	Stoichiometric coefficient	-
v	Atomic diffusion volumes	cm^3/mol
τ	Stress tensor	Pa
τ_w	Wall boundary-layer shear stress	Pa

List of Abbreviations

This following list contains the abbreviations used in this document.

Abbreviation or Acronym	Definition
ASME	American Society of Mechanical Engineers
ASTM	American Society of Testing and Materials
AVR	Arbeitsgemeinschaft Versuchs Reaktor
CFD	Computational Fluid Dynamics
DLOFC	Depressurized Loss Of Forced Coolant
FZJ	Forschungs Zentrum Jülich
GUI	Graphical User Interface
HTR	High Temperature Reactor
HTGR	High Temperature Gas-cooled Reactor
HTTF	High Temperature Test Facility
IAEA	International Atomic Energy Agency
ISO	International Organization of Standardization
JAERI	Japanese Atomic Energy Research Institute
KAIST	Korean Advanced Institute of Science and Technology
KTA	Kern Technischer Ausschuss
NACOK	Naturzug im Core mit Korrosion
NQA	Nuclear Quality Assurance
MIT	Massachusetts Institute of Technology
PBMR	Pebble Bed Modular Reactor
QA	Quality Assurance
SI	International System of Units
THTR	Thorium High Temperature Reactor
UDF	User Defined Function
UK	United Kingdom
USA	United States of America
V&V	Validation and Verification
VDI	Verein Deutscher Ingenieure

CHAPTER 1: INTRODUCTION

1.1 Background

Globally, the demand for energy surpasses the supply. Climate change has become the latest topic of discussion internationally. Green house gases produced from the burning of fossil fuel to produce energy are a major contributing factor to climate change.

One of the alternatives for power generation, steam and process heat is the use of nuclear energy. Some of the main obstacles in the development of nuclear technology have been the public and political perception on safety, nuclear waste, radiation and cost.

One of the many nuclear designs is that of a High Temperature Gas-cooled Reactor (HTGR). HTGR technology began with research in Germany and lead to the building of the experimental Arbeitsgemeinschaft Versuchs Reaktor (AVR) in 1967. This experimental reactor operated for 21 years and offered a clean and compact energy source with high efficiency and a modular design. The benefits of this design and the modularity were identified by Reutler and Lohnert [70] in their 1984 paper. Walmsley [96] presents the historical aspects of high temperature gas-cooled reactors before 1995. Other than the AVR project, these included the Dragon (UK) and Peach Bottom (USA). Both the Dragon and the Peach Bottom proved the basic concept of a high temperature reactor and worked well. Demonstration reactors were the Fort St. Vrain in the USA and this operated from 1977 to 1992; and Thorium High Temperature Reactor (THTR) in Germany which operated from 1985 to 1989. The THTR closed due to political pressure after the Chernobyl era. The designs had marginal, repairable operational issues but were never developed further. Hereafter, most development on nuclear technology stagnated in the western countries, however some eastern countries continued with development efforts. Japan is one of the countries that continued with the development of high temperature reactors and constructed the experimental reactor at Tokai [30]. Recent developments with high temperature gas-cooled reactors emerged from China [36]. With the assistance of Germany, they designed and built the HTR-10 pebble bed 10 MWt reactor in 2000 and they are presently building a 190 MWe demonstration plant.

The need for safe nuclear energy is of the utmost importance. The safety features of High Temperature Reactor (HTR) technology, combined with no carbon emissions makes it an attractive alternative energy source.

South Africa identified the need to consider alternative fuel sources due to environmental issues and the finite life of coal reserves in the country. The South African power utility 'ESKOM' began research on the subject of high temperature reactors. This lead to the formation of the Pebble Bed Modular Reactor (PBMR) project, which is a joint venture between industry and government. A 400 MWt demonstration power plant has been designed [84]. The general layout of the PBMR demonstration plant is presented in Figure 1.

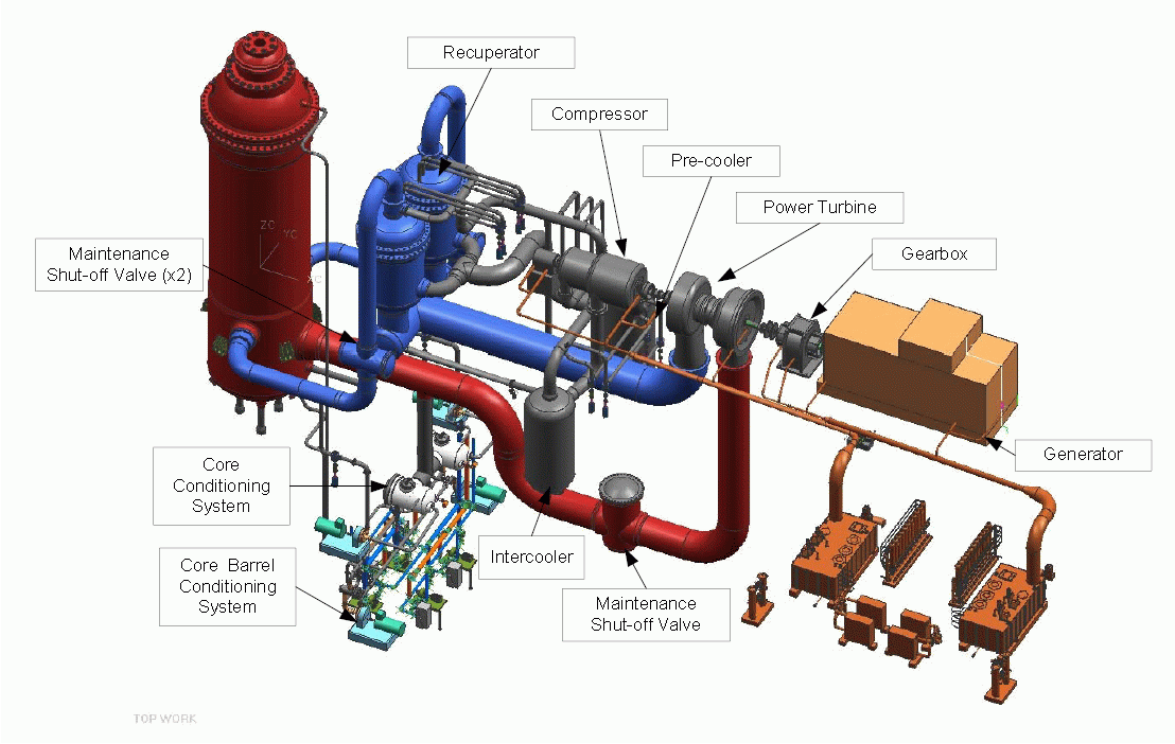

Figure 1: PBMR Demonstration Power Plant Layout

(Adopted from Slabber [84])

The PBMR concept is based on the Interatom HTR-Modul design [70]. The reactor is a high temperature gas-cooled reactor with spherical fuel elements and graphite as internal structural material. The choice of coolant fluid is helium since it is chemically and radioactively inert. It also has a high thermal capacity and good neutron physics properties. The fuel elements provide numerous advantages such as on-line continuous fuelling which will increase the availability of the reactor and the ability for the reactor to operate at high temperatures.

The fuel element to be used in the PBMR reactor is shown in Figure 2. The fuel kernel is protected by a TRISO coating consisting of a layer of Pyrolitic Carbon (PyC), Silicon Carbide (SiC) and a further later of PyC on the outside. The SiC layer forms the primary fission

product barrier. The fuel kernels are embedded in a graphite matrix and surrounded by a 5mm layer of graphite to form a pebble of 60mm diameter.

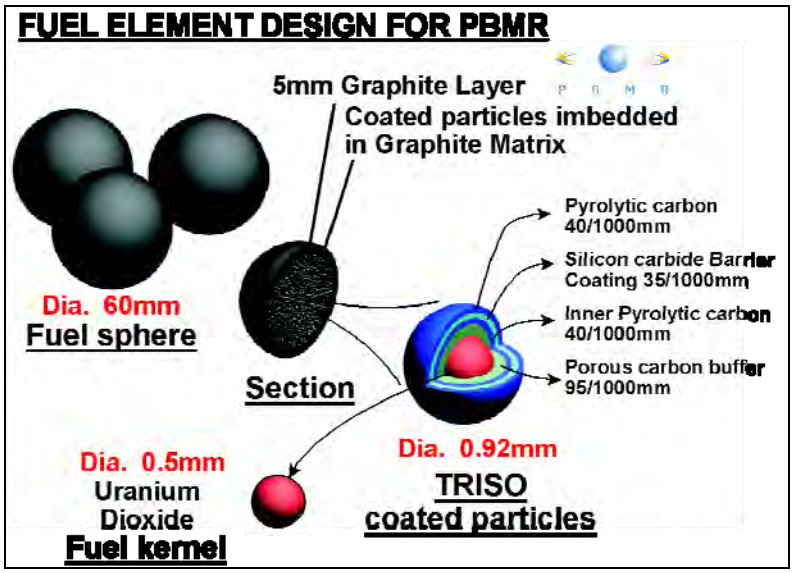

Figure 2: Fuel Elements for the PBMR Reactor

(Adopted from PBMR web site [67])

One of the intrinsic safety features of Uranium-238 is the negative temperature coefficient. In the event of loss of cooling, the fuel will heat-up due to insufficient heat removal. The fuel has enhanced neutron absorption properties at higher temperatures, which means that it will automatically cause the nuclear chain reaction to shutdown, resulting in a reduction in power levels. This inherent property of the reactor control is independent of operability or reactor equipment, because it is solely based on the laws of physics. Thus, in the event of a loss of cooling, the reactor will automatically shut down without having to insert control rods or other shutdown systems. The reactor is designed to heat up (due to decay heat produced) to a temperature to which the fuel remains intact without releasing fission products.

Due to the high temperature and neutron irradiation, the material of choice as a reflector and moderator (internals of the reactor) is graphite. The internals are multiple complex shaped blocks of graphite. The reactor has multiple gas flow paths, namely the primary coolant flow path, the secondary coolant flow path (designed flow paths for component cooling) and leakage flow paths (undesired flow paths but present due to construction). The cooling flow paths are gaps or engineered holes in the graphite blocks. Figure 3 illustrates the complexity of the flow path between the graphite blocks in the lower region of the reactor.

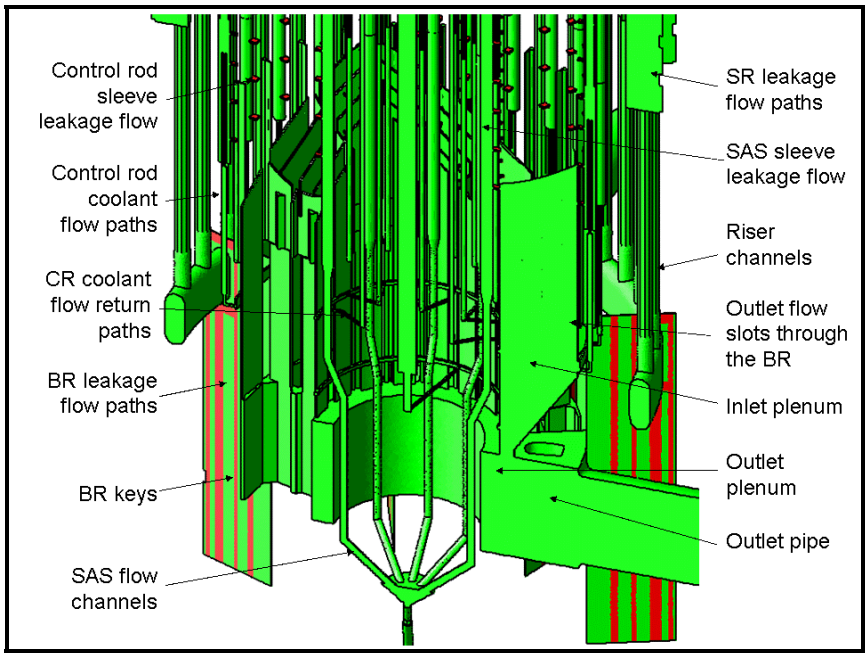

Figure 3: Flow Path in the Lower Region of the PBMR Reactor

(Adopted from Van Rensburg [93])

1.2 Introduction

After the Chernobyl incident, even greater emphasis is placed on safety. One of the concerns with high temperature reactors is what would occur should air enter the reactor. During startup of the plant, it is standard procedure to bake out the graphite to remove moisture from the system and purge the reactor with nitrogen during the heat-up cycles. Hence, air in the reactor during normal operation would therefore be negligible. The other possibility of air entering the reactor is from a rupture in the pressure boundary. The plant is designed in such a way that the pipe works are multiple annulus pipes with the inner most pipe leading to the core. This means that a large event needs to first occur to form a complete guillotine break in the pipe work. The expected occurrence of a large guillotine pipe break is in the order of less than one in a million years [16]. The size and location of the break would influence the flow behavior and the subsequent phenomena.

Simultaneous large ruptures at the top and bottom of the reactor will result in loss of coolant and the immediate flow of air into the reactor. This is one of the reasons for not having much pipe works at the top of the reactor. However, a large rupture at the core inlet or outlet pipes will result in the helium coolant escaping from the reactor. The loss of coolant will trigger a

shutdown of the reactor. For the purposes of this study, we will assume that the trigger event retains the core intact and all the components remain in place (no geometric deformation). The helium remaining in the reactor will equalize in pressure to that of the atmosphere due to the density difference of air and helium. The reactor core will still be hot while the inlet riser and outer most graphite blocks in the reactor will be cold. This sets up an inverse U tube geometry with a temperature gradient. Air will slowly diffuse through the helium and enter the reactor in small quantities. Eventually, after numerous hours of diffusion, the density gradients will dominate and there will be a rapid change when larger quantities of air will enter the reactor by means of natural convection driven buoyancy forces. The long period before which natural convection forces dominate, will allow sufficient time for mitigating action to be taken, such as inert gas injection etc.

The oxygen content of air will react with the heated graphite. The by product will be carbon monoxide (CO) and carbon dioxide (CO_2). The temperature in the pebble bed needs to be below 1600 °C to prevent fuel degradation and radio-nuclide particle release. However, besides the fuel temperature and the formation of toxic gases, oxidation of graphite is known to influence the density of graphite and hence the mechanical strength of the structural graphite within the reactor may be affected.

1.3 Importance of the Study

Previous nuclear designs were based extensively on experimental data and empirical correlations. With advances in computer technology, most of the newer generation reactors are designed with the aid of computer aided design. Software used still need proper verification and validation. At present, it is found that numerous studies concentrate on the subject of air ingress and determining the onset time to natural convection. Most studies are two dimensional approaches in a highly three dimensional geometry. The common trend of combining the two dimensional flow analyses with an external code for chemical reactions were found or the use of custom written software.

PBMR presently uses the strategy of solving up to the natural convection stage with the use of CFD. The mass flow rates determined by CFD are then used in a two dimensional code ‘Tinte’ to calculate oxidation with either air or water. This proves effective for transient simulations. From previous work at PBMR, it is known that the natural convection stage reaches some sort of stability in terms of mass flow rate into the reactor. The flow path in the lower region of the reactor is extremely three dimensional with multiple graphite blocks. It is known that air ingress would depend on temperature, geometry considered, gas and graphite properties and oxidation parameters.

The aim of this study is to develop a CFD simulation approach to consider graphite oxidation under conditions of air ingress. The parameters for oxidation and a strategy for implementation to the PBMR reactor are studied by benchmarking CFD simulations against known experiments. The results of such a study, once applied to a reactor, will allow more precise assessment of the graphite and possible areas where change in strength would occur due to oxidation. The heat release due to the chemical reactions has to be accounted for since it may influence the fuel temperature. Fuel temperature must be limited to remain at a safe level to prevent fission product release.

1.4 Problem Statement

The flow path of the lower reflector of the reactor is extremely complex and the temperature of the graphite would be dependent on the flow path. For this reason, PBMR would like to develop a steady state analysis technique for the three dimensional lower reflector of the reactor. Graphite oxidation of the lower blocks of the reflector would influence the mechanical strength of the blocks. Heat release from the chemical reactions needs to be quantified to determine if the fuel temperature remains within a safe band and avoid the release of fission products.

This study will focus on the use of commercial CFD software to develop an approach to simulate nuclear graphite oxidation.

In order to understand oxidation behavior, a literature survey was conducted and essential parameters were determined. Controlled basic experiments of oxidation will be consulted to aid in understanding basics of graphite oxidation. The end intention of the study will be to benchmark the simulation approach against the NACOK experiments. Two sets of experiments are selected. The first considers two reaction types and is applicable to packed beds and would require a porous medium approach. The second test is with more complex reflector blocks. The feasibility of a surface oxidation approach will be investigated and compared with a porous medium approach. Both the NACOK configurations represent simultaneous top and bottom pipe breaks and will be analyzed with a steady state approach.

1.5 Limitations

This study only considers the steady state approach to oxidation since it is computationally more feasible. The phenomena of oxidation are transient and dependent on graphite burn off.

For this investigation, the approach adopted is the benchmarking of simulations against published experimental data. The integrity of the experimental data needs to be assessed.

The benchmark of the NACOK test does not have specific data pertaining to the graphite chemical kinetics during oxidation. The oxidation characteristics for the grade of graphite used are not well known neither is the purity of the graphite.

The simulation of the PBMR reactor and the changes in strength of the graphite are beyond the scope of this study.

The distribution of the heat generated from the chemical reaction will partially heat up the solid and the balance will heat the gas stream. The proportions are not exactly known and therefore may not be correctly implemented.

It is expected that particles would dislodge from the parent surfaces and accumulate in some areas. This could influence the flow field and result in a change in geometry of the original surface. Effects of particle accumulation and change in shape are not accounted for in this study. At present, CFD is capable of methods such as moving and deforming meshes with known and well defined changes in shape. Alternative possible methods are based on mesh reconstruction based on physics and time change. The latter approach is not a standard feature within the software code and would be expensive in terms of the required computational resources and time for simulation. It is for this reason that these methods are not explored further or considered for this study.

1.6 Summary

Nuclear energy has recently received renewed interest as an energy source. High temperature gas-cooled reactors are one of the new generation nuclear technologies. Due to the high temperature and neutron irradiation most of the internal material is graphite. The fuel spheres in the PBMR reactor also contain an outer layer of graphite. Flow profiles through the reactor are extremely three dimensional and complex. Since the Chernobyl incident, more emphasis has been placed on safety and analysis of low probability events. One event analyzed is the ingress of air into the reactor. The oxygen content of air would result in the formation of CO and CO_2. Oxidation will also reduce the mechanical strength of the graphite blocks. The effect of chemical reaction increase in fuel temperature needs to be quantified. Previous simulations of air ingress mainly employed two dimensional flow codes coupled with other software for chemical calculations or custom written codes. This study considers the use of a commercial CFD code to predict a three dimensional steady state analysis approach for nuclear graphite oxidation. This is done by benchmarking against oxidation experiments.

CHAPTER 2: LITERATURE

2.1 Introduction

Nuclear energy is being considered as an energy source for power generation and process heat. Some of the main stumbling blocks in the development of nuclear technology has been the public and political perceptions on safety, nuclear waste, radiation, cost and regulation stability as detailed by Kadak et al. [35]. Since the Chernobyl incident in 1986, public and political issues have become important factors. Previous nuclear power plants were of large capacity and complex designs; this meant high capital cost and staff requirement as well as high decommissioning cost at the end of life of the plant. Reactors were characterized by a high power density and active cooling systems (amongst other factors); this made the design prone to possible core meltdown in the event of multiple system failure.

With the renewed interest in nuclear power generation, research on nuclear power plants has resumed. The need for change of the previous designs was identified. The main reasons for the anticipated changes were an enhanced emphasis on safety, the avoidance of nuclear proliferation, reduced construction time to aid better economics, mass production, increased availability due to on-line fuelling, higher plant efficiency, the need to design plants with commissioning in mind and the need to simplify the operating of plants. The new reactors are termed ‘Generation 4’ reactor designs and will have a low power density and have passive decay heat removal systems, meaning minimal human intervention and no core melt down.

Multiple groups around the world are conducting research initiatives. The high temperature gas-cooled reactors have emerged as the most suitable Generation 4 reactors [60]. High temperature gas-cooled reactors are divided into two broad categories depending on the fuel design. They are either prismatic (block fuel) reactors or pebble bed reactors. The first has fuel compacts with embedded coated particles placed within graphite blocks while the latter has coated particle fuel agglomerated and formed into a pebble with an outer coating of graphite. South Africa began research on the Pebble Bed Modular Reactor in the mid 1990’s. The concept was based on the German AVR experimental reactor and the high temperature demonstration plant in Germany as explained by Nicholls [60]. South Africa purchased most of the research from Germany and continued to evolve the design. The South African design is characterized by features such as a fixed central column, small emergency planning zone and low core power density that requires no active cooling systems and excludes the possibility of core melt-down. These factors were highlighted by Koster et al. [44]. Their paper also detailed the proposed gas cycle to improve cycle efficiency and the basic core design.

The report from the International Atomic Energy Agency (IAEA) [37] detailed the numerous global activities in the area of high temperature gas-cooled reactor research. South Africa is one of the members of the IAEA and participates in the areas of graphite development and fuel research. The European Union has an extensive program [92] with the main focus being in areas of materials development, component development (such as heat exchangers) and fuel technology. Corwin [12] detailed the USA perspective for the USA Department of Energy for research into metals and graphite used in high temperature gas reactors while Murthy and Charti [59] detailed the materials used in high temperature reactors and the challenges faced as well as areas of opportunity. The need for modularity in new designs to aid cost effective construction and flexible needs of the customer was highlighted by Kadak [34].

Packed beds of spheres have been studied for many years with the main applications ranging from catalytic and chemical beds through to fluidized beds. The application to nuclear technology has been under development since the 1950's. Simulation of all of the actual pebbles in immense detail is still in the distant future, hence the approach of bulking the solids into a porous zone is generally used. With this approach the characteristics of heat and flow need to be understood. The subject of heat transfer and flow profiles are studied by numerous groups throughout the world and Achenbach [1] commented that over 150 papers are produced per year on this subject. Research activities as detailed by Achenbach [1] focused predominantly on pressure drop, prediction of convective heat transfer, effective thermal conductivity, wall heat transfer, flow channeling and braiding effects. This is not the main focus of the study, hence the subject is not discussed in much detail, and relevant theories applicable to this study are discussed in more detail when used.

Nuclear plants are designed to withstand a multitude of events both natural and human. Events such as seismic activity and impact from airplanes are considered during the design phase as described in the technical description of the PBMR demonstration plant by Slabber [84].

Extensive efforts are invested in probability risk assessment as detailed by Fleming [16]. Items such as pipe breaks on the pressure boundary have a frequency of occurrence of less than one in a million years. These events are typically classed as beyond design events. With nuclear plant design it has become good design practice to analyze events with probabilities of occurrences of less than one in a million years should they influence safety to plant and have a perceived risk to the public.

One of the beyond design events is the possibility of air entering the reactor on a large scale. For this to occur there needs to be a relatively large incident where the reactor inlet or outlet lines rupture. These lines are typically multi-layer annular pipes with a very low frequency of

complete rupture. Should air enter the reactor the oxygen content of air will react with the heated graphite that makes up the majority of the internals of the reactor and react to form CO or CO_2.

In the event of a pipe break, the pressurized and heated helium from the reactor would escape leading to what is termed the depressurized loss of forced coolant (DLOFC). This would typically trigger a sequence of subsequent plant action. Thereafter, it is expected that the helium pressure will be equal to the environmental pressure. Air will diffuse into the reactor. Due to the difference between the density of helium and the density of air the diffusion of air into the reactor will be a very slow process. This will eventually give way to natural convection flow due to gravity forces and thermal gradients and result in air ingress into the reactor. The final stage occurs when larger quantities of air or oxygen enter the reactor and results in graphite oxidation. Should the postulated break occur in the core inlet pipe or the turbine inlet pipe, convection driven flow would result immediately.

With the increased capacity of computational simulation, most of the present designs are evaluated with a host of numerical computational tools. With the use of computational tools the validation of the tools becomes essential for use in a nuclear environment. In the chemical industry it was typical to couple more than one mathematical code each to perform a specific function. Presently, commercial computational fluid dynamics (CFD) codes have the ability to predict flow, heat transfer and reaction chemistry phenomena.

The following section will focus on previous work on air ingress and oxidation. This will be expanded to areas of further development and used to form the objectives of this study.

2.2 Previous Work

This section highlights the previous work in the areas of diffusion and natural convection for air ingress. Following this baseline, attention is then focused on graphite oxidation.

Ita and Sonntag [32] performed experiments into separation of helium and nitrogen based on two filled bulbs with a temperature gradient in 1976. Kerkhof and Geboers [38] considered an extensive mathematical analysis of diffusion between two bulbs and flow within the capillary tubes. A multitude of flow conditions were considered. The end result was the solution of the modified Stefan-Maxwell equations.

The Japanese Atomic Energy Research Institute (JAERI), specifically the work conducted by Takeda and Hishida pertained to gas diffusion and air ingress. A series of publications were

produced from 1991 to 2004. In 1991 [88] and 1992 [26] they developed a custom two dimensional code to calculate molecular diffusion and onset times of natural convection based on a two component gas system. The prediction by the code was compared with the results of an inverse U tube experiment (hereafter referred to as the JAERI experiment) and expanded to the Japanese high temperature test reactor which is a prismatic reactor. By 1996 [89], the experiment was modified to include combustion of a graphite pipe and expanded to include multi-component gases. The focus of their work changed to air ingress prevention by helium injection in a paper published in 2000 [90]. The last paper by Takeda [91] was in 2004 and focused on the development of a two dimensional mathematical code called 'FlowGR', based on the finite difference scheme and further work on the prevention of air ingress.

The Germans at Forschungs Zentrum Jülich (FZJ) developed a series of experiments as part of their research on high temperature reactors, one such experiment (the NACOK facility) was developed to study the effects of pressure drop in packed beds, molecular diffusion, natural convection and graphite oxidation in a geometry representative of the hot and cold passes of the reactor. Initial work at FZJ on gas diffusion began in 1993, with the work of Zhang et al. [100]. They developed a one dimensional diffusion code to analyze high temperature gas reactors. The results predicted by the code was compared with the results of the JAERI experiment and applied to the NACOK facility in the design stage with a return tube configuration. Moormann and Hilpert [54] (also part of FZJ) explained the release of metals from fuel in their paper published in 1991 and stressed the reasons why fuel should not exceed the temperature limit.

Lim and No [49] developed a two dimensional code called 'Gamma' to predict diffusion and the onset time of natural convection. Their code produced results that compared well with available experimental results and the results from other two-dimensional numerical analyses.

Multi-component gas diffusion was predicted by No et al. [64] who worked on the coupling of the custom codes 'Gamma' and 'Relap5'. They benchmarked the coupled codes against a series of experiments, beginning with two bulbs, the JAERI experiment and the NACOK facility.

Also relating to the coupling of codes was the study by Haque [22] who considered a prismatic reactor for air ingress. A two dimensional model was considered with a coupling of the codes 'React' and 'Thermix'. He concluded that air ingress does not substantially change the peak fuel temperature as compared to accidents with no air ingress. The findings included a period of 50 hours before limiting temperatures were reached with an inlet mass flow rate of 0.6kg/s. Scenarios of delayed air ingress were also considered.

Ball [4] conducted sensitivity studies on high temperature gas reactors and found that there were good margins of operating conditions to potential damage conditions and that the response time of peak temperatures occurred in the order of days. His predictions show that oxygen was depleted before it reached the core. This work was further expanded and published in 2008 [5]. The sensitivities show that the configuration considered would influence the location of oxidation, this was linked with the degree of cool down that occurred in the core. Possible mitigations to delay air ingress were also discussed. The work was conducted with a custom code called 'Grsac'.

Oh et al. [65] proposed that the density difference of air and helium would lead to a much quicker onset of natural convection than compared to the diffusion process. They proposed that this scenario be analyzed as well.

Significant efforts were invested by PBMR into the research and simulation of air ingress. Work into the subject began in 2003 and is still ongoing. The strategy of PBMR was to conduct the diffusion and onset to natural convection with the aid of CFD and to use the two-dimensional code 'Tinte' for the calculation of air and water ingress into the reactor. Schmitz [73] initially worked on heat transfer parameters applicable to the pebble bed and the comparison of CFD and Tinte for this purpose. Analysis for air ingress concentrated on various models of the complete system pressure boundary, and investigated the influence of different break sizes and varying locations of the breaks. This work is detailed in reports [75] and [76]. The effect of inert gas injection to delay the onset of natural convection during air ingress was also tested and was detailed in report [78]. The papers published on the subject were presented at the HTR conference in 2006 [81].

At the same conference, Schmitz [82] presented a second paper related to air ingress simulations with CFD and the verification and validation of the simulations. Recent work focused on the effect of pipe break, gap sizes [79] and the large pipe break analysis [80]. CFD analyses were conducted with the commercial CFD code 'Fluent'. The increase of air ingress simulations can be linked to the increased computational solver capacity of the CFD team at PBMR in recent years. Computational solver capabilities changed from 6 cores in 2003 to 160 cores in 2009. Amongst the documents produced by Schmitz was a test requirement specification for the NACOK simulations [74] in 2004. In this document, Schmitz reviewed the German facilities for oxidation. It was found that most of the German facilities for oxidation were decommissioned. These facilities included experiments such as 'Nova', 'Hoeberg' and 'Veluna'. The 'Thera' and 'NACOK' facilities were identified as operational experiments. Thera was identified for small sample testing to obtain oxidation parameters.

Literature revealed that most of the investigations on molecular diffusion and onset times to natural convection were conducted with custom written two-dimensional codes or the coupling of more than one numerical code. In addition the IAEA recognized the NACOK and JAERI experiments in the field of air and water ingress [37]. The European Union identified the NACOK facility for studies into air ingress as future work [92] and for the validation of numerical methods for nuclear design. Contescu et al. [10] emphasized the need for standard test methods to have comparable results.

The following paragraphs concentrate specifically on carbon / graphite research. The process to manufacture nuclear graphite is discussed in a latter section of this report along with more detailed theory of graphite oxidation.

Balden et al. [3] investigated the corrosion of seven different types of graphite in a temperature range from 327°C to 727°C. Some samples were mixed with silicon and titanium. They employed detailed surface analysis using electron microscopy. The authors noted the temperature dependence of oxidation. Microscopic effects of graphite oxidation were also studied by Hahn [21]. He concentrated on the effect of oxidation in the two lattice directions and the formation of pores at high temperature. Ishihara et al. [31] considered the design of graphite components of HTGRs. It is known that graphite is brittle, and due to the absence of design criteria, the group from JAERI set up some design criteria for graphite. The study by Lim et al. [50] investigated the change in properties of graphite grade IG-11 after oxidation. Electron microscopy was also used to evaluate the samples after oxidation. Air oxidation resulted in a change in shape and weight of the samples at temperatures above 900°C. They found that crater like pores were created. In air the oxidation was a surface effect and if the sample was exposed to 1100°C for three hours the weight changed by an average of 46%. They noted no change in shape after CO_2 oxidation. However, when exposed to high temperatures for prolonged periods of time, graphite damage occurred. Large changes in bending strength of the material were noted depending on the temperature of the experiment.

Snead et al. [85] composed a comprehensive handbook of SiC properties for fuel performance. This is one of the layers that form the pebble fuel. Properties of non-irradiated and irradiated SiC were compiled along with various strength properties. Zhu et al. [101] considered fuel graphite improvements for oxidation resistance. Dense gradient silicon carbide was used to coat the spheres. It was reported that this coating greatly improved the resistance to oxidation and also had good thermal shock resistance, which means that the spheres were less prone to cracking in adverse temperature gradients.

Walker [95] conducted research in the field of gas reactions of carbons and graphite. Reaction rates were determined by weight of the samples at set temperatures and time intervals. His research showed an increase in reaction rate up to 5% burn-off, a constant range from 5 to 30% burn-off, and a decrease in reaction rate above 30% burn-off. This was linked to the surface area. With the general use of carbon, the impurities in carbon influence the reaction rates; hence the grade and properties of the graphite are important.

Fuller and Okoh [19] considered the kinetics and mechanism of nuclear graphite oxidation. They considered the Japanese graphite, grade IG-110 in a temperature range from 450°C to 700°C. The burn-off link to reaction rate was explained as follows. The reactions initially occur only on the outer surface and as time passes, the reaction rates increase as the pore walls oxidize. The pore walls grow larger and join each other, hence the surface area decreases, leading to a decrease in the reaction rate once it has reached a peak (at approximately 40% burn-off). The kinetics of oxidation were explained as diffusion of reactants to the graphite surface followed by absorption of the reactants at the surface. This then results in a chemical reaction on the surface and within the pores. Following the reaction, desorption of the products occur, products then need to diffuse away from the surface and pores of the graphite into the flow stream. The activation energy of IG-110 was quoted as 188kJ/mol. This compares favorably with earlier research as detailed in paper [19]. The Arrhenius curve of log reaction rate versus inverse temperature was also explained. The slope was activation energy over the universal gas constant and the natural logarithm of the intercept was the pre-exponent factor in the reaction rate. They proposed that air oxidation occurred in three stages, but stress that at the stage of research, further work was required.

Around the same period Takeda and Hishida [89] developed a custom numerical code for the analysis of high temperature reactors and considered the detail of the chemical reactions. The partial and complete reaction of carbon and oxygen to form CO or CO_2 was expressed as one equation. The activation energy used for IG-110 graphite was 209kJ/mol. The ratio of CO/CO_2 was introduced and shown in the algebraic expression to calculate the quantity of CO and CO_2. The CO reaction with oxygen to form CO_2 was also stated along with the calculation of a volumetric reaction rate.

Heintz and Parker [23] studied the influence of impurities on graphite oxidation. They found that boron and phosphorous offer some reduced oxidation rates, while most other metals act as catalysts and speed up the reaction rate. They provided a detailed look at the micro-structure of carbon.

Initial work of Moormann et al. [55] was for the Institute of Nuclear Safety Research in Germany, now called FZJ. Moormann et al. [55] conducted corrosion rate tests on A3 fuel matrix graphite in oxygen. Their intention was to develop a Hinshelwood-Langmuir correlation that was linked to the partial pressure of oxygen. Moormann [57] investigated air ingress with the aid of the code 'React' and 'Thermix'. He quoted the reaction of carbon and CO_2 (Boudouard reaction) as a partial pressure of CO_2 as used in 'React'. Later Moormann et al. published a paper [56] on the oxidation behavior of the fuel matrix graphite in oxygen compared with standard nuclear graphite. Block reactors have small quantities of fuel graphite where as pebble reactors have large quantities of fuel graphite due to the difference in their designs. Moormann et al. [56] considered the activation energy of the filler and binder that make up the fuel matrix graphite. The filler and the binder were found to have activation energies of 166kJ/mol and 123kJ/mol respectively. Tests at 750°C show that fuel graphite grade A3-27 had a peak burn-off at approximately 25%, while that of structural graphite (grade V483T) was closer to 40%. Moormann [58] highlighted that the fuel temperature should be below 1500°C and provided a theoretical basis for the behavior of graphite oxidation. Essential reactions and changes in enthalpy were also documented.

Continuing with work from the early 1990's and from FZJ, Kugeler et al. [45] investigated the formation of dust or aerosols due to water and air ingress into the core of a high temperature reactor. Particle size distributions were measured. Kugeler and Roes [46] investigated the mass concentration of particles from structural and fuel matrix graphite. The mass of structural particles was found to be large and they concluded that particle release would be unlikely due to particle mass and the flow stream that may be present. They suggested further work into the release of particles from the fuel matrix. Sun et al. [87] conducted initial simulation work with 'Tinte' for the construction of the NACOK facility. Mass flow rates under natural convection conditions were calculated. Conclusions at the time were that 'Tinte' required further development to deal with the onset of natural convection. Roes [71] used the VELUNA experiment to determine the parameters of graphite oxidation. The reactions obtained at the time were for the development of two-dimensional codes or analysis with known flow conditions, hence the quoted reaction rates accounted for both chemical and flow conditions. The inclusion of the flow parameters do not make the results amenable to analysis with CFD since the flow parameters are calculated by the CFD program. Similarly Gerwin et al. [20] reported on the reaction rates applicable to high temperature graphite oxidation. It was found that flow and chemistry parameters were included in the results.

Blanchard [6] composed an Appendix in an IAEA technical document on thermal oxidation of graphite. The document detailed the essential reactions of carbon and the energy changes.

The mechanisms of oxidation were also discussed along with the regimes. Standard formulations for change in mass were documented for standard shapes such as slabs, cylinders and spheres. Rate constants were linked to the Arrhenius parameters and an activation energy of the range of 170kJ/mol was given as a reference. The document detailed the parameters required to conduct an oxidation analysis.

Kuhlmann [47] conducted flow experiments at NACOK in 2002. This work provided data on mass flow rates through the NACOK facility based on a temperature gradient on the return tube geometry. His work also included pressure drop calculations for the packed bed. He proposed new coefficients for the KTA formulation of the pressure drop under very low flow conditions. The rest of the report focused on the development of the two-dimensional code 'Direkt' for flow simulation.

Xiaowei et al. [97] tested IG-11 (marginally different to IG-110 through chlorination) graphite. The air flow rate was 20ml/min. The findings pointed to an activation energy of 159kJ/mol in the temperature range from 400°C to 600°C, and 72kJ/mol in the range from 600°C to 800°C. Samples had sizes of 10mm diameter and 10mm height.

Massachusetts Institute of Technology (MIT) emerged with a series of investigations pertaining to the NACOK facility under the supervision of Kadak. The initial work was in 2003 by Zhai [99]. His study considered the simplified heat transfer from the reactor with a custom code called 'Heating 7.' He then proceeded to benchmark his study against the JAERI facility with the work of Takeda and Hishida [89] for diffusion and natural convection. This was further expanded to benchmark Fluent against the corrosion experiment conducted at JAERI. The NACOK facility was simulated for mass flow rates under varying temperature conditions. Parks [66] considered the simulation of pressure drop on a NACOK experiment and began incorporating basic reactions for oxidation. Brudieu [7][8] expanded the reaction chemistry work and compared a blind benchmark CFD investigation against the results of the NACOK open chimney and return-duct experiments.

A series of publications by the Korean Advanced Institute of Science and Technology (KAIST) were studied. The first paper by Kim and No [40] concentrated on the geometric effects of graphite during oxidation. Graphite grade IG-110 in regime I was considered. Multiple samples were tested and a geometric factor was determined to account for surface area to volume ratios changes. The second paper [41] considered the oxidation of graphite over a large range of temperatures. A controlled experiment was devised. Two experiments were conducted. The initial tests were in regime I at a temperature range from 540°C to 600°C, and a velocity of 0.072m/s with varying oxygen concentrations. This was used to determine the activation energy

and the order of reaction. A total number of 33 tests were conducted in this region to ensure repeatability. In the second set of tests the temperature ranged from 700°C to 1500°C, for a velocity of 0.16m/s and varying oxygen concentrations. The data was used to form an Arrhenius curve of reaction rate versus inverse temperature. The data was also used to form a ratio of CO/CO_2 and this data was compared with results obtained from literature. Some basic CFD analyses were conducted of the experiment. The experimental data was intended for use in a semi-empirical model. Amongst the data were an activation energy of 218kJ/mol and an order of reaction of 0.75. The tests did not consider the effect of burn-off. The experimental facility was modified to consider the reaction of carbon with carbon dioxide [42]. A temperature range up to 1400°C was considered. The results indicated an activation energy of 290kJ/mol and an order or reaction of 0.9. The final paper [43] considered the changes in density and mechanical strength of graphite due to oxidation. The paper also detailed the inclusion of the oxidation parameters in the software code 'Gamma' for two-dimensional analyses.

Chi and Kim [9] conducted work on two grades of Japanese graphite (IG-110 and IG-430) and two grades of German graphite (NBG-18 and NBG-25) with the intension of comparing oxidation based on the filler coke types. The IG-110 and NBG-25 are made from petroleum coke, while IG-430 and NBG-18 are made from pitch coke. Temperature was varied from 600°C to 960°C. The finding was that oxidation was highly temperature dependent. The oxidation rates of all of the samples followed a similar trend through the temperature range considered. The exception was in the range from 700°C to 800°C, where the petroleum coke graphite showed a higher oxidation rate. At higher temperatures this effect did not occur. The average activation energy determined by this study was 161.5kJ/mol.

The work of Contescu et al. [11] stemmed from the Department of Energy in the USA. This paper identified that the test methods along with the sample shape and size have an influence on the results. They attempted to form the baseline for the American Society of Testing and Materials (ASTM) to be used on graphite oxidation testing. At lower temperatures, oxidation depends on the oxygen concentration and material reactivity, which was linked to the micro structure of the materials. As the temperature increases the oxidation rate becomes more sensitive to surface oxygen concentration or air flow conditions, and the mechanism of oxidation becomes more in-pore diffusion controlled. At even higher temperatures the material dependence is removed since oxidation becomes limited by the surface layer and is controlled by mass transfer of species. The air flow rate was found to influence the linearity of the Arrhenius curve. This paper proposed a set air flow rate and temperature range in which samples should be tested as well as a standard shape and size of the test sample to remove the dependence of surface to volume ratios. Activation energies were found to be similar, but

depending on the test methods used, the intercept of the Arrhenius curve or the pre-exponent factor would vary.

Studies by Hinssen et al. [24] found that no standard test method was available for graphite testing. The link of reaction rate to sample size was also found and raised the question of a standardized test method. The work detailed the need for the testing of the graphite to be used on the PBMR. The order of reaction and the kinetics in regime II need to be quantified. The paper also identified the need for experimental tests on the fuel matrix graphite and the inclusion of high temperature reactions with CO_2.

Sikik [83] highlighted studies conducted by PBMR on the subject of air and water ingress for transient simulations of the PBMR with the two dimensional code 'Tinte'. One of the findings was that the air that enters the reactor has a cooling effect on the fuel temperature. The air ingress cases with an outlet pipe break represented the most severe cases.

Adams et al. [2] considered coal combustion, but summarized the reaction of CO and oxygen to form CO_2. The rate parameters were determined from an intensive series of chemical reaction steps into radical formation. The activation energies, pre-exponent factors and the rate concentrations were compared; all were relatively similar to the original parameters proposed by Dryer and Glassman (as quoted in the Fluent manual [17]) in the temperature range below 900 °C. Similarly, work by Roesler et al. [72] considered the radical formation in the reaction of CO and oxygen to form CO_2. They considered fuel mixtures and looked in depth at radical formation that makes up this simplified one step reaction. Again it emerged that the constants used were based on several experiments and were global values to fit a range of temperature applications.

Perkins and Sahajwalla [68] provided insight into the modeling of chemical reactions within Fluent with a paper published in 2007. This paper was related to coal combustion. Stanmore et al. [86] considered soot formation and the comparison between the results of CFD simulations and experimental data. The work was also intuitively used as a guide for the CFD approach followed in this study.

The findings of this literature study, areas of future work and objectives of this literature study are detailed in subsequent sections of this Chapter.

2.3 Findings

High temperature reactors are identified as the future nuclear reactors. Numerous reasons are given for the suggested changes in the new rector designs(compared to the previous generation of reactors). One feature was the enhanced safety and elimination of forced cooling of the reactor core. This feature would prevent core melt down without human intervention.

The field of air ingress and graphite oxidation is a concern for all parties involved in the development of high temperature reactors. The NACOK facility is internationally recognized as an experimental facility to test graphite oxidation.

Older experimental work quoted reaction rates with a combination of flow and chemistry effects. This, however, does not make them suitable for use in CFD analyses since the flow portion is calculated by the software. Experimental data for reaction rates were found to be expressed as an Arrhenius curve of reaction rate and inverse temperature. The slope of the curve is used to derive the activation energy and the intercept on the reaction rate axis is used to form the pre-exponent factor in the Arrhenius equation. Experimental data showed similar activation energies for nuclear graphite. However, depending on the sample surface area to volume ratio and factors such as flow rates etc, the pre-exponent factor would change. Experimental tests were not guided by a set procedure; this was proposed in 2008.

Most previous numerical work used custom written codes to calculate molecular diffusion and onset times for natural convection. The majority of the studies that included chemistry coupled two-dimensional analysis codes for flow and a second package for the chemistry, or were custom written. Custom written numerical codes require extensive validation and verification for use in a nuclear environment.

Only two sets of investigations focused on the use of CFD. The investigations by KAIST [41] concluded that CFD was computationally too expensive and continued to develop a custom written program. However the experiments conducted were well documented and can be used as benchmarks.

The investigations performed at MIT [8] showed success with the use of CFD but identified the need for better experimental data. Details of the Boudouard reaction were very limited. Fixed stoichiometric values were used for reaction chemistry and the user coding for chemistry was not optimized. The study showed success with the transient analysis for diffusion and onset times to natural convection.

Studies conducted at PBMR by Schmitz ([75] to [80]) demonstrated success with the use of CFD to simulate molecular diffusion and onset times to natural convection. 'Tinte' was used to conduct oxidation calculations [83]. This approach was well suited to transient and two-dimensional analyses. The 'Tinte' code has the correlations of the VELUNA oxidation experiments implemented for oxidation. These were based on the Hinshelwood-Langmuir correlation. While being the most accurate kinetic model to describe graphite oxidation, it is very dependent on graphite grade and incorporates multiple activation energies for the different regimes.

2.4 Areas for Further Work

Previous work conducted by PBMR and external teams show that the transient effects such as molecular diffusion and onset times of natural convection can be correctly determined using CFD. It is known that the flow path within the reactor bottom reflector is complex and three dimensional. In the event of air ingress the exact locations of oxidation would be essential since oxidation influences the mechanical strength of the graphite blocks. It is also important to quantify the amount of oxygen that may reach the pebble bed since this may influence the temperature and fuel integrity. This however is dependent on the location of the break.

Studies by KAIST [41][42] detailed the experimental procedure for their oxidation tests and the results they obtained. The understanding of graphite oxidation behavior and the graphite reactions were highlighted by MIT. This is essential to explain the analysis to regulatory bodies. Experimental data was detailed as a stumbling block for MIT. The reaction rates used fixed stoichiometric values and the user coding for chemistry was not optimized.

Literature has provided numerous sources that provide explanations of the mechanisms and regimes of graphite oxidation. This aided in the understanding of graphite oxidation. The work by KAIST can be used as benchmarks to develop a modeling approach using CFD. Although the grade of graphite is not the same as that to be used in the PBMR, benchmarking the CFD will aid in understanding oxidation behavior and the essential parameters required by CFD in a controlled environment. PBMR has identified the need for experimental tests on the graphite to be used and this is a future exercise.

The use of singular stoichiometric values by MIT was not fully explained but is most likely due to the version of Fluent used by them. It is known that user coding may be applied to reaction chemistry. A focus on this area may improve the oxidation results.

With the use of CFD, reaction rates may be accommodated in two ways. The first is by explicitly modeling the surface walls on which reactions would occur along with the region in which it resides. The second method is an implied method whereby the reacting surface area forms a ratio to the volume within which a chemical reaction occurs. For this study the first approach is termed the surface reaction approach and the second is termed the porous approach. For example, modeling the actual pebbles within the pebble bed is impractical due to the required resources. With the porous approach, the pressure drop and reacting surfaces are estimated and lumped into a porous cell zone. The study by KAIST [41], which included CFD simulations, employed the surface reaction approach. The investigation by MIT [8] employed the porous approach. For the present study it is proposed that a comparison be done to compare the two approaches of simulation on the same geometry.

2.5 Objectives of this Study

The flow path of the lower reflector of the reactor is extremely complex and the temperature of the graphite would be dependent on the flow path, hence PBMR would like to develop a steady state analysis technique for the simulation of the three dimensional lower reflector of the reactor. Graphite oxidation of the lower blocks of the reflector may influence the mechanical strength of the blocks.

This study will focus on the use of commercial CFD software to develop an approach to simulate nuclear graphite oxidation.

Literature would provide an understanding of oxidation behavior and the reactions of graphite with air. Exploring the manufacturing of graphite will aid in understanding the oxidation thereof. Literature has shown that oxidation mechanisms, regimes and the effect of burn off are important. These subjects will be explored further.

The stages of molecular diffusion and natural convection flow will be briefly explored since it is relevant to air ingress. More emphasis will be placed on benchmarking the CFD approach against the results of the KAIST oxidation experiments. This will aid in understanding graphite oxidation behavior and the essential parameters required for reaction chemistry, and implementation within CFD. Benchmarking against the NACOK tests will also establish feasibility on a larger scale. Steady state analyses will be conducted on two sets of experiments. The first has two pebble bed regions at different temperatures; this will hence include the reactions of graphite with oxygen and carbon dioxide with a porous approach. The second has complex reflector geometries. This test will be used to compare a surface reaction

approach and a porous approach to oxidation. Both NACOK tests are of the open chimney configuration.

2.6 Conclusions

Historically, most of the numerical analyses for air ingress and graphite oxidation were performed using two dimensional codes as shown by Takeda and Hishida [91] and Lim and No [49] amongst others. Most were custom written or required the coupling of more than one code, one for flow effects and another for reaction chemistry such as that by No et al. [64] and Haque [22]. Custom written codes within a nuclear environment require large amounts of validation and verification.

The inclusion of flow and chemistry in the reaction rates as detailed in Roes [71] are not suitable for CFD analysis since the flow parameters are solved for by the CFD software. Only the base chemistry portion of the equations are required.

Experimental data for different nuclear graphite show that activation energies are within similar ranges; however the scatter of pre-exponent factors is quite large [10]. This is attributed to the experimental conditions and the ratio of surface area to volume of the test sample. There is no international standard test procedure for graphite testing. This was proposed in 2008 by Contescu et al. [11]. PBMR has identified the need for oxidation tests [24]. However, this is a future task.

Limited three dimensional analyses with commercial software have been conducted. The investigations by MIT ([7] and [8]) highlight the need for experimental graphite oxidation results to perform simulations. The publications by KAIST ([41] and [42]) document the experimental process to determine oxidation and the reaction rates.

PBMR presently adopts the approach of calculating onset times to natural convection with CFD, and determining the effects of oxidation with a two-dimensional code ‘Tinte’. It is known that the flow path within the reactor bottom reflector is complex and composed virtually entirely of graphite. Obtaining a three dimensional location of oxidation would aid in determining the change in mechanical strength that may occur.

This study will focus on developing a CFD approach to simulate nuclear graphite oxidation. While a mixed source of data will be used, it will provide the essential background knowledge for the understanding of graphite oxidation and the manner in which experimental data needs to be implemented for CFD applications. The effects of diffusion and mass flow under natural convection conditions will be briefly considered since they are of relevance to the overall air

ingress process. Experiments by KAIST ([41] and [42]) will be used as a benchmark to provide a controlled environment in which the effects of oxidation may be studied, along with the implementation of parameters within CFD. The benchmarking against two open chimney tests on the NACOK facility ([25] and [62]) will demonstrate the ability to simulate more than one chemical reaction and the feasibility of larger more complex geometries in steady state. The main intention of this study is to develop a strategy to simulate graphite oxidation.

It is known that once natural convection begins the flow rate converges to a constant mass flow rate; hence, a steady state analysis would still be valid.

The limitations of the approach are that changes in geometric shape are not accounted for due to the resources required. Changes in the shape of the graphite may occur with oxidation. The effect of deformation and accumulation of particles may influence the gas flow path; these effects are beyond the scope of this study. The change in mechanical strength of the graphite after oxidation is also not included in the scope of this study.

CHAPTER 3: THEORY

3.1 Introduction

This section is intended to provide background on the subject of graphite oxidation. The data on oxidation was obtained from the literature and aids in understanding the oxidation process and the essential parameters for oxidation.

Since oxidation would be placed in context to an air ingress event, air ingress stages are also considered, in particular molecular diffusion. This process needs to be understood to enable the proper simulation thereof.

For the simulation of the NACOK experiment, some effects that occur in a packed bed of pebbles need to be considered. Most of the topics discussed are the subjects of ongoing research. The intention is to emphasize the relevant topics and how they are applied in the case of the PBMR. The relevant theoretical aspects are discussed only briefly, although each could be a field of study on its own. The theoretical aspects related to pressure drop, effective thermal conductivity and the variation in the porous structure in the near wall region are considered for this study.

3.2 Theory- Air ingress and Molecular Diffusion

In the event of a rupture of the pressure boundary of the reactor or associated pipe work, the pressurized high temperature helium which forms the working fluid of the reactor may escape. Hence the coolant of the reactor is lost. This is termed the depressurized loss of forced coolant. Following the loss of coolant, the plant is designed to automatically trigger a safe shutdown and maintain the reactor in a sub-critical state. The location and the size of the pipe break will influence the process. Simultaneous guillotine breaks in the inlet and outlet pipe areas are extremely unlikely since these are multilayer pressure pipes. However, for the purposes of analysis we will assume that if both break, this would result in hot and cold regions being present. The reactor exit flow path would be hot, while the inlet channels would be cold.

Following a rupture the pressure of the helium will reach equilibrium with the atmospheric pressure. The reactor will still be filled with helium. Air will begin to diffuse through the helium; this is known to be a slow process. Due to thermal gradients within the reactor, the fluid densities would eventually change over time. Buoyancy forces would eventually change giving

rise to natural convection. During this stage larger quantities of air will enter the reactor. The oxygen in the air would react with graphite at elevated temperatures.

Before considering oxidation, let us first consider molecular diffusion. Molecular diffusion coefficients are required as input for the CFD simulations. The mass diffusion flux formulation is discussed in Section 4.6 of this report. The base equation used to calculate the diffusion coefficients was sourced from Perry's Chemical Engineering Handbook [69].

The adapted equation is given below. The adaptation performed was to have an output in the International System of units (SI), in this case it is m^2/s.

$$D_{A-B} = \frac{10^{-7} T^{1.75} \left\{ \left(M_{w,A} + M_{w,B} \right) \Big/ \left(M_{w,A} * M_{w,B} \right) \right\}^{\frac{1}{2}}}{P \left\{ \left(\sum v \right)_A^{\frac{1}{3}} + \left(\sum v \right)_B^{\frac{1}{3}} \right\}^2} \quad (1)$$

In Equation (1) D_{A-B} is the diffusion coefficient of a mixture of gas A and B, T is temperature, P is pressure (in units of Atmospheres), $M_{w,A}$ and $M_{w,B}$ are the molecular weights of species A and species B, while $\sum v$ is the atomic diffusion volumes of the species.

The most commonly used atomic diffusion volumes for this study are detailed in Table 1, and were extracted from Perry's Chemical Engineering Handbook [69].

Table 1: Atomic Diffusion Volumes

Species	$\sum v$
He	2.88
N_2	17.9
O_2	16.6
CO	18.9
CO_2	26.9
H_2O	12.7

3.3 Theory – Oxidation

Graphite has been used in the nuclear industry since the 1940's. It is used as a moderator, reflector and a layer on the fuel matrix. It has the ability to handle high temperatures and is strong enough to be used for structural purposes. One drawback of graphite is that it is prone to oxidation during air or water ingress into the reactor. In order to understand oxidation, the manufacturing of graphite is first discussed. This is then followed by oxidation mechanisms, regimes and finally the reactions considered for this study.

3.3.1 Graphite Manufacture

This section presents a brief overview of the composition and the process of manufacturing graphite. The information discussed in this subsection was sourced from Marsden [52], Nightingale [63] and Slabber [84].

The main constituents of graphite are raw petroleum coke and coal tar pitch. Raw petroleum coke is calcinated at approximately 1300°C. The main reason for calcination is to remove volatile hydrocarbons before using it to manufacture graphite. The coke is crushed to a specific size; in this process some fine particles are created. The filler coke may also be derived from coal tar pitch in which case the filler is referred to as a pitch coke.

The binder most often comprises coal-tar pitch. Pitch is typically solid at room temperature but becomes liquid at relatively low temperatures and is characterized by high carbon content after carbonization. To start with, a mixture of various sized coke particles including fines and pitch is formed. This mix is either vibration molded or extruded into the required shape. During this process, the filler coke particles are aligned with a preferred direction, generally influenced by the direction of forming, which gives rise to the anisotropic mechanical and thermal properties of graphite. The degree of anisotropy is also influenced by the source of the coke and the particle size. Anisotropy of molded graphite is generally lower than that of extruded graphite.

Pitch will soften at a relatively low temperature of approximately 100°C. After forming, the carbon body is baked at high temperature, generally around 1000°C. This changes the crystal structure of the material and the carbon becomes very hard and brittle. The baked carbon artifact is slowly cooled in the furnace from the baking temperature to prevent the formation of cracks.

Baked carbon has a high porosity. A process known as impregnation is conducted to reduce the porosity of the carbon. Either pitch and / or polymers are impregnated into the carbon blocks to reduce the open pores that may be seen on the outer surface and thus increase the

graphite density. A process of re-baking is carried out after impregnation to carbonize the sample. The impregnation and re-baking step may be repeated several times.

Thereafter, the baked sample is heated to an extremely high temperature, generally in the range from 2500°C to 3000°C as part of the thermal treatment process called graphitization. Here, the crystal growth and internal order of the material is affected much more dramatically. The thermal conductivity improves dramatically with a corresponding reduction in electrical resistivity. Graphitization aids in removing trapped gases such as hydrogen from within the blocks and yields a product of much higher purity as compared to the baked sample. Graphitization improves the oxidation resistance of the material as compared to the non-graphitized (or baked) samples.

Some of the main requirements of nuclear graphite are the high thermal conductivity and resistance to radiation damage. Hence, raw material selection is critical. Graphitization at sufficiently high temperatures results in impurities diffusing out of the carbon. During this process chemical purification may also be conducted if required, by employing different gaseous mixtures in the graphitization furnace at different temperature ranges. Alternatively, purification can be executed separately after graphitization. The purified product will show improved oxidation resistance over the non-purified product by virtue of its much lower impurity content. The final graphite block is then machined into the required shape and size.

The pebble fuel manufacturing process differs fundamentally from that used for conventional nuclear grade structural graphite which is used in core components. The A3-3 fuel matrix graphite material adopted for the encapsulation of the PBMR fuel kernels is made up from three main constituents, namely natural flake graphite, electro-graphite and a phenolic resin binder, in measured proportions.

A key difference with the conventional graphite manufacturing process is that the process to make the matrix material starts off with already graphitized raw materials which are bonded with a phenolic resin rather than a binder pitch. After pressing the mixture of flake graphite, electro-graphite and resin binder into a spherical shape, the sphere is carbonized to drive off volatiles from the phenolic binder. This step is followed by a heat treatment at approximately 1900ºC to sinter the product and impart some order to the resin-based binder matrix. Since the starting raw materials are already quite pure, no additional purification is needed for the fuel spheres.

These spheres are not heated to extreme temperatures to avoid damaging the ceramic oxide fuel kernels and associated coatings. Due to the high purity of the raw materials started with,

the final manufactured sphere has relatively good oxidation resistance and compares well with conventionally made nuclear graphite.

3.3.2 Oxidation Mechanisms

The reflectors and fuel coating of a high temperature gas reactor are manufactured from graphite. The coolant gas within the plant cycle is helium. Amongst the main reasons for the use of helium are the inert characteristics of the gas and the good thermodynamic properties (such as high specific heat capacity). Upon start up of the reactor, efforts are made to bake out the graphite and remove as much moisture as possible by means of purging the system with inert gas, generally nitrogen. Under normal operating conditions, minor quantities of moisture may be present and will cause minimal corrosion. This study considers the severe events of air ingress when larger quantities of air would enter the reactor system.

Atmospheric air is made up of primarily nitrogen (N_2), oxygen (O_2) and water vapor (H_2O). Graphite is essentially carbon. During air ingress oxygen comes into contact with carbon at high temperature, which will initiate a chemical reaction. To understand oxidation, first consider the mechanisms that will occur. This is based on the mechanism as explained by Fuller and Okoh [19].

Figure 4 is used to explain the oxidation mechanism and was adapted from Laage [48]. In Figure 4 the block represents a piece of graphite that resides within a flow stream. The flow stream can be split into the bulk flow represented by {1} and the flow boundary layer {2} that forms between the main stream and the interface with the graphite due to the surface friction. As discussed earlier graphite is made up of a mixture of coke and pitch, which leads to a porous solid. Region {3} is the porous surface region of the graphite.

The bulk flow {1} will be made up of the different species of gases; diffusion through the flow boundary layer will occur up to the graphite surface {2}. Once the reactants reach the surface of the graphite, there will be in-pore diffusion into the porous region on the surface of the graphite {3}. Reactions will most probably occur within the graphite {4}, this will entail the breaking of the carbon – carbon bonds of the material and the formation of carbon – oxygen bonds. The products generated will have to diffuse out of the porous region of the graphite {5}. Products will then have to diffuse through the flow boundary layer by external mass transfer {6}. While diffusing back into the bulk flow {7} the gas – gas reactions have to be considered along with the generation and dissipation of heat.

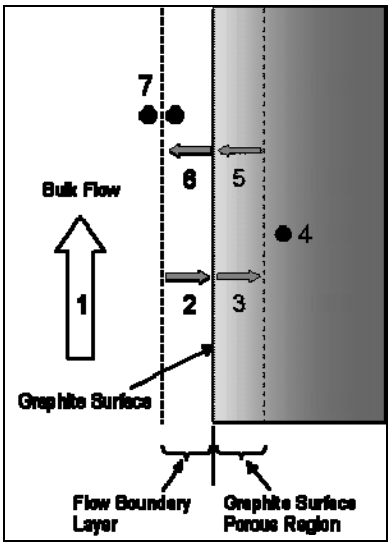

Figure 4: Oxidation Mechanisms

(Adopted from Laage [48])

Based on Figure 4 it becomes clear that oxidation will depend on several factors including: the rate at which reactants have access to the graphite surface, partial pressures of the gases, porosity of the graphite, purity of the graphite, temperature, rate of removal of the products and the diffusion coefficient.

3.3.3 Oxidation Regimes

The oxidation of graphite is highly temperature dependent. This temperature dependence is used to classify the reactions in three separate regimes, as detailed below. Data for the listed regimes were sourced from Roes [71]. It can be noted that the absolute temperatures do vary marginally depending on the reference text used; however they all remain in a similar range.

- Regime I: Kinetic regime

  The first regime is below 650°C and called the chemical kinetic regime. The reaction rate is slow due to the low temperature and depends purely on the chemical reaction rate properties. Oxygen is freely available at the surface of the graphite, including the internal surfaces created by the pores. As oxidation occurs the porosity increases and reduces the graphite density. The porosity change is uniform through the graphite and the outer shape of the structure remains unchanged. Oxidation regimes and the location on an Arrhenius curve are summarized in Figure 5. Figure 5 is an adapted version from that

sourced from Hinssen et al. [24]. It should also be noted that negligible oxidation would occur below 450°C.

- Regime II: In-pore diffusion regime

  The diffusion process into the pores of the graphite and the chemical reaction rate determine the reaction rate. This is between temperature ranges of approximately 650°C and 1000°C. As the temperature increases so does the reaction rate. The inner region of the pores becomes starved of oxygen and this limits the reaction rate. The graphite experiences a porosity and density change that develops over time. The removal of graphite is not uniform. This results in a change in the activation energy for the reaction, hence a change in slope on the reaction rate curve.

- Regime III: Mass transfer regime

  The mass transfer regime is at temperatures above 1000°C. In this case the reaction rate has increased to such a level that the outer surface of the graphite experiences oxygen depletion and the reaction is controlled by the gas transport phenomena through the boundary layer that surrounds the graphite. Since the reaction rate becomes mass transport controlled, the reaction rate curve sees a leveling of the slope.

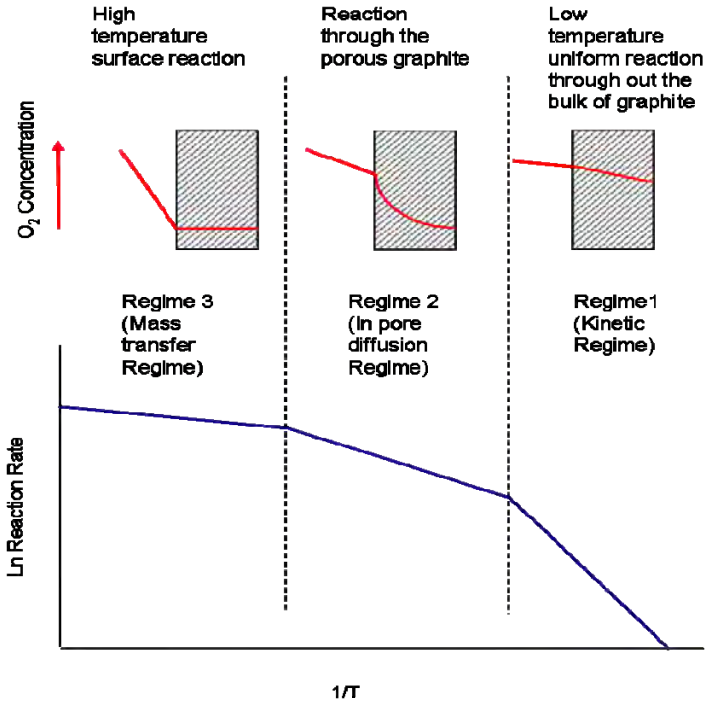

Figure 5: Oxidation Regimes

(Adapted from Hinssen et al. [24])

When considering the Arrhenius plot as shown in Figure 6, the activation energy is found from the product of the slope and the universal gas constant. The intercept on the Y axis is the natural logarithm of A, hence the exponent A is the pre-exponent factor.

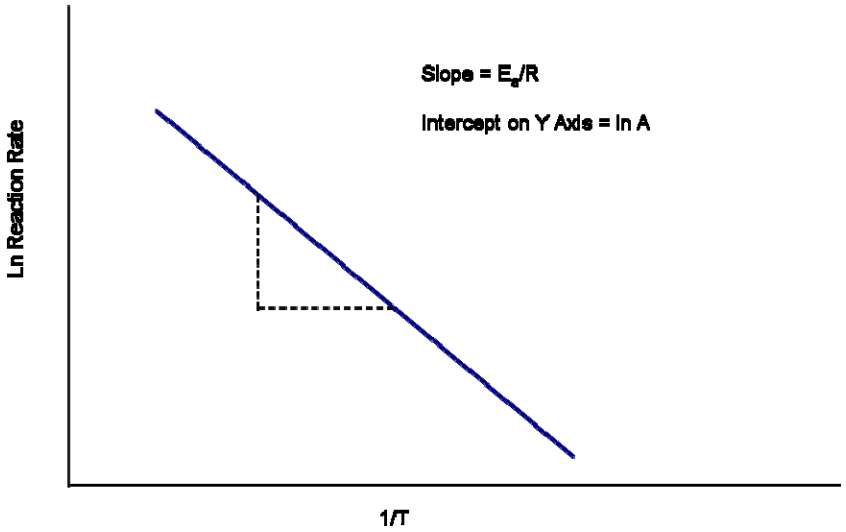

Figure 6: Arrhenius Curve Interpretation

3.3.4 Oxidation equations

For this study the chemical reactions considered and heat of the reactions (at 18°C and 101325 Pa) are listed below and were obtained from Roes [71].

The complete reaction of carbon and oxygen that produces CO_2. Δh = -394 kJ/mol.

$$C + O_2 \longrightarrow CO_2 \tag{2}$$

The partial reaction of carbon and oxygen that produces CO. Δh = -111 kJ/mol.

$$C + \tfrac{1}{2} O_2 \longrightarrow CO \tag{3}$$

The secondary reaction of CO and oxygen that produces CO_2 is considered along with the effect of moisture. Δh = -283 kJ/mol.

$$CO + \tfrac{1}{2} O_2 \longleftrightarrow CO_2 + H_2O \tag{4}$$

This reaction is included in the Fluent database of reactions and is based on the Dryer Glassman correlation. It includes a pre-exponent factor of 2.239e12 and an activation energy of

1.7e8 in J/kmol. The correlation takes the form of $K[CO][O_2]^{1/4}[H_2O]^{1/2}$. The concentration exponents are obtained from a series of experimental data based on radical formation at different temperatures as explained by Adams et al. [2]. The high temperature reaction of carbon and CO_2 in the absence of oxygen that produces CO is detailed below with Δh = + 172 kJ/mol.

$$C + CO_2 \longrightarrow 2CO \tag{5}$$

A positive heat of reaction or change of enthalpy indicates an endothermic reaction in which heat is absorbed; this will have a cooling effect on the graphite. A negative enthalpy indicates an exothermic reaction in which heat is released. The reactions above are specific to the oxidation of graphite in air with atmospheric moisture.

Should steam be considered then the reaction of carbon and steam needs to be included, this is a two step reaction, where the first reaction produces hydrogen, and hydrogen reacts to form methane.

$$C + H_2O \longrightarrow CO + H_2 \tag{6}$$

$$C + 2H_2 \longrightarrow CH_4 \tag{7}$$

Figure 7 is an extract from Roes [71]. It illustrates the diffusion of oxygen through the flow boundary layer, the generation of CO and CO_2 on the solid surface and the diffusion of species back into the flow stream.

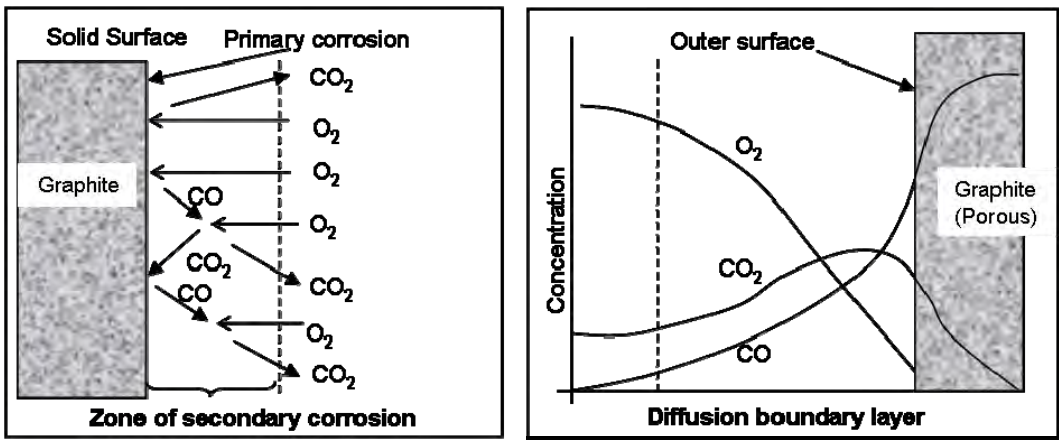

Figure 7: Oxidation Zones

(Adapted from Roes [71])

3.3.5 Burn off

With the manufacture of graphite, the porosity of graphite has to be accounted for since it would influence the available surface area on which reactions could occur. Burn-off as sourced from the works of Fuller and Okoh [19] is explained in the following paragraphs.

At low temperatures the burn-off profile is relatively low and negligible, since there is little oxidation propagation into the depth of the graphite. In the first regime of oxidation, reactions occur in the micro-pores where the available surface area is low.

In the second regime, the closed pores are opened giving rise to larger pores. There is a sharp increase in reaction rate due to the larger available surface area. The reaction rate will vary through the depth due to the gradient of available reactants. Eventually the pore walls are consumed and the reaction surface area decreases. Peak burn off is found around 35% - 40%.

Once the walls are consumed the reaction rate steadily decreases since the reaction area decreases and a change in geometry would occur.

Amongst the published data from Fuller and Okoh [19] is a curve of fractional burn-off versus the increase in reaction rate as shown in Figure 8 (Figure 8 is a recreated image since the original paper was a scanned copy). This curve also shows that peak burn-off occurs at around the 35% - 40% region. The test sample was graphite grade IG-110 at a temperature of 750°C.

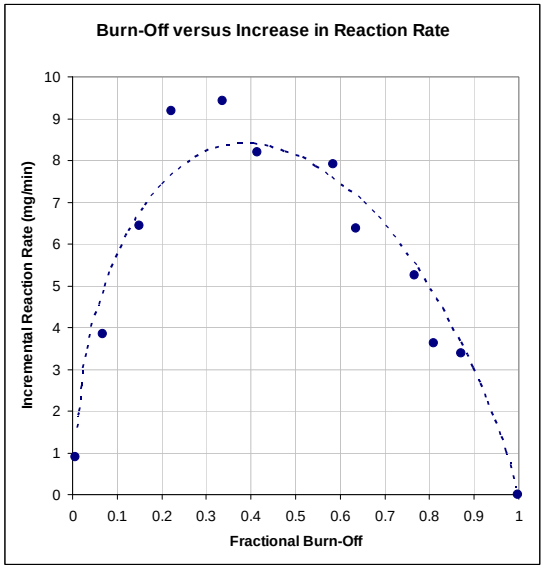

Figure 8: Burn-Off versus Reaction Rate

(Recreated from Fuller and Okoh [19])

The proper kinetics of oxidation within regime I should include a function of burn-off (if known). The general reaction rate will be expressed as shown in Equation (8).

$$r_I = K \exp(-E_a / R_{UGC} T) \left[C_A\right]^n f(B) \quad (8)$$

Where r_I is the volumetric reaction rate in regime I, K is the pre-exponent factor, E_a is the activation energy, R_{UGC} is the universal gas constant, T is temperature in Kelvin, $\left[C_A\right]^n$ is the gas concentration of species A to the power of the reaction order (n) and $f(B)$ is the function of burn-off.

3.4 Theory – Reactor model

Over several years numerous parties have investigated the technique of modeling a packed bed of spheres. With the nature of this work, research will continue as long as there is an interest in the subject. The subject of a packed bed of spheres has given rise to numerous detailed studies. From a thermo-hydraulic perspective, major development areas have been pressure drop through packed beds, the effects of wall channeling and the proper calculation of the effective thermal conductivity. These three developments areas are only a few amongst a long list; they are relevant to this study and will be briefly discussed further to place in perspective the study and some of the considerations.

3.4.1 Pressure Drop

Pressure drop through packed columns has been a research subject for over the past sixty years. Huge bodies of work have been conducted on the subject since it is not only applicable to high temperature reactors but also geometries such as fluidized beds and chemical reactors.

The PBMR is a modification of the initial German design. The Germans' nuclear safety standards commission (Kern Technischer Ausschuss, KTA) [39] formulated acceptable equations for the calculation of pressure loss, provided that given limits are adhered to. The limits are listed below

- Modified Reynolds number in the form - $\mathrm{Re}/(1-\varepsilon)$ between zero and 10^5. Where Re is Reynolds number and ε is porosity of the bed.
- Bed porosity of the bed between 0.36 and 0.42
- The height of the bed should be greater than five pebble diameters.

- A range curve of the ratio of vessel diameter to pebble diameter versus $\mathrm{Re}/(1-\varepsilon)$. (This range curve is further discussed in Chapter 5.3, where it is applied).

3.4.2 Effective Thermal Conductivity

When considering a packed bed the heat transfer mechanisms are detailed and complex. Figure 9 details the various modes of heat transfer that may occur in a packed bed.

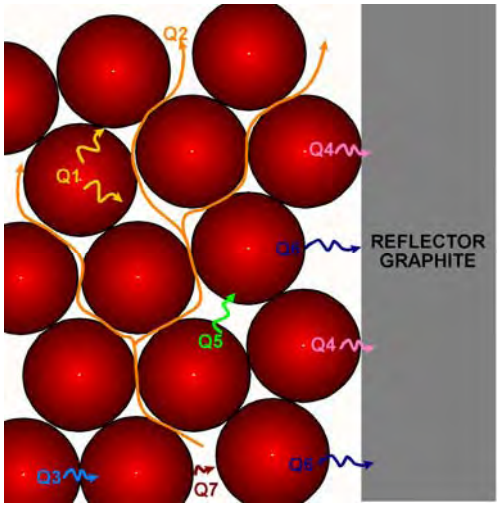

Figure 9: Heat Transfer in a Packed Bed

Based on Figure 9, the various heat transfer modes can be described as follows:

- Conduction from the centre of the pebble to the surface (Q1).
- Convection from the pebble surface to the gas (Q2).
- Point contact conduction between the pebble surfaces (Q3).
- Point contact conduction between pebble and wall (Q4).
- Pebble to pebble radiation (Q5).
- Pebble to wall radiation (Q6).
- Conduction in the gas (Q7).

During the depressurized loss of forced coolant (DLOFC) the convection heat transfer between the reflector and the gas stream and conduction heat transfer between pebbles, gas and the reflectors becomes more pronounced. When using a porous medium approach, the standard conductivity formulation in Fluent is a ratio of solid and fluid conductivity, as explained in Chapter 4.5.3 and Equation (16). With this standard formulation the effect of radiation is neglected. Work at PBMR included research on the most suitable manner to model the effective thermal conductivity of a packed bed. Schmitz [77] compared the values given by the Zehner-Schlünder [98] formulation as defined by the KTA with the values obtained from experimental data.

For this study only the axial component of the Zehner-Schlünder formulation was included. The original Zehner-Schlünder [98] text was in German, an English version appeared in Fullarton's translation of the Verein Deutscher Ingenieure (VDI) Heat Atlas [18]. Generally, the effective thermal conductivity is considered in the radial direction since it is usually the dominant component. For the NACOK experiment the radial dimensions are minimal, and under low flow conditions make the axial component essential for inclusion. For further interest on the topic the VDI Heat Atlas [18], Section Deb1 is recommended. The axial formulation is briefly detailed below.

$$k_{cond-eff,a} = k_f \left(\frac{k_B}{k_f} + \frac{Pe}{k_{shape}} \right) \tag{9}$$

In the above equation, k_{shape} is a shape factor (1.3 for spheres), Pe is the Peclet number, k_f is the fluid thermal conductivity and k_B is defined below.

$$k_B = \left(1-\sqrt{1-\varepsilon}\right)\varepsilon\left[\left(\varepsilon-1+k_G^{-1}\right)^{-1}+k_{rad}\right]+\sqrt{1-\varepsilon}\left[\varphi k_p+(1-\varphi)k_c\right] \tag{10}$$

ε is bed porosity. k_G is the thermal conductivity ratio and is inclusive of the modified free path of gas molecules. k_{rad} is conductivity due to radiation. φ is a flattening coefficient for spheres due to their weight and the resulting flattening of contact points. k_p is the conductivity of the pebble material and k_c is a composite conductivity which accounts for shape factors, radiation effects and pebble material factors. The VDI Heat Atlas [18] provides a full explanation and formulation of these terms.

3.4.3 Porosity Variation

Numerous groups around the globe have studied the porous structures of packed beds as defined by the porosity and its influence on wall channeling and mixing effects. The PBMR focuses on research conducted by the North-West University and the High Temperature Test Facility (HTTF), which was designed to study these effects.

Du Toit [13] deals with the radial variations of porosity in packed beds. It is known that the porosity profile takes the form of a damped sinusoidal wave as shown by Figure 10 (adapted from Du Toit [13]). Explicit modeling of this effect would require a large number of computational cells in the radial direction.

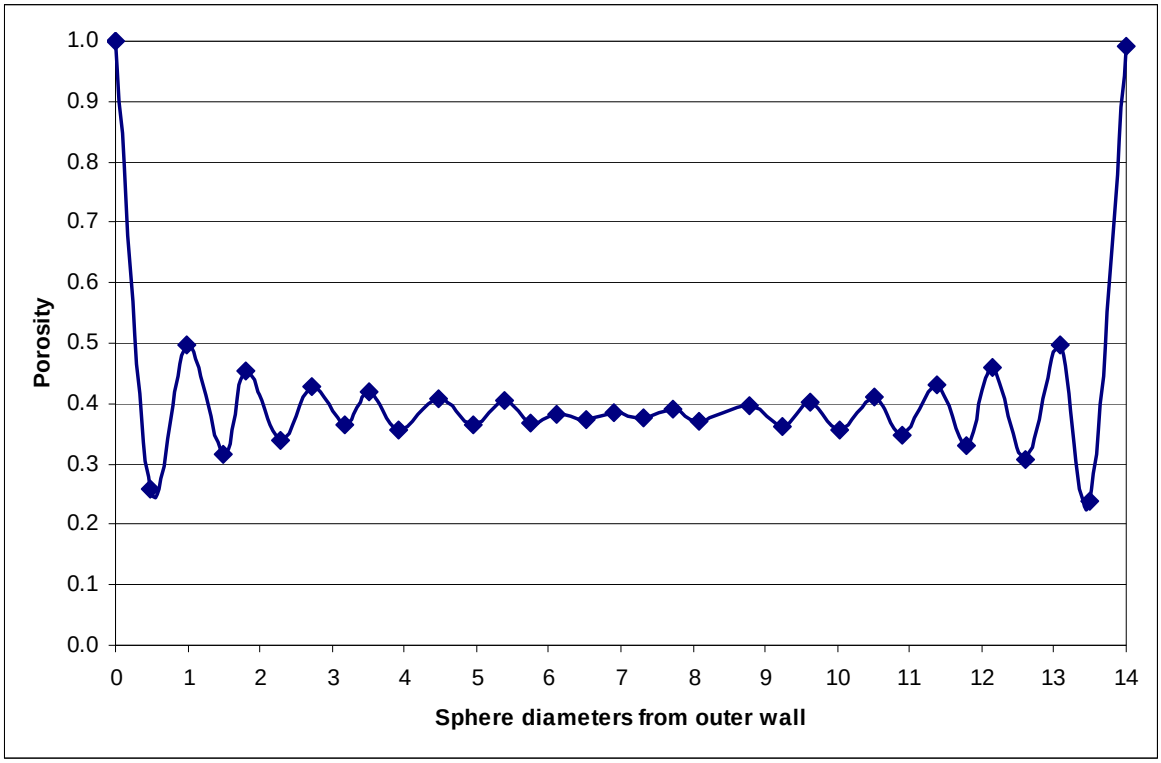

Figure 10: Radial Porosity Distribution

(Adapted from Du Toit [13])

In order to simplify the modeling approach, the porosity in the near wall region is estimated with an exponential correlation. Figure 11 is adapted from Du Toit [13] and shows the exponential function in the near wall region. Du Toit [13] found that the Hunt and Tien [29] correlation best represented the averaged porosity variation in the near wall region when compared with a numerical analysis.

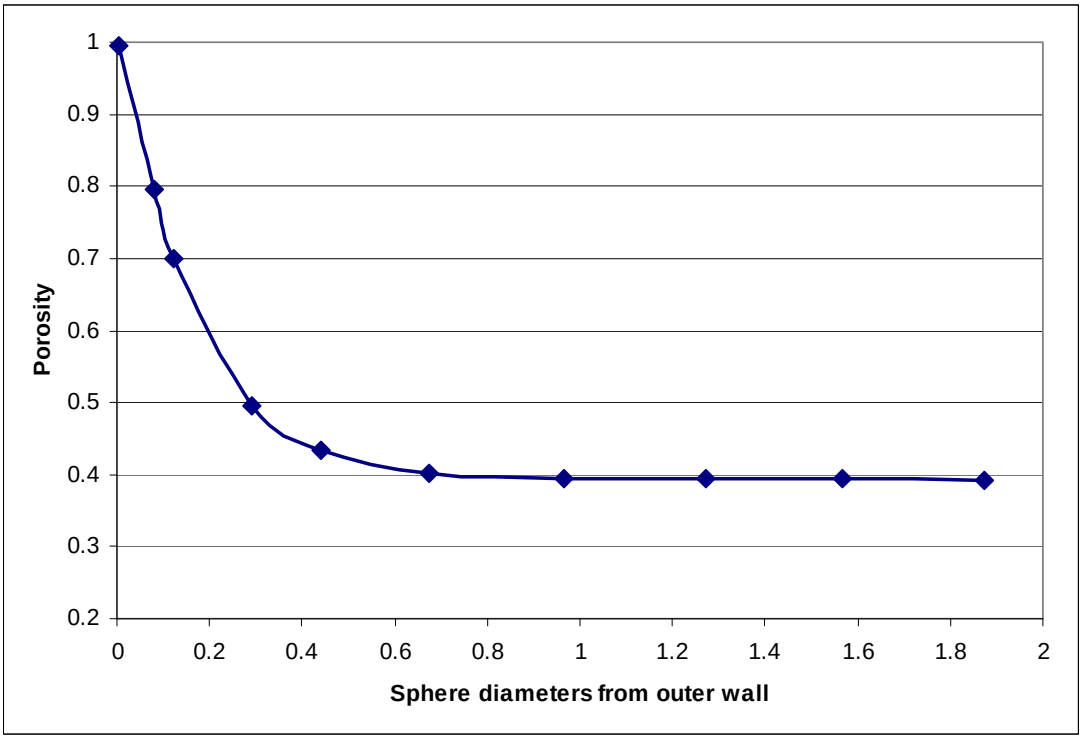

Figure 11: Near Wall Porosity Estimate

(Adapted from Du Toit [13])

The approach adopted by Van Rensburg [93] in the modeling of a nuclear reactor considers the distance of one pebble diameter from the walls. The average values of the variation of the exponential correlation to one pebble diameter are applied to the cells residing in this region. For this study the near wall region of one pebble diameter is given a higher average porosity compared to the bulk region. The values used are detailed in Table 2.

Table 2: Averaged Porosities used through the Pebble Bed

Pebble Bed Region	Porosity Value
Near-wall region	0.4737
Bulk region	0.395

CHAPTER 4: METHODOLOGY

4.1 Introduction

Computational Fluid Dynamics (CFD) is the approach of solving the Navier-Stokes equations via a discretized method. Generally, the finite volume method is used; however, the finite element and boundary element methods could also be used. Traditional areas of application were mostly in the simulation of flow and heat transfer.

The subject of numerical simulation has been studied over many years. Some excellent textbooks on the subject are for example those by Ferziger and Peric [15] and another by Versteeg and Malasekera [94].

CFD codes are structured around numerical algorithms to solve the basic conservation equations. The codes can be divided into three broad areas, the pre-processors, solver and post-processors. These are first considered and then the main conservation equations relevant to this study are considered in more detail. This is followed by an overview of validation and verification.

4.2 Pre-processor

This part of the code is used to define the geometry or computational domain. The domain has to be split into a number of smaller blocks, referred to as the computational cells, control volumes or grids. This defines the regions or points where the values of the solution will be obtained. The relevant physics to define a problem need to be selected. Material properties need to be defined, appropriate wall boundaries need to be specified. The appropriate inlet and exit boundaries from the domain need to be defined.

The accuracy of the solution is governed by the computational grid. The size of the computational grid is usually governed by the limitations of the computational hardware, specifically by the available random access memory on a computer. Larger meshes also require large resources and time for solution. Hence the grid density is a trade-off between accuracy and available resources to obtain a practical engineering solution. The software used to generate the CAD model and the computational grid is called ‘Gambit’. The problem is defined and solved with Fluent.

Part of the set up includes selection of the relevant solution methods and convergence criteria. The solution method includes the manner in which the solver shall solve equations. A coupled

solution solves the bounding momentum and continuity equations simultaneously, while the segregated solver first does the momentum equations, then continuity, updates the mass flux, pressure and velocity, then solves energy, species, turbulence and other scalars. The method of discretization is also set. A second order upwind scheme produces a more accurate result to a first order scheme.

The method of pressure and velocity coupling relates to pressure and velocity corrections to enforce mass conservation and to obtain the pressure field.

The term convergence refers to reducing the solution round off error to a small enough number before proceeding to the next step within an iterative method. The iterative method is the back bone of the solution of simultaneous sets of non-linear algebraic equations. Convergence criteria are applied to multiple levels of the solution. There are criteria to inner iteration loops and to outer iteration loops.

Within outer iteration loops there are criteria for converged solutions of the systems of linearized algebraic equations, convergence of the solution of sets of non-linear algebraic equations for a given mesh and the convergence of a solution to an exact solution as the mesh is refined. Within Fluent the overall solution criteria for a defined mesh is specified. For this study, on obtaining a solution with a defined mesh, the solution gradients are considered and adaptive mesh refinement is conducted to ensure that the end solution is mesh independent resulting in a converged solution.

It is good practice to also monitor the stability of essential parameters in the solution since convergence alone may not be sufficient to have an accurate solution. A completely mesh independent solution may not always be practical due to hardware constraints. However, if the essential variables and locations are stable the solution may still be deemed as a reasonable engineering approximation.

Under relaxation relates to the change in flux during the solution process. The equations being solved are non-linear and rapid changes may cause problems with solution convergence. The lowering of the under relaxation factor decreases the change in flux from one iteration to the next to aid convergence.

4.3 Solver

Fluent uses the finite volume method as the basis for the solver. The following steps are followed:

- The governing equations are integrated over each computational cell. The results from all the computational cells that comprise the computational domain are added to give a set of simultaneous algebraic equations.

- Discretization is the process by which the finite difference approximations are formed for the integrated equations, and by which the integral equations are converted into sets of algebraic equations.

- The algebraic equations are solved by means of an iterative method.

As the solver progresses it considers the overall solution specified convergence criteria. Convergence criteria are described in the paragraph above. Stability is defined as being associated with the damping of errors as the numerical method proceeds.

4.4 Post-processor

This is generally the graphical representation of the solution. Post-processing can be done by a multitude of methods including contour, vector plots, path line tracking, animations, formations of graphs and alpha-numeric exports. Custom written quantities may also be defined.

4.5 Conservation Equations

The four main conservation equations are that of mass, momentum, energy and species. Each equation is considered in more detail to show the specific relevance to this study. The intention of this section is to show the global equations and the relevance of specific terms. The information quoted in this section was extracted from the Fluent 6.3 User manual [17].

4.5.1 Mass Conservation

The generalized mass or continuity equation takes the differential form below.

$$\frac{\partial \rho}{\partial t} + \vec{\nabla}.\left(\rho \vec{V}\right) = S_m \tag{11}$$

In the above equation ρ is density, while ∂t is time period, ∇ is a gradient, V is velocity and S_m is the source term for mass added to the gas phase from user-defined sources.

4.5.2 Momentum Conservation

The momentum equation is expressed as follows:

$$\frac{\partial}{\partial t}\left(\rho\vec{V}\right)+\nabla.\left(\rho\vec{V}\vec{V}\right)=-\nabla P+\nabla\left(\bar{\tau}\right)+\rho\vec{g}+\vec{F}_i \quad (12)$$

In equation (12), P is pressure, τ is the stress tensor, g is gravitational force and F_i is a source term. The first term on the left hand side is the local change of momentum per unit volume per time and the second term is the convective transport of momentum per unit volume. This is balanced by a pressure gradient, a stress tensor gradient, gravitational body force and external forces acting on the body. The $\vec{F}_i$ term may also contain source terms from the resistance due to a porous medium and user-defined sources. Amongst other parameters, the stress tensor includes a term for the inclusion of molecular viscosity.

In some of the cases considered, a porous medium will be used. It is found that certain resistances such as that of the packed bed are impractical to be modeled in explicit detail due to constraints on hardware. In these cases, the overall pressure drop through the blockage is characterized and their properties are applied to a cell zone. Hence this effectively becomes a momentum sink in the momentum equation. Along with this approximation comes numerous limiting factors; amongst them is the default use of the superficial velocity inside the porous medium. This can however be switched by the user to the physical or interstitial velocity formulation. Within Fluent the physical velocity formulation is defined as

$$V_s = \varepsilon * V_{physical} \quad (13)$$

where V_s is the superficial velocity, ε is the porosity and $V_{physical}$ is the physical velocity. In this study the physical velocity formulation is used in porous zones.

The effect of turbulence is also impaired. Since the solid does not exist, the turbulence created by the solid is neglected within the porous zone. Specific heat capacity is taken as a constant in a porous zone, however specific heat capacity may be user defined.

The source term used in a porous media to define pressure losses are made up of a viscous loss term and an inertial loss term. The source term essentially creates a pressure drop that is proportional to the square of velocity. A simple homogenous form of the porous medium expression is shown below.

$$F_i = -\left(\frac{\mu}{\alpha} V + \frac{1}{2} \phi \rho V^2 \right) \quad (14)$$

Where F_i is the momentum source term, μ is viscosity of the fluid, α is permeability on the viscous loss term and ϕ is the inertial resistance factor. Fluent offers a variety of input methods for the coefficients, and they will be discussed at the relevant input areas.

When considering reaction chemistry within a porous media additional inputs are required for the reaction mechanisms and the surface to volume ratios. This is discussed in further detail in the reaction chemistry section.

4.5.3 Energy Conservation

The Fluent form of the energy equation is:

$$\frac{\partial}{\partial t}(\rho E) + \nabla.(\vec{V}(\rho E + P)) = \nabla.\left\{ k_{cond-eff} \nabla T - \sum_j h_j \vec{J}_j + (\overline{\tau}_{eff}.\vec{V}) \right\} + S_h \quad (15)$$

In Equation (15) E is energy. The terms on the right hand side show energy transfer due to conduction, species diffusion, viscous dissipation and a source for heat from chemical reactions or a volumetric heat source. The conduction term for a porous media would be the effective thermal conductivity which is defined as

$$k_{cond-eff} = \varepsilon k_f + (1-\varepsilon) k_s \quad (16)$$

Where $k_{cond-eff}$ is the effective thermal conductivity, k_f is the fluid phase thermal conductivity and k_s is the solid medium thermal conductivity.

In Equation (15) above:

$$E = h - \frac{P}{\rho} + \frac{V^2}{2} \quad (17)$$

The sensible enthalpy h for an ideal gas is defined as:

$$h = \sum_j Y_j h_j \quad (18)$$

Y_j is the mass fraction of species j and h_j accounts for the specific heat of the species in the form:

$$h_j = \int_{Tr}^{t} C_{p,j}.dT \tag{19}$$

where $C_{p,j}$ is specific heat capacity of species j.

4.6 Reaction Chemistry

Reaction chemistry has to account for the reaction and production of various species; hence the species conservation equation needs to be included in the solution. This takes the form of:

$$\frac{\partial}{\partial t}.(\rho Y_i) + \nabla.(\rho \vec{V} Y_i) = -\nabla \vec{J}_i + R_i + S_i \tag{20}$$

In Equation (20) Y_i is the mass fraction of species i. $\vec{J}_i$ is the diffusion flux of species i due to the concentration gradient, R_i is the net rate of production of species i by chemical reaction and S_i is the rate of creation of species i from the dispersed phase.

Should a concentration gradient exist between chemical species in a mixture, mass transfer would occur to establish a state of equilibrium, hence the diffusion flux needs to be considered. The diffusion flux term and chemical reaction term (rate of production of a species) in the above equations are explored in further detail. For laminar flow and low concentration gradients the diffusion flux is determined with Fick's law, the generalized form is shown in Equation (21).

$$\vec{J}_i = -\rho D_{i,m} \nabla Y_i \tag{21}$$

In the above equation, ρ is the density of the mixture. $D_{i,m}$ is the mass diffusion coefficient of species i in the mixture. For the cases considered in this study, the mixtures considered are treated as multi-component systems. Density is specified to be formulated with the ideal gas law, hence density for multi component mixtures is formulated with Equation (22).

$$\rho = \frac{P_{total}}{R_{UGC} T \sum_i Y_i / M_{w,i}} \tag{22}$$

In Equation (22), P_{total} is the sum of the gauge and operating pressure, R_{UGC} is the universal gas constant, Y_i is the mass fraction of species i, and $M_{w,i}$ is the molecular weight of species i.

The mass diffusion coefficient of Equation (21) is computed with Equation (23).

$$D_{i,m} = \frac{1 - X_i}{\sum_{j,j \neq 1} X_i / D_{ij}} \tag{23}$$

Where X_i is the mole fraction of species i and D_{ij} is the binary mass diffusion coefficient of spatial component i in component j.

For full multi-component diffusion within Fluent the mass diffusion coefficients per binary pair of gases $D_{i,m}$ may be specified and the solver then calculates the binary mass diffusion coefficient D_{ij}, based on the solution of a vector matrix of ratios of mole fraction, diffusion coefficient of spatial components and molecular weight. This is based on the Maxwell-Stefan Equations as detailed in the Fluent manual [17]. The defined term of D_{ij} is expressed in Equation (24).

$$D_{ij} = [D] = [A]^{-1}[A_b] \tag{24}$$

Note $[A]$ and $[A_b]$ are $(N-1)$ x $(N-1)$ matrices, with N being the total number of species, while $[D]$ is a $(N-1)$ x $(N-1)$ matrix of the diffusion coefficient D_{ij}. Within Fluent the solver utilizes $N-1$ species, and the balance is taken as the most abundant species or the back ground fluid. Full details of the formulation of constants A and A_b can be found in the Fluent manual [17].

For this study the laminar finite-rate model was used. This model implements the chemical source terms with the aid of the Arrhenius expression. The net source of chemical specie i due to the reaction is calculated as the sum of the Arrhenius reaction sources over the N_r reactions.

Hence reaction R_i is expressed as

$$R_i = M_{w,i} \sum_{r=1}^{N_r} \hat{R}_{i,r} \tag{25}$$

where $M_{w,i}$ is the molecular weight of species i and $\hat{R}_{i,r}$ is the Arrhenius molar rate of generation or consumption of species i in reaction R_i.

The molar reaction rate is defined as

$$\hat{R}_{i,r} = \left(\varpi''_{i,r} - \varpi'_{i,r}\right)\left(K_{forward,r} \prod_{j=1}^{N} \left[C_{j,r}\right]^{\eta'_{j,r}} - K_{back,r} \prod_{j=1}^{N} \left[C_{j,r}\right]^{\varpi''_{j,r}} \right) \tag{26}$$

Where $\varpi''_{i,r}$ = Stoichiometric coefficient of product i in reaction r.

$\varpi'_{i,r}$ = Stoichiometric coefficient of reactant i in reaction r.

$K_{forward,r}$ = Forward rate constant for reaction r.

$C_{j,r}$ = Molar concentration of species j in reaction r.

$\eta'_{j,r}$ = Rate exponent for reactant species j in reaction r.

$K_{back,r}$ = Backward rate constant for reaction r.

$\varpi''_{j,r}$ = Stoichiometric coefficient of product j in reaction r.

Finally, the Arrhenius expression for the forward reaction, $k_{f,r}$, is calculated with

$$K_{forward,r} = A_r T^{\beta} e^{-E_a / R_{UGC} T} \tag{27}$$

Where A_r = Pre-exponent factor constant

T = Temperature

β = Temperature exponent

E_a = Activation energy of the reaction

R_{UGC} = Universal gas constant

Within Fluent the chemical reaction in the form of Equation (26) is input via the 'Reactions' panel of reacting species. Multiple reactions may be specified and named. Reactions may then be grouped to be applied to specific geometry via the 'Reaction Mechanisms' panel.

When applied to a porous zone an additional panel for input of the 'surface to volume ratio' is activated. The porous zone requires input for the inertial and viscous coefficients relating to pressure drop as discussed in Equation (14). This relates to the packing of the porous media. The input of surface to volume ratio relates to the available surface area for reactions to occur within a defined volume of the porous zone.

4.7 Validation and Verification

Within the nuclear industry, emphasis is placed on safety being of the utmost importance. Hence all calculations produced have to be of the highest quality and standards and must be as accurate as possible given the available resources at the current time. To ensure that quality and high standards are maintained, the PBMR has numerous quality assurance (QA) procedures and processes of validation and verification (V&V).

The official definitions of QA and V&V are detailed in the PBMR Demonstration Power Plant Qualification Process White Paper [33]. The V&V approach to CFD analyses at PBMR is detailed in a paper by Schmitz et al. [82] and is dealt with in more detail by Hoffmann [28] in his report on the Validation and Verification Plan for CFD analyses at PBMR.

The term QA can be simplified to say that QA deals with processes and procedures that need to be followed to complete a given task. Several high level documents are used to form company procedures for items such as document control and calculations (to name a few that pertain to CFD analyses). These high level procedures are based on several legal legislation and guidelines, including the Occupational Health and Safety Act; SA Nuclear Regulator licensing document (LD-1094); ISO 9001:2000 - Quality management systems and ASME NQA1-1994 (Quality assurance requirements for nuclear facility applications).

V&V relates more to the tools used for a specific task. Validation focuses on the physics, i.e.: ensures that the correct phenomena have been identified and represented by valid equations. Verification is related to working through the code to ensure everything is implemented correctly. Comparison with analytical solutions, experimental data or alternative numerical solutions are generally used as an indirect method of verifying a code. These cases are generally small enough to be solved without constraint of resources.

V&V is subdivided into four main groups namely: software verification, software validation, model verification and model validation. For software verification, the commercial codes are cross checked by manufactured solutions and certified correct before release for use on any project. This also applies to version changes of the software. Software validation is conducted by running a series of simulations with different phenomena which are relevant to PBMR. Model verification is implemented with different methods such as review of assumptions, simplifications, geometry and input data. Model validation has to be comparisons with analytical solutions, experimental data or alternate numerical solutions. For this study mainly experimental data is used.

The details of QA and V&V can be quite complex and involved. Large volumes of work were conducted to ensure that the best quality and highest standards are always maintained. Most industries do not generally follow such a stringent process.

Besides being guided by several procedures, the PBMR CFD group has compiled a CFD Best Practice Guide, as detailed in [27]. This is based on a best practice guide compiled for the European Commission [53]. This demonstrates that analyses conducted at PBMR are internationally recognized.

CHAPTER 5: INITIAL EXPERIMENTS AND SIMULATIONS

5.1 Introduction

The events preceding oxidation in an air-ingress occurrence are molecular diffusion and natural convection. This chapter considers firstly an analytical solution for diffusion and then compares this analytical solution with the numerical CFD solution. The second benchmark case for the CFD simulations is an experiment at NACOK to demonstrate mass flow rate calculations under conditions of natural convection.

5.2 Diffusion Tube Benchmark

To demonstrate molecular diffusion a simple case of two gases mixing within a tube was considered. The analytical solution for this problem was conducted by Lourens [51]. This work by Lourens forms the baseline of the validation and verification of phenomena conducted by the CFD group at PBMR for new software releases. The CFD simulation of this analytical solution would demonstrate the ability of the CFD code to predict pure diffusion in the absence of a gravity field.

Molecular diffusion is known to be a slow process; the experiment was a simple case that would enable the optimal balance between demonstrating the ability to simulate diffusion without spending excessive time on the subject. Previous work conducted by Schmitz and Koster [81] at PBMR has successfully demonstrated the ability of the code to predict diffusion on large complex geometries. However, the required resources for such simulations are intensive.

The test case was a pipe of 2m length, with a mix of nitrogen in the lower part of a tube of diameter 65mm, and helium in the upper half (The first 1m was nitrogen and the upper 1m was helium as shown in Figure 12). The gases were then allowed to mix by diffusion. The mole fractions were monitored with time, along the height at locations of 0m, 0.5m, 1.5m and 2m. Analytical solutions were obtained for temperatures of 27°C, 500°C and 900°C. Initial mole fractions of nitrogen at time zero would be 1 at height 0m and 0.5m and 0 at height 1.5m and 2m. This would change with time, and the species concentration would reach equilibrium over the entire length of the tube.

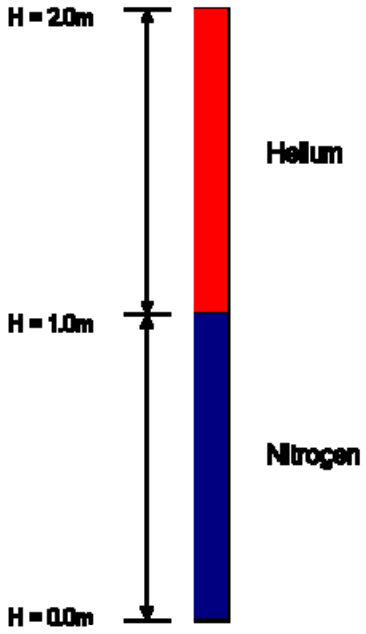

Figure 12: Diffusion Tube Geometry

To simulate this experiment, a two dimensional CFD model was created. The outputs of the analyses were curves of mole fraction of species versus time at a set temperature; hence these simulations were time dependent or transient solutions. The computational grid had five cells in radial direction and sixty cells along the axial direction leading to a total of 300 cells.

Monitor locations were pre-defined at the stage when the mesh was generated in 'Gambit'. The model was also created with two fluid zones, one for helium and another for nitrogen.

Diffusion coefficients for the binary mix of helium and nitrogen were calculated with Equation (1). This equation was varied with temperature to form a curve of diffusion coefficient versus temperature (Figure 13). The data was used to perform a curve fit and the coefficients of the polynomial curve fitted equation were input into Fluent. Note that the inputs for diffusion coefficients for Fluent are in the form of a Taylor expansion and in SI units as shown in the graph.

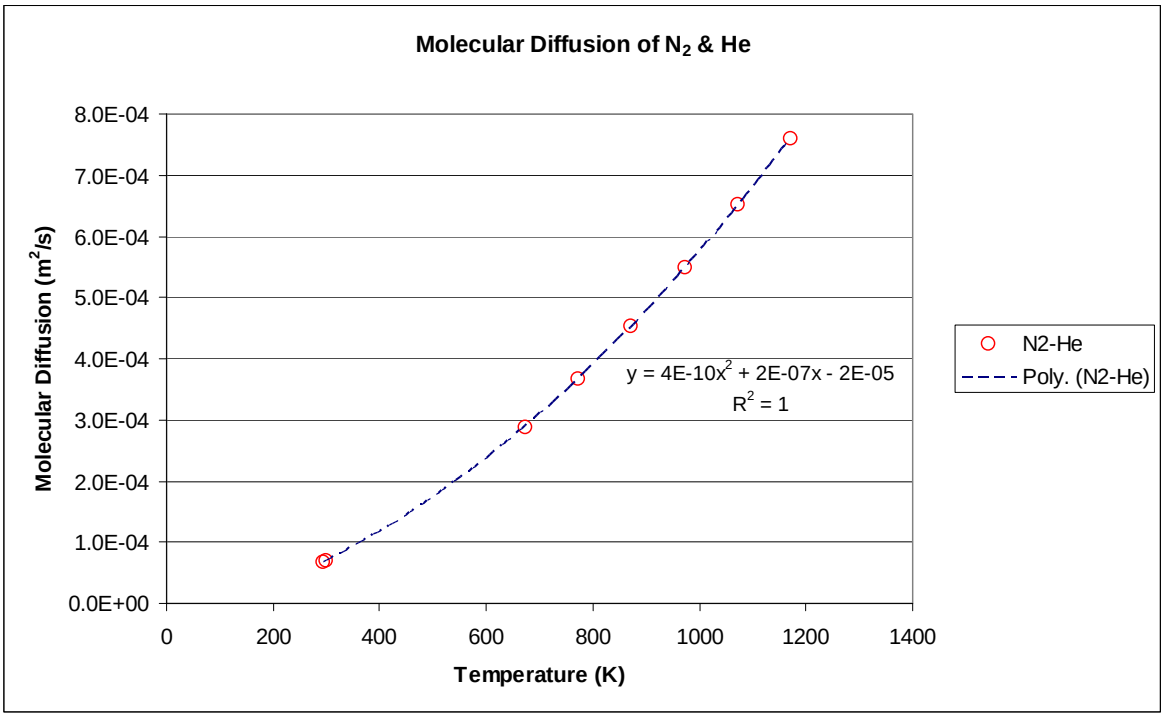

Figure 13: Mass Diffusivity of Nitrogen and Helium

Simulations were conducted with the default under-relaxation factors. The pressure-velocity coupling method of PISO was selected and the second order upwind discretization scheme was used. The relevant temperature was specified at the stage of the solution initialization.

From the analytical solution it was known that high temperatures would have the shortest diffusion period.

The first simulation was conducted at a temperature of 900 °C and with a CFD time step size of 2.5 seconds. Figure 14 presents the results. Monitor locations were defined at heights of 0.5m intervals and the mole fraction of nitrogen was monitored with time. Analytical solutions are the point values while CFD results are the smooth lines. Good comparison was obtained between the two. It takes approximately 3000 seconds for the two gases to fully mix at a temperature of 900°C.

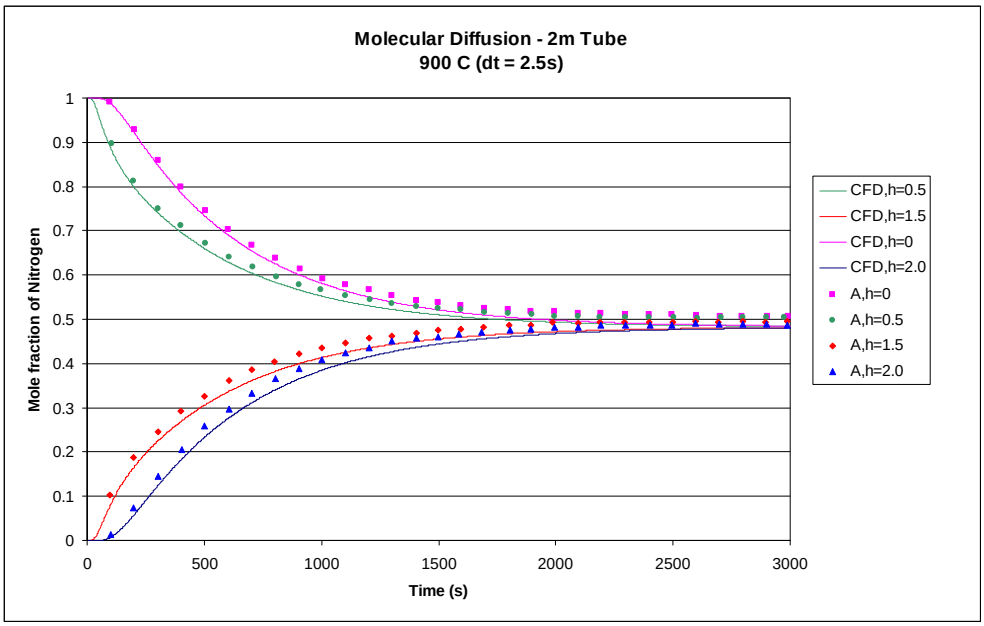

Figure 14: Mole Fraction of Nitrogen at 900°C – Analytical and CFD Results

For the next test, the time step size was doubled to 5 seconds to determine sensitivity to the time step size. The results are presented in Figure 15. The simulation with the 5 second time step is shown by the broken lines. From this figure it can be seen that the 2.5 second time step is closer to the analytical solution when compared to the 5 second time step.

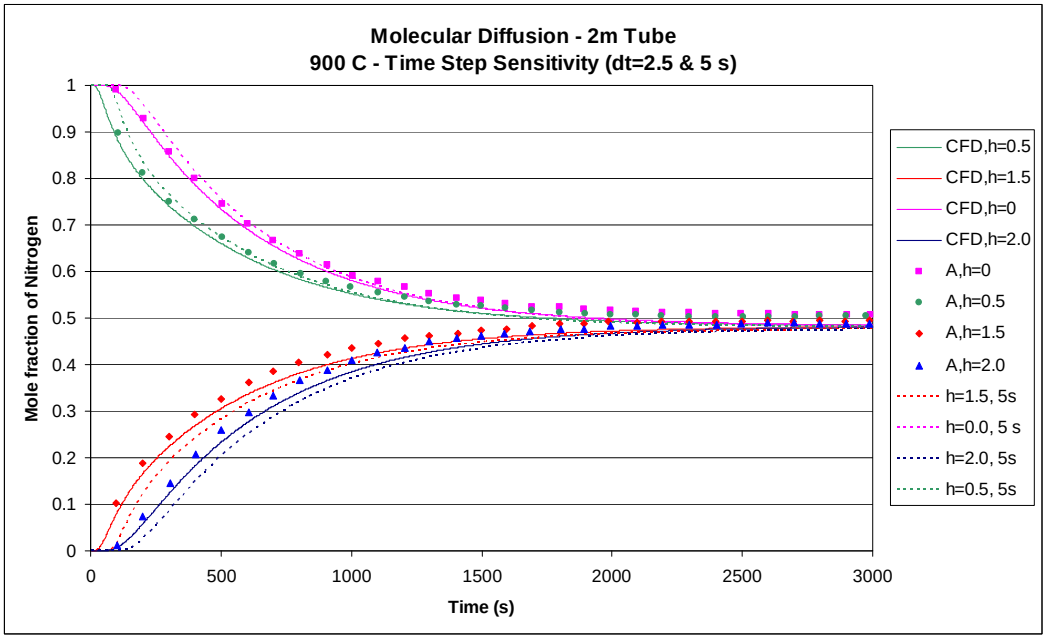

Figure 15: Mole Fraction of Nitrogen at 900°C – Analytical and CFD Results (CFD Time Step Sensitivity)

The next check was to determine the grid sensitivity of the solution as illustrated by Figure 16. The grid was double in both the radial and axial directions. The broken line shows this simulation. Results show that minimal variation was obtained by increasing the grid from 300 cells to 1200 cells. Further simulations were conducted on the original grid and with a time step size of 2.5 seconds.

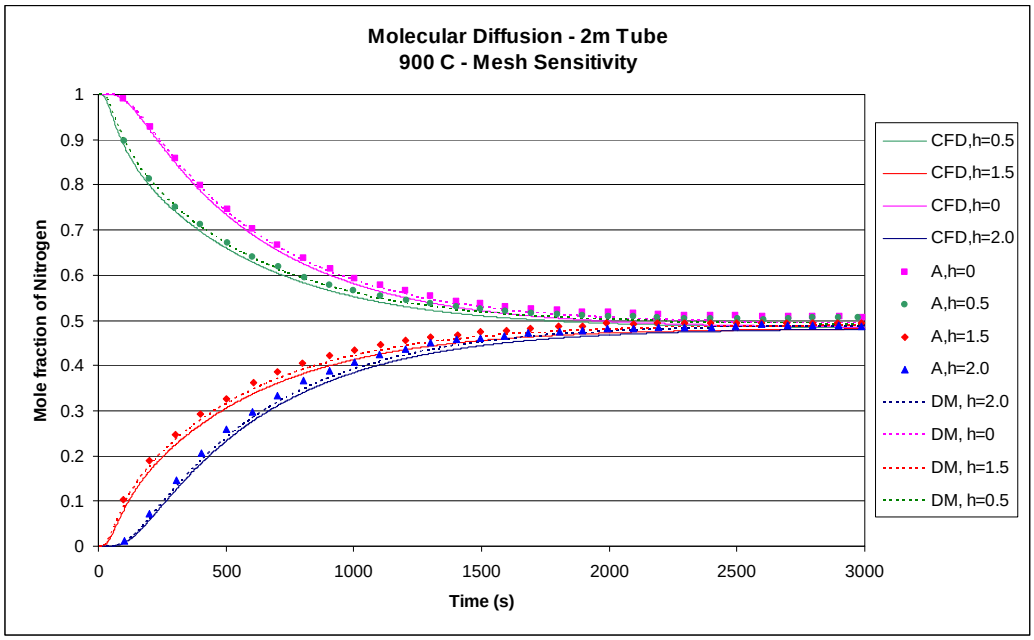

Figure 16: Mole Fraction of Nitrogen at 900°C - Analytical and CFD Results (CFD Grid Sensitivity)

The next simulation was conducted with a temperature of 500°C. It was found that the results of the CFD simulation closely follows the analytical solution as detailed in Figure 17. At 500°C it takes approximately 4500 seconds for the two gases to mix completely.

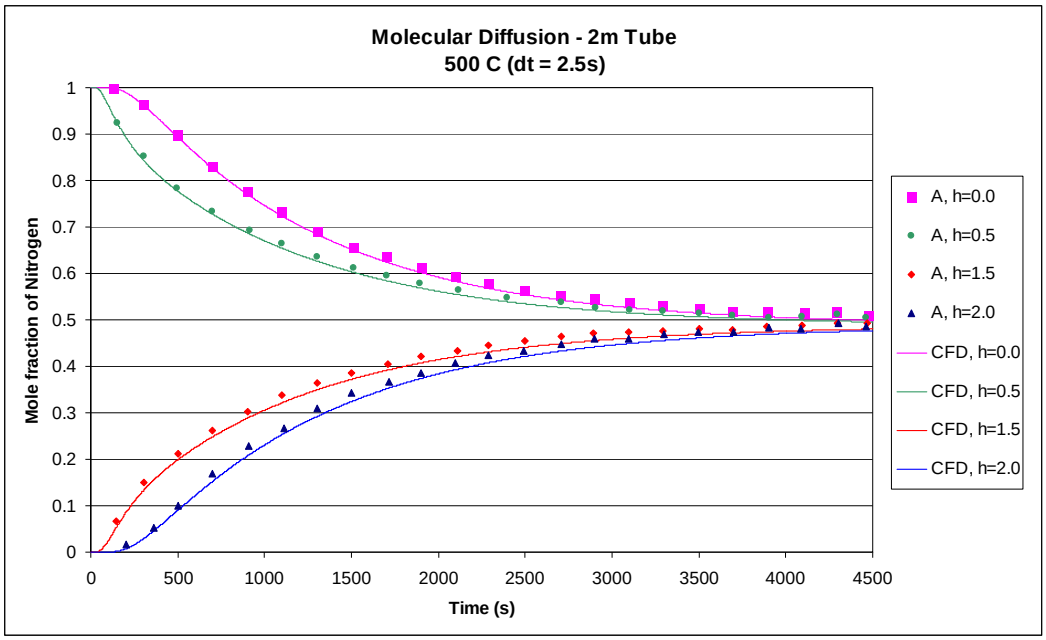

Figure 17: Mole Fraction of Nitrogen at 500°C – Analytical and CFD Results

The final diffusion test was conducted at a temperature of 27°C. Figure 18 details the results obtained from the analytical solution and the results of the CFD simulation. Again good comparison was obtained between the CFD prediction and analytical solution. At 27°C the mixing time of the two gases is approximately 15000 seconds.

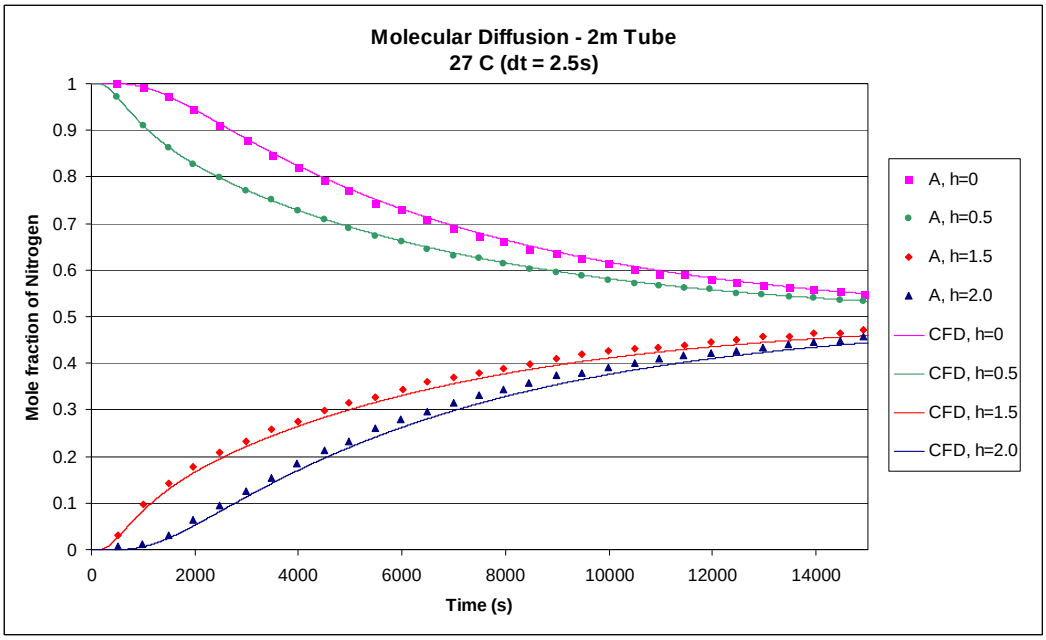

Figure 18: Mole Fraction of Nitrogen at 27°C – Analytical and CFD Results

This demonstrates that molecular diffusion can be simulated accurately. A simple test case was used to become familiar with the required input for the CFD simulation of diffusion. The computational grid and a few of the results are detailed in Annexure A.

5.3 NACOK - Flow Under Natural Convection

The German Institute for Safety Research and Reactor Technology designed and operates numerous experiments. One such facility, operated by Forschungs Zentrum Jülich (FZJ), is the NACOK (Naturzug im Core mit Korrosion) facility. This experiment was designed to study graphite oxidation under natural convection conditions which would equate to accidental air ingress on a nuclear reactor.

The test configuration can be either a return tube or an open chimney. The return tube is basically an inverted U-tube with one heated and one cooled leg. This would be similar to the cooling paths found in a high temperature reactor. The open chimney is a heated column that is vented to atmosphere at the top. This would represent a double break at the top and bottom of the reactor to create a chimney effect. The facility is designed so that the test segments are modular and removable. The benefit of this is that the test specimen could be changed to suit the customers' requirements. Figure 19 shows a schematic of the facility while Figure 20 is a photograph of the facility.

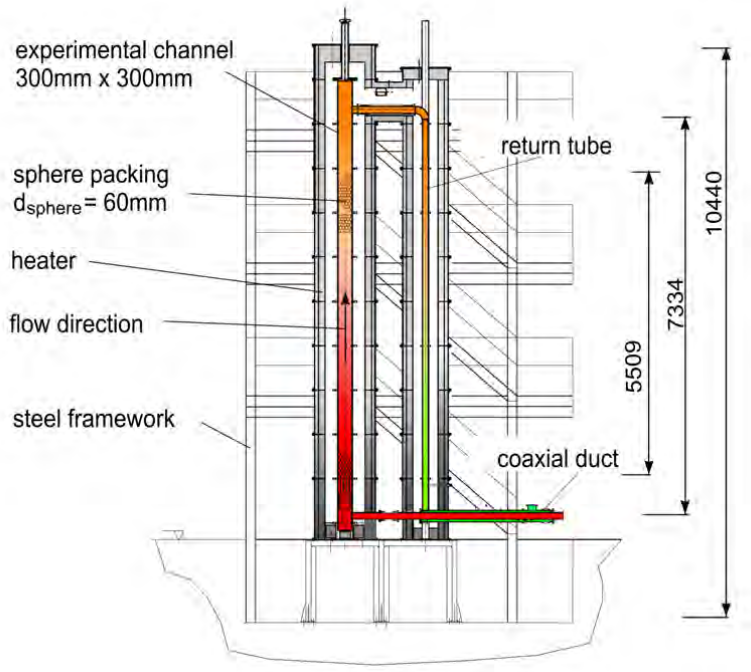

Figure 19: Schematic of the NACOK Test Facility

Figure 20: Picture of the NACOK Facility

Amongst the earlier studies conducted at NACOK was one by Kuhlmann [47] in 2002. His investigation was on a five meter column of ceramic (non-reacting) pebbles. Part of his objectives included determining the mass flow rate under conditions of natural convection, by varying the temperature on the hot and cold legs of the return tube configuration.

Simulation of this part of the experiment would demonstrate the ability to determine the mass flow rate through the system under natural convection conditions.

The experiment can be described as follows. The main test channel was 300 mm x 300 mm in cross sectional area. The horizontal exit pipe and the down pipe were of 125mm diameter. Flow was induced by natural convection only, i.e.: no forced flow. The experimental channel was filled with a 5m high column of ceramic pebbles. The experimental channel was set to a known temperature and the temperature was then changed in 50°C intervals while the return pipe was set to 200°C, 400°C, 600°C or 800°C. The return pipe was always cooler than the experimental channel. The mass flow rate through the system was measured for each case.

With the finite volume approach used in this study, the simulation of the individual pebbles is not practical. A porous cell zone was characterized with the pressure drop properties of the actual column to simplify the model. The porous approach was discussed in the Methodology (Section 4.5.2). An essential parameter in this flow analysis was the determination of the pressure drop through the packed column. As shown in the Theory (Chapter 3.4.1) the KTA rule [39] is generally used to determine the pressure drop in a packed bed. However, one of the limiting factors for application of this rule is a curve of the ratio of vessel diameter to pebble diameter versus the modified Reynolds number. The applicable range of the KTA rule is the shaded region shown in Figure 21. For this case the diameter ratio would be approximately 5, and the modified Reynolds number in the form $\mathrm{Re}/(1-\varepsilon)$ is below 300, as shown by the red lines on Figure 21. Hence this test was out of range of the KTA rule. Kuhlmann [47] addressed this by conducting experiments in the low Reynolds number region and proposing modified constants to the KTA equation for pressure drop in the low Reynolds region.

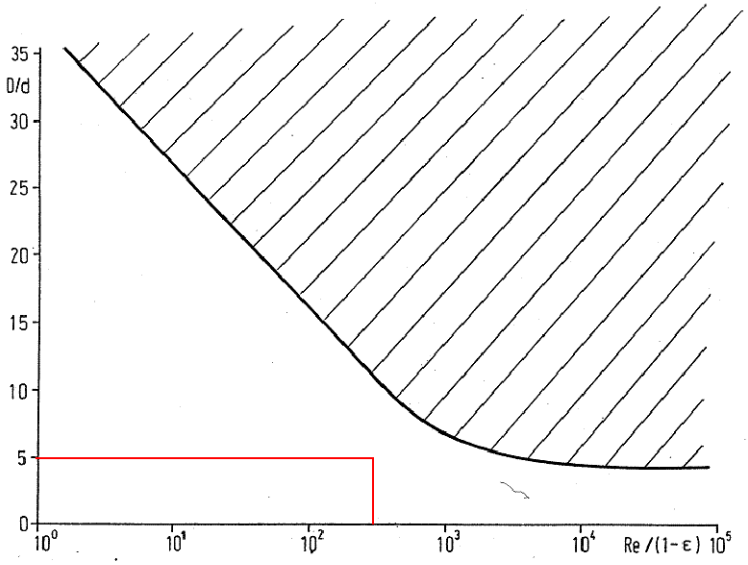

Figure 21: Limiting D/d Curve of KTA Rule

(Adapted from KTA [39])

An alternative to determine the pressure drop in a packed column is the Ergun [14] equation. This equation is used as one of the standard input methods of resistance coefficients in Fluent. Equation (28) shows the pressure drop with the KTA formulation, while Equation (29) shows the Ergun formulation. The main difference is the Reynolds number term in the KTA formulation. For the Reynolds range considered the Reynolds term is calculated to be approximately 0.51, resulting in the constant changing from 3 to approximately 1.5, as compared to the 1.75

constant in the Ergun formulation. The Ergun formulation is easier to use since it does not require any future manipulation or user coding.

Pressure drop per unit length via the KTA rule [39] is expressed as follows:

$$\frac{\Delta P}{l} = \frac{160\mu(1-\varepsilon)^2 V}{\varepsilon^3 D_p{}^2} + \frac{3\rho V^2(1-\varepsilon)}{D_p\varepsilon^3}\left(\frac{1-\varepsilon}{\mathrm{Re}}\right)^{0.1} \tag{28}$$

Where:

$\frac{\Delta P}{l}$ = Pressure drop per unit length

μ = Viscosity

ε = Porosity of the bed

V = Velocity

ρ = Density

D_p = Diameter of the pebbles that make up the bed

Re = Reynolds number

The Ergun Equation [14] is expressed as follows:

$$\frac{\Delta P}{l} = \frac{150\mu(1-\varepsilon)^2 V}{\varepsilon^3 D_p{}^2} + \frac{1.75\rho V^2(1-\varepsilon)}{D_p\varepsilon^3} \tag{29}$$

Fluent has a standard input method for porous media based on the Ergun Equation. For Equation (14), the permeable loss coefficient (α) is expressed as

$$\alpha = \frac{D_p{}^2\varepsilon^3}{150(1-\varepsilon)^2} \tag{30}$$

Whereas the inertial loss coefficient (ϕ) of Equation (14) is calculated from

$$\phi = \frac{3.5(1-\varepsilon)}{D_p\varepsilon^3} \tag{31}$$

Prior to considering any simulations, the KTA and Ergun equations were compared to show the deviation under the low mass flow rates considered in this experiment set. The Ergun and KTA equations were placed in an Excel spread sheet. Pressure was taken as atmospheric (101325 Pa). Calculations were performed at three temperatures, 25°C, 500°C and 900°C. These temperatures are sufficient to envelope the operating range of the NACOK experiment. The density and viscosity were calculated as stipulated by the KTA rule, and the pebble diameter, porosity and bed cross sectional area were specified.

Based on a specified velocity the Reynolds number was calculated, along with the pressure drop using with both the KTA - Equation (28) and Ergun – Equation (29). Mass flow rates were calculated based on velocity, density and the cross sectional area of the experimental channel. The mass flow rates were selected as a comparison parameter since the NACOK experiment under consideration has a comparison of mass flow rate versus temperature. From the experimental data it is known that the maximum mass flow rate was approximately 4.5g/s. Figure 22 shows the comparison between the Ergun and KTA pressure drop calculations. As temperature and mass flow rates increase the difference between the two also increases. At 900°C and 5g/s, the difference between the two methods is approximately 7% as shown by Figure 22. Although differences do occur the variations are sufficiently small for the mass flow rates considered. For this portion of study the Ergun equation was used to implement the pressure drop in packed beds.

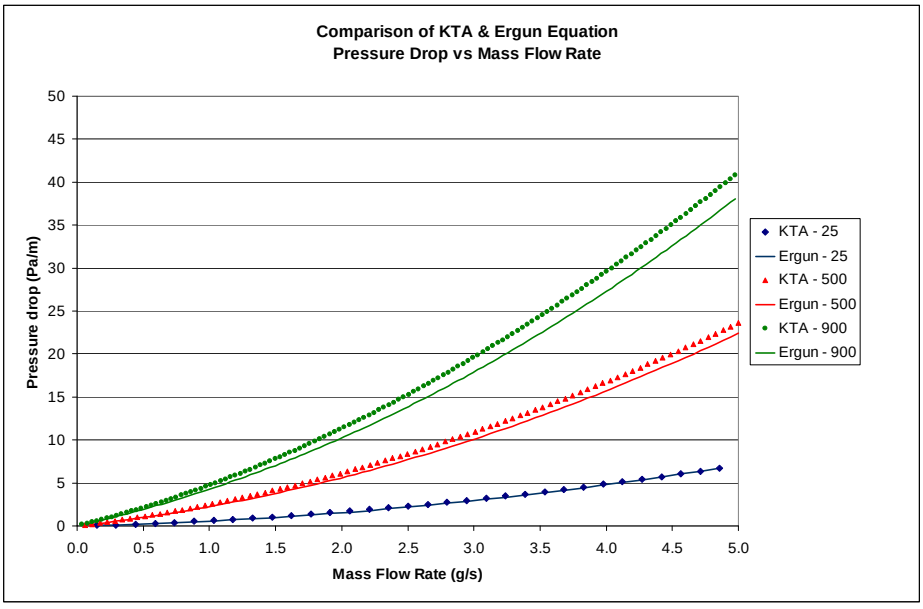

Figure 22: Comparison of Mass Flow Rate versus Pressure Drop for KTA and Ergun Equations

It is also known that leakages were found in the NACOK experimental facility after these tests were conducted. For this reason, there are uncertainties relating to the experimental results. Variations could not be quantified. However, the intention was to establish that the correct estimate of the mass flow rate could be simulated and to establish a trend.

The CFD model for this return duct case comprised approximately 64 300 cells. These simulations were three dimensional, steady state solutions, with a double precision solver. The mixture of species was nitrogen and oxygen in parts that constitute air. This step was not necessary for these tests, but provided insight for future work in this investigation that required species for reactions. The inlet and exit boundary conditions were specified as pressure boundaries with an inlet flow temperature of 20^0C. The experimental channel and the return pipe had conditions of fixed temperature.

The pebble bed was simulated with a uniform porosity of 0.395. Wall channeling was not considered in this sub-study. The pressure velocity coupling was via the PISO method as recommended by the Fluent manual [17] for simulations of natural convection. The discretization scheme for pressure was set to body force weighted and all other parameters to second order upwind. The solution required changing the default under-relaxation factors to lower settings; these are documented in Table 3. With the solution being under conditions of natural convection, it is good practice to monitor the solution stability since solution convergence alone may not be representative. Multiple monitor surfaces were created through the domain and they were monitored for stability in mass flow rate. In conjunction with the solution convergence criteria, the monitors were considered for stability before the solution was taken as complete.

Table 3: Under Relaxation Factors for NACOK Flow Test

Parameter	Under Relaxation Factor - Used	Under Relaxation Factor - Default
Pressure	0.2	0.3
Density	0.8	1.0
Body Forces	0.8	1.0
Momentum	0.5	0.7
Oxygen	0.9	1.0
Energy	1.0	1.0

Figure 23 details the geometry of the simulated domain in which the overall boundaries are shown along with the regions of the experimental channel and the return pipe. The experimental channel was 300 x 300 mm in cross section, while the return pipe had a diameter of 125 mm.

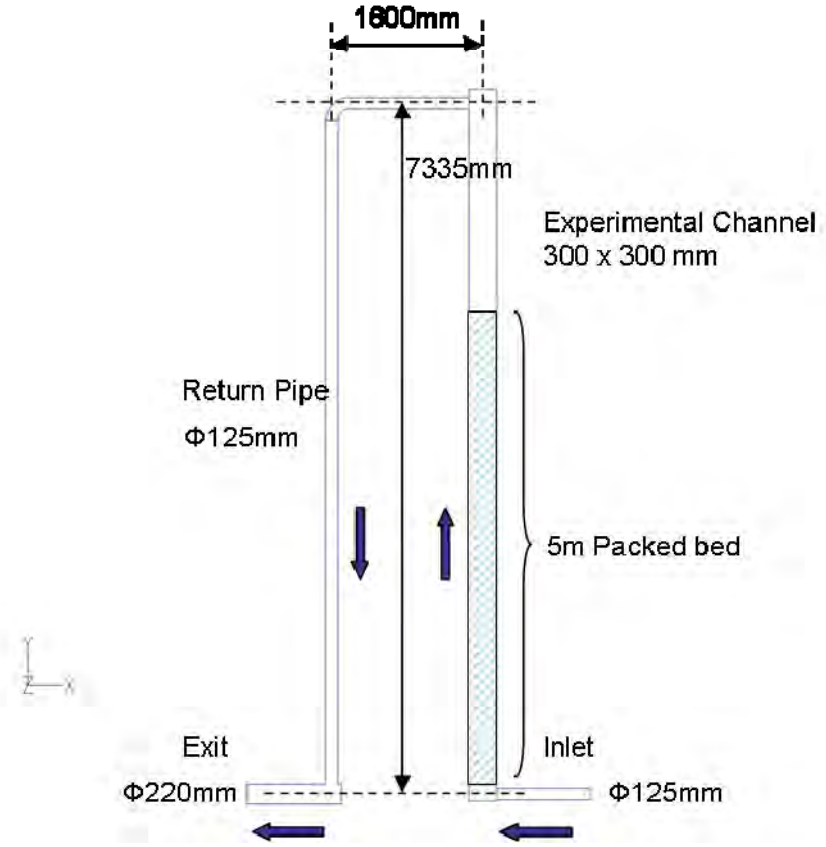

Figure 23: NACOK 2002 – CFD Geometry

Approximately thirty individual simulations were conducted to obtain this comparison of experimental results and simulation. Some of the results are included in Annexure B. The polynomial coefficients for material properties used for the simulations are documented in Annexure C.

The results are presented in the form of a graph as shown in Figure 24. The temperature in the heated experimental channel is expressed on the X axis and the temperature in the return pipe are the color coded points. The blue points are the return duct at 200°C, similarly the return pipe at 400°C is in red, 600°C is in green and 800°C is in black.

The solid points are the measured values from the experimental data and the hollow points are values predicted by the CFD simulations. From the results it is observed that the CFD simulations over predicts the mass flow rate in the high temperature region above 800°C. For the case with the return duct at 800°C, the difference in results is larger than the other cases.

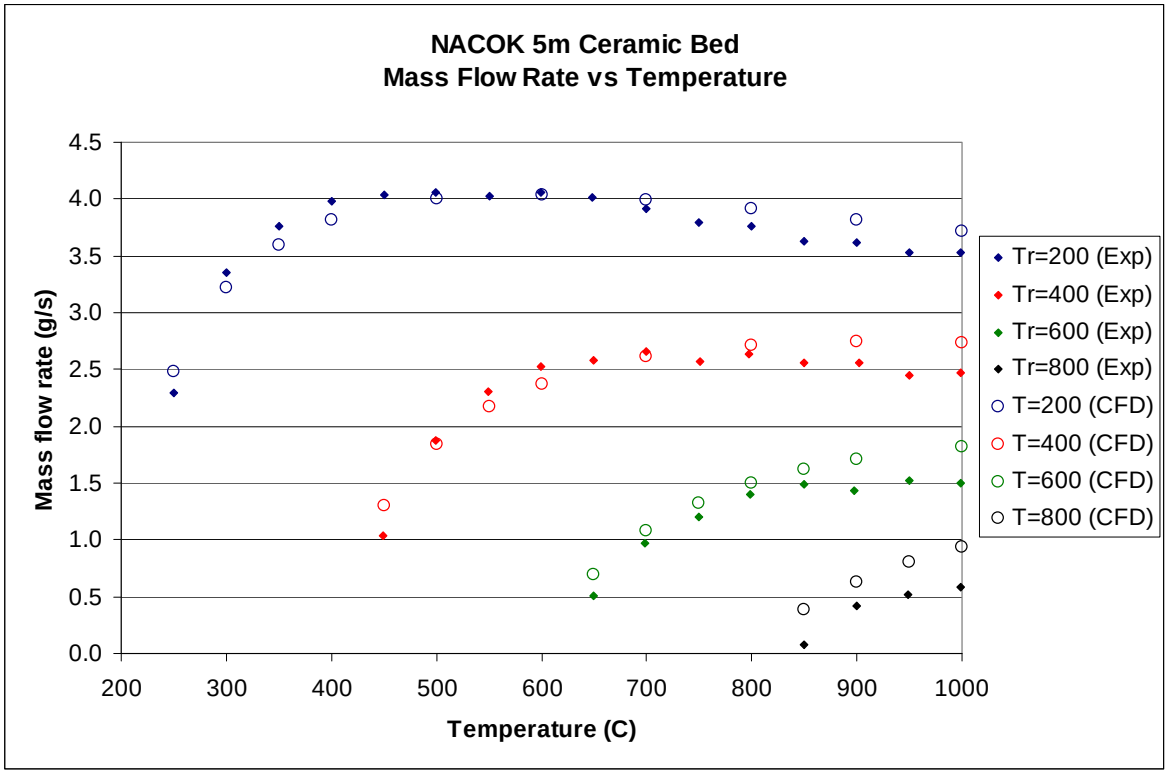

Figure 24: Mass Flow Rate versus Temperature on the NACOK Inert 5m Pebble Bed

A possible reason for the difference in results could include the accuracy of the experimental measurements of the mass flow rates under the low flow conditions for the 800°C return pipe case. Another possible reason is that the packing variation of the bed in the near wall region may influence the mass flow rates and measurement locations. Measurements would typically be with a probe at a fixed point location, whereas the CFD results quoted are area weighted average results across a sectional plane. The near wall effects of a packed column were not studied and can be considered to improve accuracy of the results.

Based on Figure 21, the flow was shown to be in the laminar region. The Ergun equation would generally neglect the second term of Equation (29) in these conditions to form the Blake-Kozeny equation. The constants of the Ergun equation have also been the subject of research for the past sixty years.

A further limitation was that the detailed temperature maps of the experimental conditions were not published. For the CFD simulation, the entire experimental channel and top of the link line were simulated at the hot temperature and the cold leg at a fixed low temperature. A sensitivity analysis to the temperature profile along the cold leg showed that the mass flow rate could be changed by inserting a graded temperature profile to the cold leg. This graded temperature profile on the cold leg is what would actually occur with an experimental setup. The thermal control on the experiment was by means of external heaters. The temperature would fluctuate within certain limits on each of the legs since they are at different temperatures. It is also known that leakages were discovered on the experimental facility after these tests were conducted.

Despite the limitations listed above, the results show that a similar trend was followed by both the experiment results and the results from the CFD analyses. More accurate results may be possible by considering some of the issues discussed above, but for this study the focus is oxidation, hence the trend of a correct mass flow rate prediction was taken as sufficient.

5.4 Summary

The phenomena of diffusion and mass flow rate under conditions of natural convection were explored in this chapter since they are of relevance to air ingress.

Diffusion was benchmarked by comparison of the CFD prediction against an independent analytical solution. A long tube was filled with helium and nitrogen and the gases were allowed to mix purely by diffusion. The simulation of this basic experiment aided in understanding the parameters of diffusion and the simulation thereof. Transient analyses were conducted to test the influence of computational time step size and grid sensitivity. Simulations were conducted at three different temperatures. The results of the analytical solution and the predicted results by the CFD simulations compared well.

The tests conducted in 2002 at the NACOK facility by Kuhlmann [47] considered the return duct experiment to determine mass flow rates under conditions of natural convection. The configuration was basically an inverse U tube with a temperature gradient on each leg. The temperature gradient gives rise to a density variation which results in a difference in buoyancy forces and leads to natural convection flow. Aspects of pressure drop in a packed bed were also explored in this section since they were applicable to the simulations of this experiment.

The KTA rule is generally applied for the pressure drop in a packed bed consisting of uniform spheres. However, it was found that the rule has certain guidelines and the NACOK

configuration does not fall in the guideline that governs the ratio of pebble diameter to vessel diameter. The use of the standard Ergun formulation was explored since it forms the baseline for a standard pressure loss input in Fluent. The considered mass flow range of the experiment was very low. The deviation of the pressure drop for a variable mass flow rate was investigated.

Small differences occur at the low mass flow rates of the experiment. Multiple simulations were conducted with varying temperature differences. A reasonable comparison was obtained between the experimental results and the values from the CFD simulations. The general trend was closely followed with loss of accuracy at the high temperature ranges and very low mass flow rates. The accuracy of the results could possibly be improved by considering some of the issues discussed with the results. These were the accuracy of measurements at low mass flow conditions, measurement location, CFD sensitivity to sphere packing and wall channeling, temperature gradients on the experiment and CFD, the issue of leakages, etc. However, since the main focus of this study is oxidation, and a correct trend was observed, it is reasonable to say that although the accuracy of the simulation may be improved, the trends are nevertheless predicted correctly.

This demonstrates the ability of Fluent to simulate conditions of molecular diffusion and natural convection.

CHAPTER 6: KAIST EXPERIMENTS AND SIMULATIONS

Oxidation experiments conducted by the Korean Advanced Institute of Science and Technology (KAIST) were found in literature [41][42]. The CFD approach was benchmarked against the experiments. Each set of experiments is discussed in detail in this chapter.

The KAIST experiments that were mentioned in the Literature Survey will be explored in more detail here. This is then followed by the CFD simulation with the input for reaction chemistry. Finally the results of the CFD simulations are compared with the experimental results.

6.1 Experimental Data

The experiments conducted by KAIST are detailed in papers by Kim and No [41] and [42]. The work in paper [41] pertains to the $C-O_2$ reaction and details the experimental work, some CFD simulations by KAIST and the development of their custom code. The second paper by Kim and No [42] pertained to the experiment with the $C-CO_2$ reaction.

6.1.1 Carbon - Oxygen Experiment

For this experiment, work was conducted in two stages. The first stage was called the pre-test and was conducted to measure the activation energy and order of reaction. The second stage was conducted to measure the oxidation rate and the produced gases. These tests were conducted in the induction period, meaning that it still had no or negligible graphite burn-off. A schematic of the experimental apparatus sourced from [41] is shown in Figure 25.

Oxidation reaction rates were calculated from the gas concentration data. A helium - oxygen mixture of gas was injected into the test section. The concentration of oxygen and mass flow rates were controlled. The graphite sample was heated by an induction heater. The temperature was measured by two infrared thermometers. After oxidation the gaseous mixture was fed to gas analyzers.

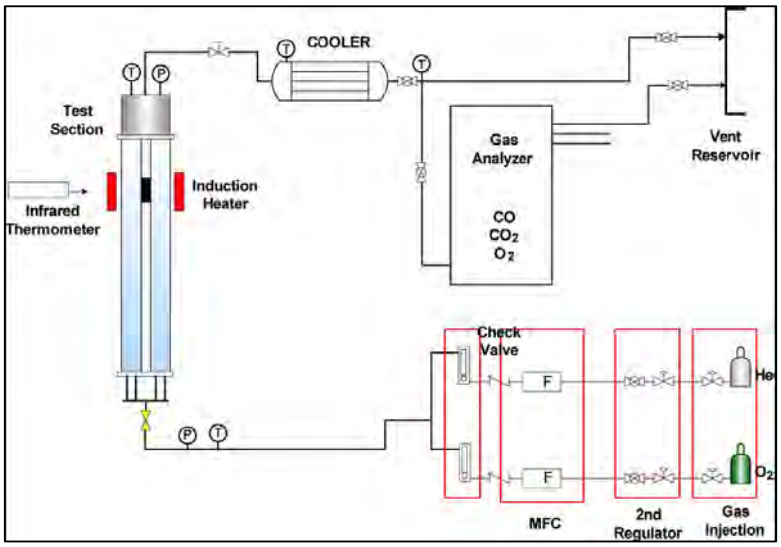

Figure 25: KAIST Experiment Schematic

(Adopted from Kim and No [41])

The test section was a quartz tube with a diameter of 76mm. The graphite sample was held in position by a ceramic rod. The graphite sample had a diameter of 21mm and a height of 30mm. Figure 26 shows a picture of the test section and main dimensions extracted from [42]. The graphite sample was IG-110, manufactured by Toyo Tanso (a Japanese company).

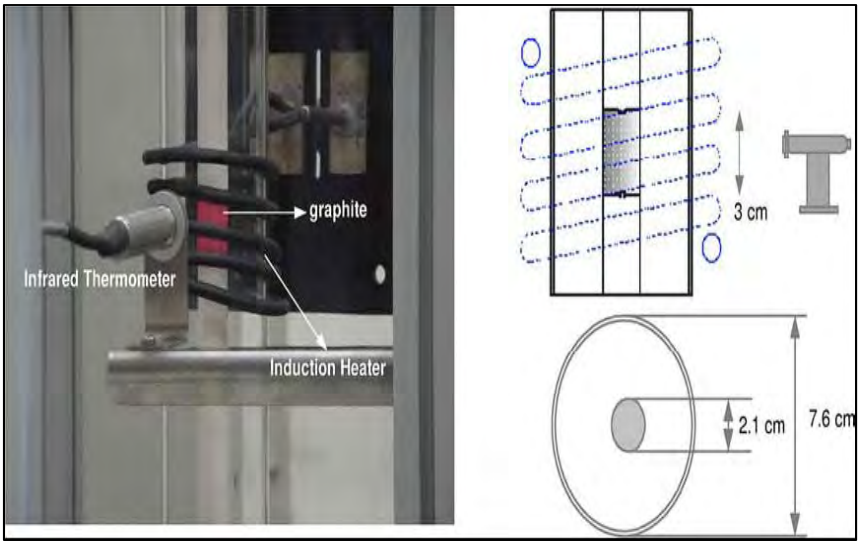

Figure 26: KAIST Experiment – Test Section

(Adopted from Kim and No [42])

The experimental procedure could be summarized as follows. Helium was injected into the test section; when the oxygen concentration reached zero, the graphite heating began. When the desired set temperature stabilized, oxygen was injected into the test section. The emitted gases were continuously sampled and concentration data was recorded. The reaction rate and CO/CO_2 ratios were calculated from the measured data.

The CO/CO_2 ratios from KAIST [41] are shown in Figure 27. Here the results obtained by KAIST were compared with the results obtained by Takahashi, Arthur and Rossberg (as detailed in [41]). As explained in the paper by KAIST [41] Takahashi conducted work on the same grade of graphite as KAIST, whereas Aurthur used coal and natural graphite and Rossberg used electrode carbon, results compare favorably and the present result is relevant to nuclear graphite. In the legend of Figure 27 the percentage values are concentration of oxygen and the relevant test velocity in slugs per minute.

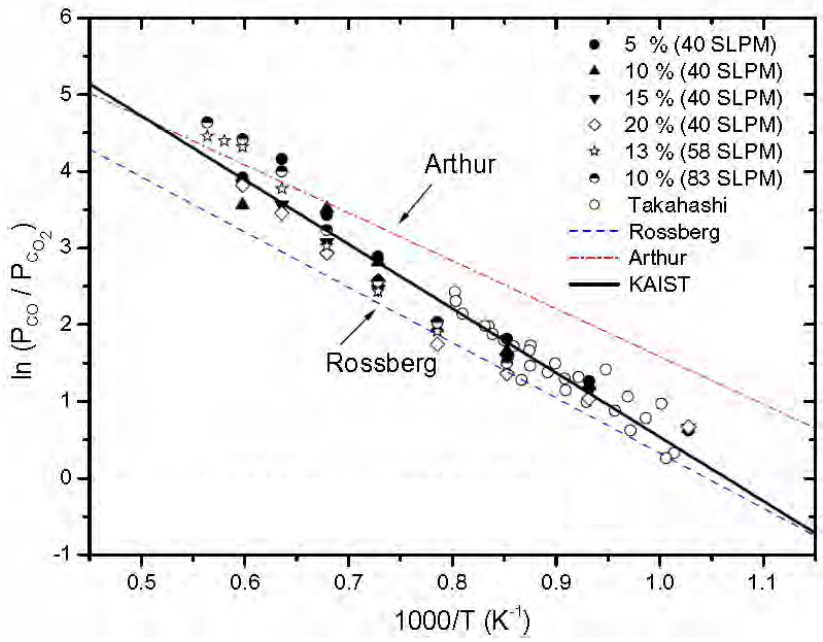

Figure 27: KAIST – Ratio of CO/CO_2

(Extracted from Kim and No [41])

The CO/CO_2 ratio was quoted as $f_{CO/CO_2} = 7396\exp\left(\frac{-69604}{R_{UGC}T}\right)$. The oxidation rates from [41] are shown in Figure 28. Note that this figure is an Arrhenius plot with the logarithmic scale of the reaction rate as a function of the inverse of temperature. The temperature range would be

approximately 700°C on the far X axis to 1500°C (located on the near X axis). The 'scatter' in the data is the result of the different inlet concentrations of oxygen used in the experiment.

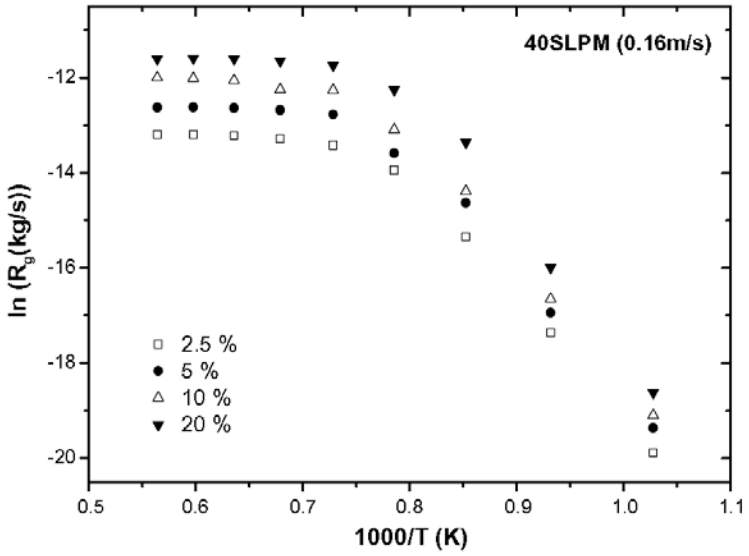

Figure 28: KAIST – Reaction Rate versus Temperature for $C-O_2$ Reaction

(Extracted from Kim and No [41])

The main findings of Kim and No [41] can be summarized as follows:

- Activation energy was equal to 218 kJ/mol
- Activation energy was not affected by oxygen concentration
- Burn-off does not influence activation energy
- The order of reaction (n) varies between 0.6 and 0.9, with an average of 0.75 and
- CO/CO_2 ratio of $f_{CO/CO_2} = 7396\exp\left(\frac{-69604}{R_{UGC}T}\right)$.

6.1.2 Carbon - Carbon-Dioxide Experiment

The second paper from KAIST by Kim and No [42] explored the carbon reaction with CO_2 to produce CO. This is the high temperature Boudouard reaction. The experimental setup was the same as discussed earlier, however the injected gas was CO_2, instead of oxygen.

The test range was from 600°C to 1400°C. The mole fraction of CO_2 was varied from 5% to 20%. Results of the reaction rate versus inverse temperature are shown in Figure 29. A note was made that there was not sufficient product below 1000°C for the gas analyzer.

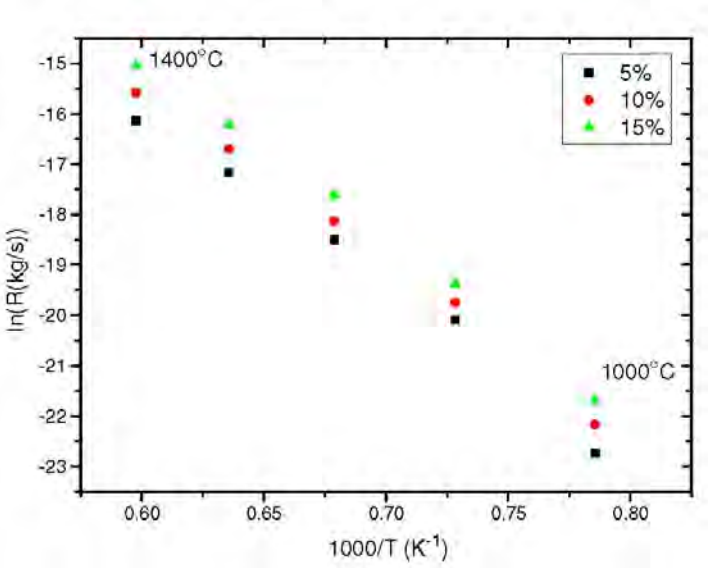

Figure 29: KAIST – Arrhenius Curve for $C-CO_2$ Reaction

(Extracted from Kim and No [42])

The published results include an activation energy of 290 kJ/mol and an order of reaction of 0.9. Some investigations were also conducted to determine the effect of burn-off. The peak reaction rate was found with a burn-off around 35% - 40%. According to Kim and No [42], at the maximum burn-off the reaction rate can be up to three times faster than in a case with no burn-off.

6.2 CFD Simulation of the KAIST Experiments

For the CFD simulation the emphasis was on understanding the input required for oxidation. The geometry was basic and allowed a simple two dimensional axi-symmetric model to be created of the fluid region. Figure 30 shows a block inserted in the location of the graphite sample to aid visualization of the domain. The graphite wall was provided with a fixed temperature as per the experiment. With the inlet air entering at 20°C, and a known velocity this yields a Reynolds number of approximately 800, hence the simulations were taken as laminar and turbulence was neglected. The fluid medium was initialized with helium and oxygen at the known concentrations and mass flow rates were used as inlet boundary data. A pressure boundary was used on the outlet. The rest of the walls were taken as adiabatic walls.

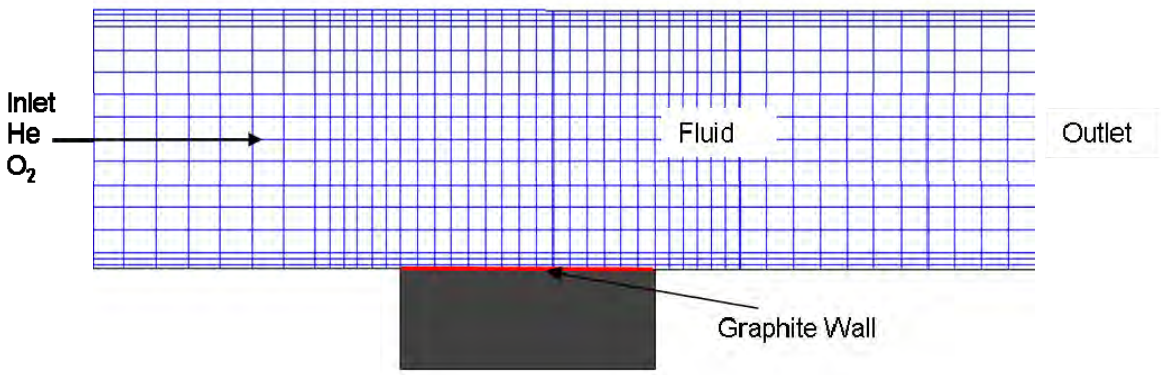

Figure 30: CFD Mesh for KAIST Experiment

The mesh size was varied from 1 000 to approximately 10 000 cells to test the sensitivity of results for grid size dependence. For this portion of the study the default CO - air reaction was used as a starting point. Species included were O_2, CO_2, CO, H_2O, He and site carbon (C <s>) for the solid species. Note that the most abundant species needs to be placed at the end of the species list (in this case He). This species is not solved for and forms the balance in the Fluent solver calculation. Should N be the number of species present, the solver solves $N-1$ species, and the balance is taken as the most abundant species or the background fluid.

The formulation of the gaseous mixture has to be specified. The parameters used are tabulated below in Table 4.

Table 4: Material Mixture Formulation

Parameter	**Formulation**
Density	Ideal gas
Specific heat	Mixing law
Thermal conductivity	Ideal gas mixing law
Viscosity	Ideal gas mixing law
Mass diffusivity	Full multi-component
Thermal diffusion coefficient	Kinetic-theory

As illustrated earlier, oxidation is highly temperature dependent. Temperature ranges considered in this study varied from 500°C to 1500°C. For each material that participates in the mixture, one has to specify the temperature dependent properties. Default values are constant in Fluent. Density was specified as an ideal gas, while the specific heat, thermal conductivity and viscosity are specified with polynomial profiles. Annexure C details the polynomial coefficients for material properties used in this study.

Mass diffusion coefficients were calculated based on Equation (1). It should be noted that the input in Fluent was per binary mix of gases. The total number of possible mixes in this case is 15. Microsoft Excel was used to calculate the mass diffusion values. The mass diffusion values are documented in Table 5 to a maximum temperature of 1200°C. The curve fit values are input as Taylor expansions in Fluent. The polynomial coefficients of the temperature dependent diffusivity calculation are detailed in Annexure C.

Table 5: Diffusion Coefficient (m^2/s) for Binary Gas Mixtures

Temperature					
K	$N_2 - O_2$	$N_2 - CO$	$N_2 - CO_2$	$N_2 - He$	$N_2 - H_2O$
293	1.985E-05	1.964E-05	1.572E-05	6.711E-05	2.526E-05
473	4.589E-05	4.540E-05	3.634E-05	1.552E-04	5.840E-05
673	8.507E-05	8.415E-05	6.736E-05	2.876E-04	1.083E-04
873	1.341E-04	1.327E-04	1.062E-04	4.535E-04	1.707E-04
1073	1.924E-04	1.904E-04	1.524E-04	6.506E-04	2.449E-04
1273	2.595E-04	2.567E-04	2.055E-04	8.775E-04	3.303E-04
1473	3.351E-04	3.314E-04	2.653E-04	1.133E-03	4.264E-04
K	$H_2O - O_2$	$H_2O - CO$	$H_2O - CO_2$	$H_2O - He$	$He - O_2$
293	2.529E-05	2.478E-05	2.017E-05	8.025E-05	6.878E-05
473	5.848E-05	5.729E-05	4.664E-05	1.855E-04	1.590E-04
673	1.084E-04	1.062E-04	8.645E-05	3.439E-04	2.948E-04
873	1.709E-04	1.674E-04	1.363E-04	5.422E-04	4.647E-04
1073	2.452E-04	2.402E-04	1.956E-04	7.780E-04	6.668E-04
1273	3.307E-04	3.240E-04	2.638E-04	1.049E-03	8.993E-04
1473	4.269E-04	4.182E-04	3.405E-04	1.354E-03	1.161E-03
K	$He - CO$	$He - CO_2$	$CO_2 - O_2$	$CO_2 - CO$	$CO - O_2$
293	6.555E-05	5.477E-05	1.546E-05	1.545E-05	1.949E-05
473	1.516E-04	1.266E-04	3.575E-05	3.573E-05	4.506E-05
673	2.809E-04	2.347E-04	6.626E-05	6.623E-05	8.352E-05
873	4.429E-04	3.701E-04	1.045E-04	1.044E-04	1.317E-04
1073	6.355E-04	5.309E-04	1.499E-04	1.498E-04	1.889E-04
1273	8.570E-04	7.160E-04	2.022E-04	2.021E-04	2.548E-04
1473	1.106E-03	9.244E-04	2.610E-04	2.608E-04	3.289E-04

6.2.1 Volumetric Reaction

The volumetric reactions considered are the oxidation of carbon monoxide. Equation (4) is repeated below. This equation is available from the Fluent database.

$$CO + {}^{1}\!/\!_{2}\, O_2 \longleftrightarrow CO_2 + 0H_2O \tag{4}$$

This reaction is based on the Dryer Glassman correlation (as found in the Fluent Manual [17]) and accounts for moisture. The default reaction was used in this experiment, but moisture is not considered in the experiment. Hence the water vapor term of the equation falls away. The default Fluent database equation brings in the reverse reaction of CO_2 to form CO and oxygen. This reaction was not used as part of the present study, but provides a template to input further reactions.

6.2.2 Surface Reaction

When considering any generic reaction, the stoichiometric values of the reaction are required, along with the concentration data. Other parameters will include the activation energy, pre-exponent factors and temperature exponent.

The main focus of this experiment was the primary reaction of C with O_2. The complete reaction would produce CO_2 while the partial reaction produces CO. The mathematical combination of these two equations is expressed as follows:

$$C + xO_2 \rightarrow yCO + zCO_2 \tag{32}$$

The stoichiometric values of x, y and z are expressed as functions of the ratio of CO/CO_2. If

$$F = {}^{CO}\!/\!_{CO_2} \tag{33}$$

Then the stoichiometric value for O_2 depletion, x, would be:

$$x = {}^{F+2}\!/\!_{2(F+1)} \tag{34}$$

While the stoichiometric value for CO generation, y, would be:

$$y = F/(F+1) \tag{35}$$

And the stoichiometric value for CO_2 generation, z, would be:

$$z = 1/(F+1) \tag{36}$$

The ratio of CO/CO_2 published by KAIST [41] was as follows

$$f_{CO/CO_2} = 7396 \exp\left(\frac{-69604}{R_{UGC}T}\right) \tag{37}$$

Where R_{UGC} is the universal gas constant (8.314) and T is temperature in Kelvin.

Equation (37) was used to obtain the curve shown in Figure 31. It is read as follows, for 1 mol of carbon used at a set temperature x moles of oxygen is required to produce y moles of CO and z moles of CO_2.

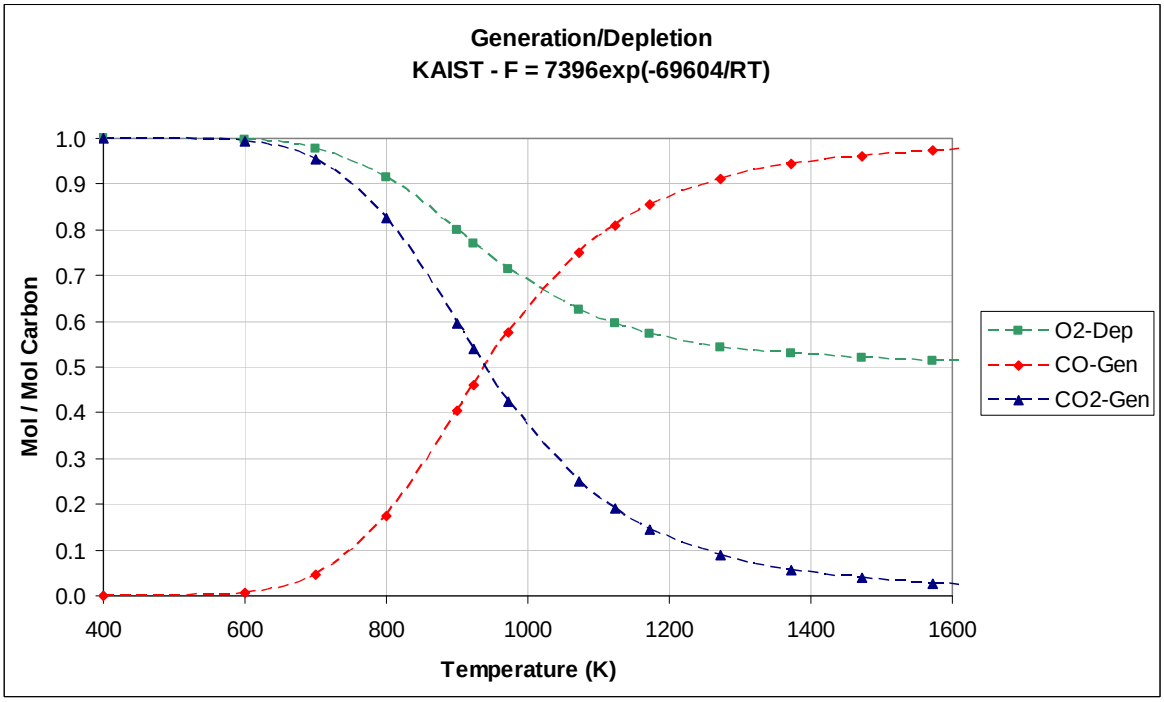

Figure 31: Ratio of CO/CO_2

From Figure 31 it is evident that the stoichiometric values can vary substantially between 800K and 1200K.

6.2.3 Reaction Inputs

For the reaction of $C-O_2$, the surface reaction rate for Fluent would be

$$R_{C-O_2} = K_{forward} * \left[C_{O_2} \right]^n \tag{38}$$

in units of kg.mol/m^2.s. This is the generic form of Equation (26). $K_{forward}$ is based on Equation (27), and

$$\left[C_{O_2} \right] = P_{o_2} \Big/ R_{UGC} T \tag{39}$$

Equation (38) expands to:

$$R_{C-O_2} = A * T^{\beta} * \exp\left(-E_a \Big/ R_{UGC} T \right) * \left(P_{o_2} \Big/ R_{UGC} T \right)^n \tag{40}$$

With the grouping of terms this equation becomes

$$R_{C-O_2} = A * T^{(\beta - n)} * R_{UGC}{}^{(-n)} * \exp\left(-E_a \Big/ R_{UGC} T \right) * P_{o_2}{}^n \tag{41}$$

The conventional manner to express the reaction rate (in units of kg/m^2.s) of carbon and oxygen as found in most literature was as follows:

$$R_{c-o_2} = K_o * \exp^{(-E_a / R_{UGC} T)} P_{o_2}{}^n \tag{42}$$

Fluent requires an input in units of kg.mol/m^2.s. Hence $K_o \Big/ M_{w,c}$, with $M_{w,c}$ being the molecular weight of carbon. To solve the above, let Equation (41) equal to Equation (42) and group similar terms. The term $K_o \Big/ M_{w,c}$ can then be expressed as

$$A * T^{(\beta - n)} * R_{UGC}{}^{-n} = K_o / M_{w,c} \tag{43}$$

For this study the influence of the temperature exponent was unknown, hence it is assumed that $\beta = 0$. The temperature exponent was found to stem from the inclusion of a reference temperature for reactions to reduce the temperature term to a dimensionless group. With $\beta = 0$, the temperature term becomes temperature to the power 1.

The equation above reduces to:

$$A = \left(K_o \Big/ M_{w,c} \right) \left(R_{UGC} T \right)^n \tag{44}$$

Where A is the Fluent pre-exponent factor input. Note that the input units of activation energy is (J/kmol). It is generally expressed as 218kJ/mol. The input unit in Fluent was 2.18e8.

In Fluent the mechanism panel can be used to specify a specific reaction or combination pertaining to a specific region in the geometry. For this case both the volume and surface reactions are grouped into one mechanism. Details relating to the 'site' in the mechanism panel are neglected, as this relates to thin walls with a concentration such as catalyst applications.

From the KAIST experimental data [41], the activation energy and order of reaction are stated. However, the pre-exponent factor is not given. To obtain the required data, the reaction rate curve (Figure 28) was digitized. The change in slope on this figure represents the regime that is mass transport controlled. This region was neglected when considering the kinetic parameters. Strictly speaking the kinetic parameters should be considered in Regime 1 as discussed in the Theory Section, however due to lack of information; Regime 2 was used to obtain a starting point, and adjusted by trial and error. The linear region data before 1000°C was used to conduct a curve fit. The average data was then used.

6.2.4 Boundary Data

The region representing the heated graphite wall was specified with a fixed temperature corresponding to the experimentally measured temperature. Reactions and mechanisms were specified on this wall for the chemical reaction.

The inlet flow condition was taken as 20°C. For Fluent version 6.3 the required boundary data for species concentration was in mass fraction. The papers by KAIST quote mole fraction. Data needed to be transposed before use to mass fraction. The mass flow rate was calculated from given data.

The PISO method was used for the pressure-velocity coupling. The discretization method for pressure was specified as body force weighted, to account for buoyancy. The rest of the parameters used the second order upwind scheme.

The solution convergence criteria for species were as stipulated by the Fluent User Manual [17] and were set to 1e-6 for all species solved. The mole fractions of the gases produced were monitored on the exit of the domain to judge solution stability.

6.3 Results

Once a converged solution was obtained, the results were analyzed using a mass approach. A mass fraction balance of each species was obtained. The mass flow rate was extracted at the exit. Each species was split to its mass proportion. The products of the reaction were CO and CO_2. The percentages of carbon in products were considered by ratio of the molecular weights. The sum of the carbon in the exit gases would be the sum of carbon lost on the reaction surface. The data was input in the appropriate form on an Arrhenius curve for comparison with the experimental data.

First static stoichiometric values were tested at set temperatures on the bounding cases. Pre-exponent factors were tested until an optimal value was obtained. Although the intercept values were relatively close, the pre-exponent factor is the exponent of that number, hence the data ranged from 500 to 2600. It was found that the best fit over the range of data was a K_o value of 2100. Once the best static fit was obtained, the information was used to develop a user defined function (UDF) that would calculate the stoichiometric values based on the surface temperature. The 'define sr_rate' UDF of Fluent was used. With this being the first attempt at using this UDF, numerous iterations were required to obtain the best manner of coding the input. This UDF was further evolved later in the investigation. A final version will be discussed in more detail later in the study.

Figure 32 shows a comparison between the experimental results and the CFD results for the reaction rate of graphite versus time in the carbon oxygen reaction. Grid adaptation was conducted to refine the boundary layer cells to obtain the change of slope in the illustrated curve. The solid points are the experimental data from KAIST and the hollow points with the smooth lines are the results obtained with the CFD simulation. Temperature ranges from 700°C (1.03 on the X axis) to 1500°C (0.56 on the X axis) in 100°C intervals. It was found that the CFD results compare well with the experimental data. There are minor fluctuations but these would be within the tolerance of the experiment and the overall fit of the CFD results is

satisfactory over the entire range of temperatures that were tested. The results of the CFD simulations capture the change in slope of the mass transport regime, however it was found that a fine boundary layer mesh was required to capture this effect. This is illustrated later on in this chapter.

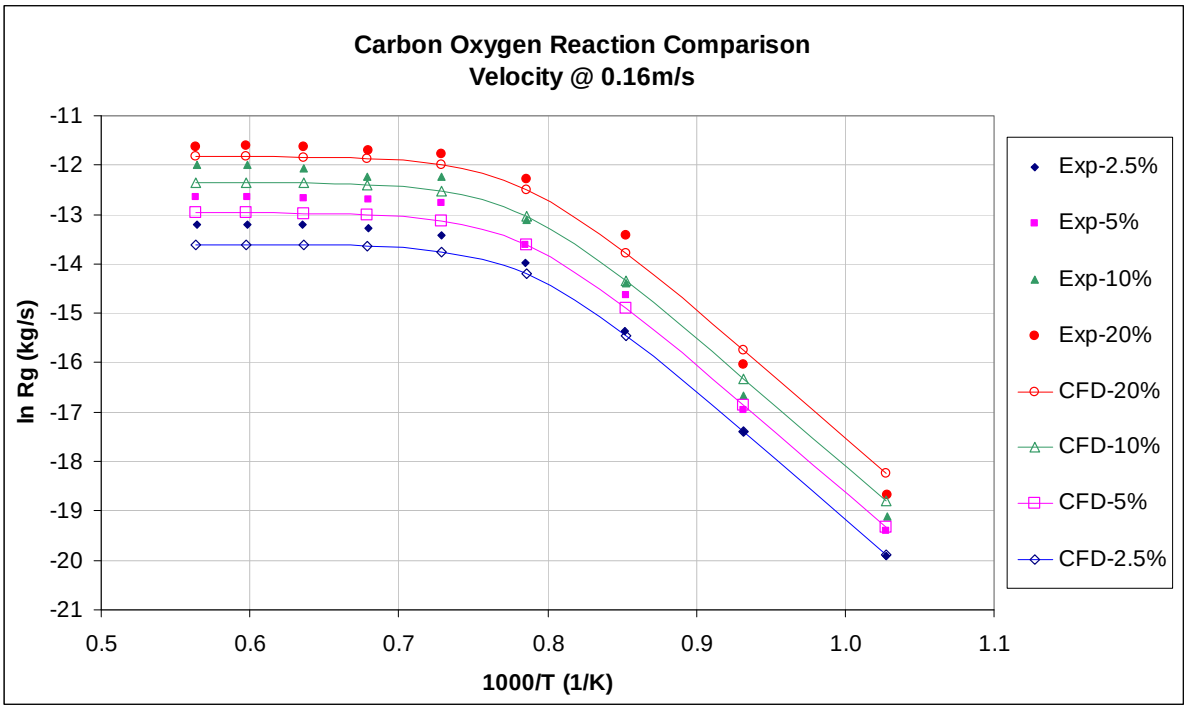

Figure 32: KAIST $C-O_2$ Reaction - Comparison of CFD and Experimental Results

Each complete set of results stems from thirty six individual simulations. The results of the simulation with a heated wall at 1100°C and a mole fraction of 20% are discussed in more detail below. Figure 33 shows a zoomed picture around the heated surface. The surface is seen at 1100°C and the incoming gas is at the ambient temperature of 20°C.

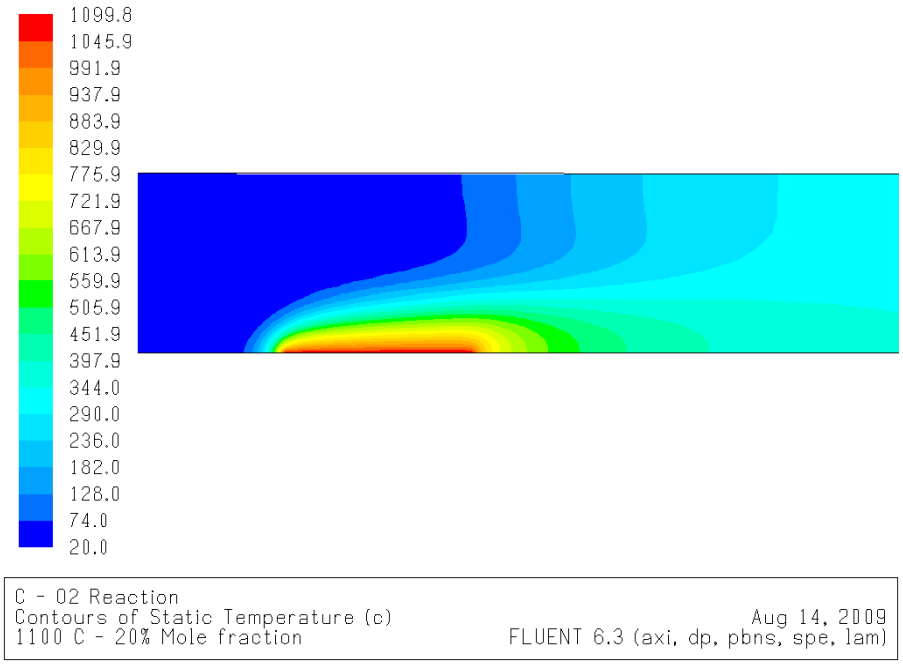

Figure 33: Temperature Distribution at 1100 °C and 20% Mole Fraction of Oxygen

Figure 34 shows the mass fraction of oxygen. Here oxygen is depleted on the heated surface.

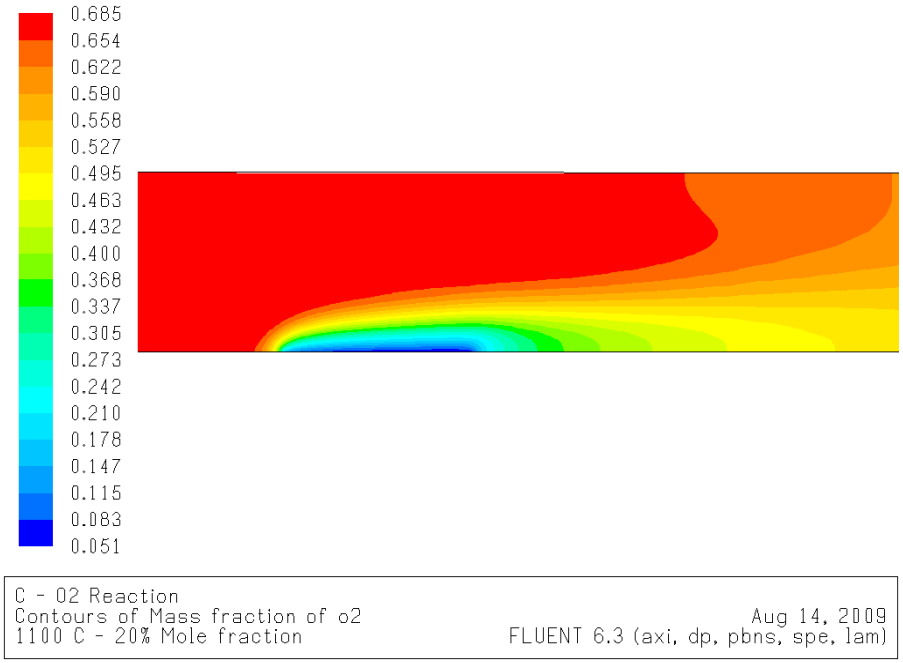

Figure 34: Mass Fraction of Oxygen

Figure 35 and Figure 36 are the generation of CO and CO_2 respectively. Here the ratio of product is controlled by the UDF.

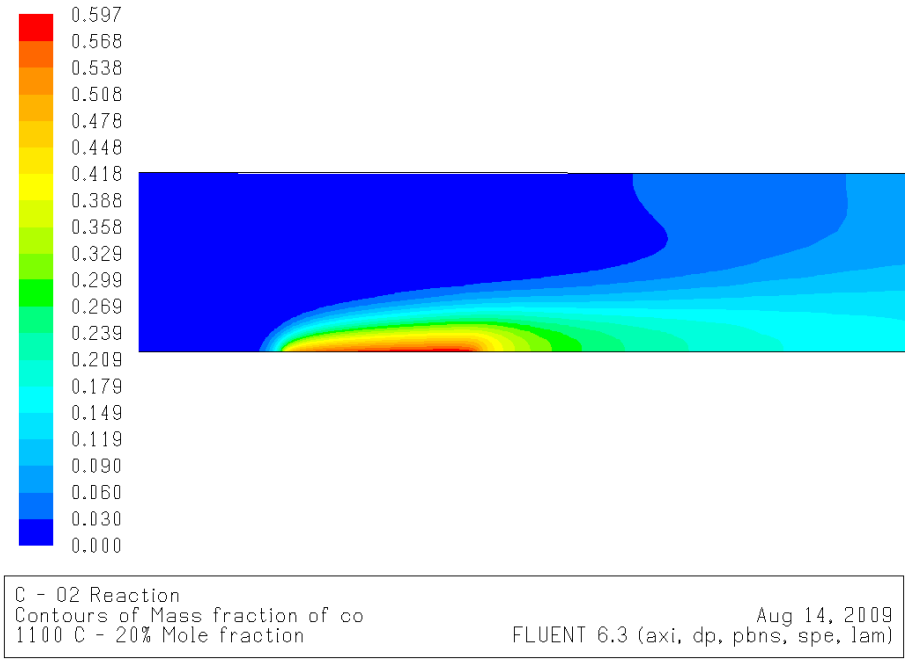

Figure 35: Mass Fraction of CO

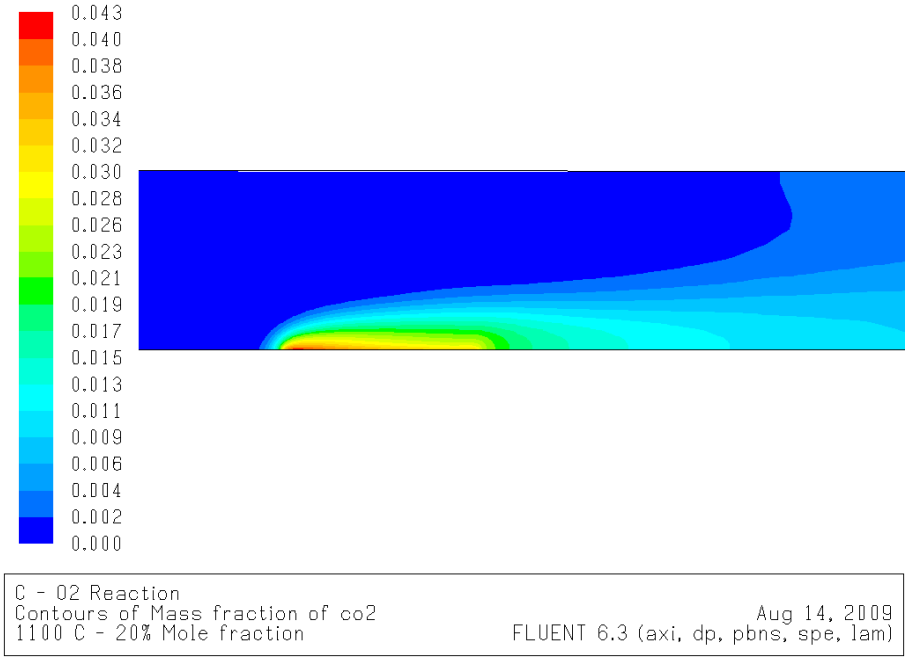

Figure 36: Mass Fraction of CO_2

It was earlier stated that a fine boundary mesh was required in the mass transport regime. As explained in the mechanism section, the reaction occurs on the surface and the cells adjacent to the reacting wall, obtains source terms to include back into the bulk flow stream. Figure 37

shows a velocity vector plot colored according to the radial velocity component of flow. The reacting heated surface is highlighted on the image and the figure shows the orthogonal disturbance created by the cells that feed information back into the flow stream due to the chemical reaction. A well-defined y^+ value (approximately in the order of 10) was required in the mass transfer regime to resolve the feedback from the reacting surface.

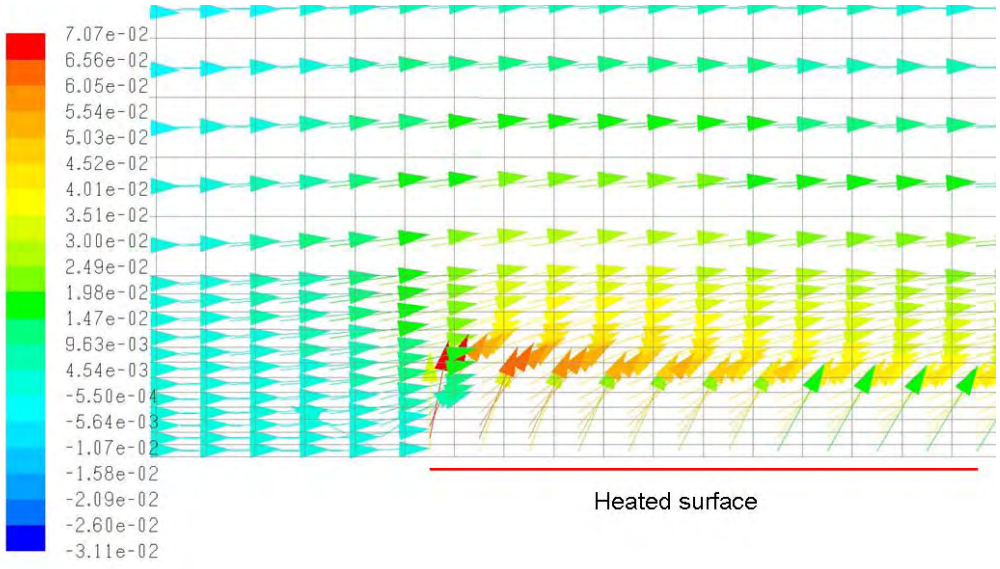

Figure 37: Radial Velocity Vector Plot on a Reacting Wall

6.4 Carbon – Carbon Dioxide Reaction and Results

This set of simulations considered the reaction of $C - CO_2$ that produces CO. This reaction was detailed in Equation (5) which is repeated below.

$$C + CO_2 \longrightarrow 2CO \tag{5}$$

This reaction is called the 'Boudouard' reaction and occurs at high temperatures and in the absence of oxygen.

The modeling approach was similar, in that the same grid was used. Since this reaction does not have varying stoichiometric values the input of the reaction directly via the Graphical User Interface (GUI) was used. This reaction occurs once oxygen is depleted hence the volumetric reaction does not need to be taken into account.

For the $C - O_2$ reaction the partial pressure in the reaction rate was that of oxygen, for this reaction the partial pressure P_{CO_2} is that of CO_2 and is shown below.

$$R_{C-CO_2} = A * T^{(\beta-n)} * R_{UGC}{}^{(-n)} * \exp\left(-E_a \Big/ R_{UGC} T\right) * P_{co_2}{}^{n} \quad (45)$$

To remove the dependence of the pre-exponent factor on temperature the following assumptions were made. If $\beta = n = 0.9$, then $T(\beta - n) = T^0 = 1$. The term for the pre-exponent factor then reduces to:

$$A = K_o \Big/ 12 * R_{UGC}{}^{n} \quad (46)$$

It is important to note that the temperature exponent was taken as equal to the reaction rate exponent; hence this value had to be included in the GUI. With this assumption the pre-exponent factor is independent of temperature and can be implemented via the GUI. The sensitivity of $\beta = n = 0.9$ and $\beta = 0$ was tested with a simulation. The magnitude of the pre-exponent factor changes but the rate exponents for the reaction order also comes into effect; hence the end result is the same with both methods. The reaction rate input stipulates consistent input units are required by Fluent. The input sequence allows the flexibly of implementation with the same result.

As with the previous experiment, the activation energy values were published but not the pre-exponent value. The experimental reaction rate curve was converted to an electronic format and a curve was fitted. The exponent of the Y intercept was used as an initial starting point for the pre-exponent factor. As stated in the previous section the pre-exponent factor is the exponent of the natural logarithm (ln) value given on the curve, hence small variations can change this number substantially. The pre-exponent factor was changed by trial and error until a suitable correlation was obtained to the experimental data.

It was found that the best fit was with $K_o = 39.5$. Solution controls etc. were similar to the initial KAIST simulations. The results were analyzed in a similar manner to the previous experiment. However in this case CO_2 is the input gas; the exit balance has to remove the input to obtain the carbon lost. The results of reaction rate of graphite versus temperature are shown in Figure 38. The solid points are the experimental data, while the hollow points with the smooth line are the CFD results. Some differences between the experimental and CFD results are detected around the 1000°C (0.786 on the X axis) mark. The paper made a note that the experiment was attempted from 600°C with 100°C intervals, but that the gas analyzer only detected sufficient product at around 1000°C. Since a good fit was obtained with experimental data at

higher temperatures, the possible inaccuracy of the measurements at 1000°C could account for the difference in results at this singular location.

Some of the results for the simulation at 1300°C and an input mole fraction of CO_2 at 10% are detailed in Annexure D.

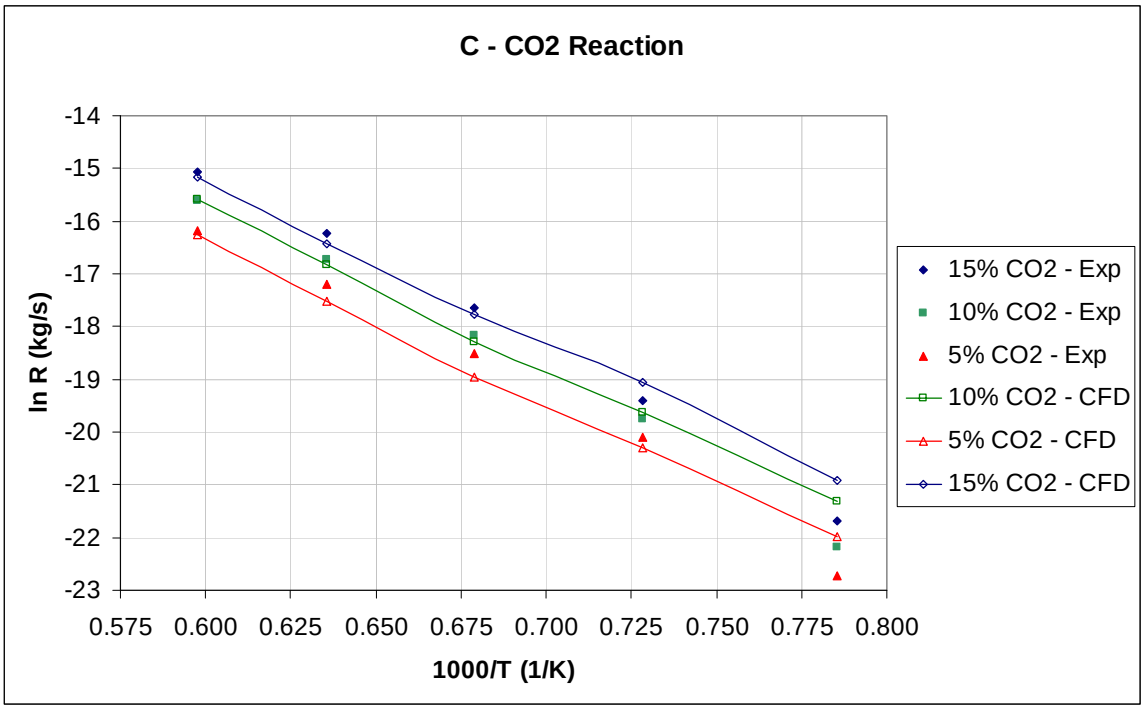

Figure 38: KAIST $C-CO_2$ Reaction - Comparison of CFD and Experimental Results

6.5 Summary

The KAIST experiments were basic oxidation experiments for the primary reaction of $C-O_2$ and the reaction of $C-CO_2$. Results show that it is possible to obtain good comparison between experimental data and CFD simulations. It was found that the basic tests aided in determining the information required for reaction chemistry and their appropriate form for input in Fluent.

The 'Define sr_rate' UDF was explored, and used to automate the input of stoichiometric values and recalculate the pre-exponent factors based on the reacting surface temperature. It was also found that a fine boundary layer is essential on reacting surfaces for source input from the reaction in the mass transfer dominated regime.

CHAPTER 7: NACOK CORROSION EXPERIMENTS AND SIMULATIONS

Through the years, numerous tests were conducted at the NACOK facility for various reasons. The focus of this Chapter is on two of the corrosion tests, both of which are with the open chimney configuration. The discussion in Chapter 5.3 focused on a return duct configuration. The open chimney is a once through flow of gas, representing the normal upward flow of gas through the reactor. The first test was a multiple pebble bed test conducted for PBMR in 2005; the other was with a combination of structural graphite conducted in 2004. These tests, as well as the simulation of the tests, are discussed in detail in this Chapter.

7.1 NACOK 2005 Experiment

PBMR contracted FZJ to conduct an oxidation experiment in 2005. Niessen et al. [62] documented the experimental data for PBMR. In addition to this report the main author, Hans-Ferdinand Niessen [61], visited PBMR in 2009. Some information was sourced from personal communication with the author.

7.1.1 Experimental Configuration

The open chimney experiment represents a double break at the top and bottom of the reactor. The bottom zone was kept at a temperature of 650°C. The reasoning for this temperature was that no significant oxidation would occur below 550°C. The helium temperature in the upper regions of the reactor would generally be around 900°C; the pebbles would be in the range of 950°C in this region. For this experiment the upper region was tested at a temperature of 950°C. Should all the oxygen react with carbon in the lower regions, CO_2 will be produced. The upper bed would experience the Boudouard reaction, with carbon reacting with CO_2 to form CO.

The inlet and exit pipes were of diameter 125mm. The main test section was 300 mm x 300 mm in cross section. The first 3 layers of pebbles were made of ceramic, which is chemically inert. The 60mm ceramic pebbles allowed a distributed flow at entry to the experiment without corrosion occurring in this inlet region. This was followed by layers of graphite fuel matrix pebbles for a height of approximately 1000 mm. These pebbles were a mixture of old Necsa pebbles and old FZJ pebbles. The material properties of A3-3 are used for these pebbles (A3-3 is a grade of fuel matrix graphite). Figure 39 depicts the schematic of the experiment. Above

the graphite pebbles was an open cavity followed by a layer of 10mm ceramic pebbles. This simulated the resistance (created by an actual large column of pebbles as found in the reactor) and throttled the flow. A large open cavity resided over the small pebble region. The experimental channel was changed to a cross section of 200mm x 200mm in cross section. The reduced area segment had a height of 2230mm and was filled with 60mm fuel matrix pebbles. The lower test region was tested at a temperature of approximately 650°C, while the upper region was tested at a temperature of approximately 950°C. The heat sources were from external electric resistance heating elements. Figure 40 is a combined extract from the configuration drawing of the experiment supplied by FZJ; the locations of the gas meters are included on this diagram.

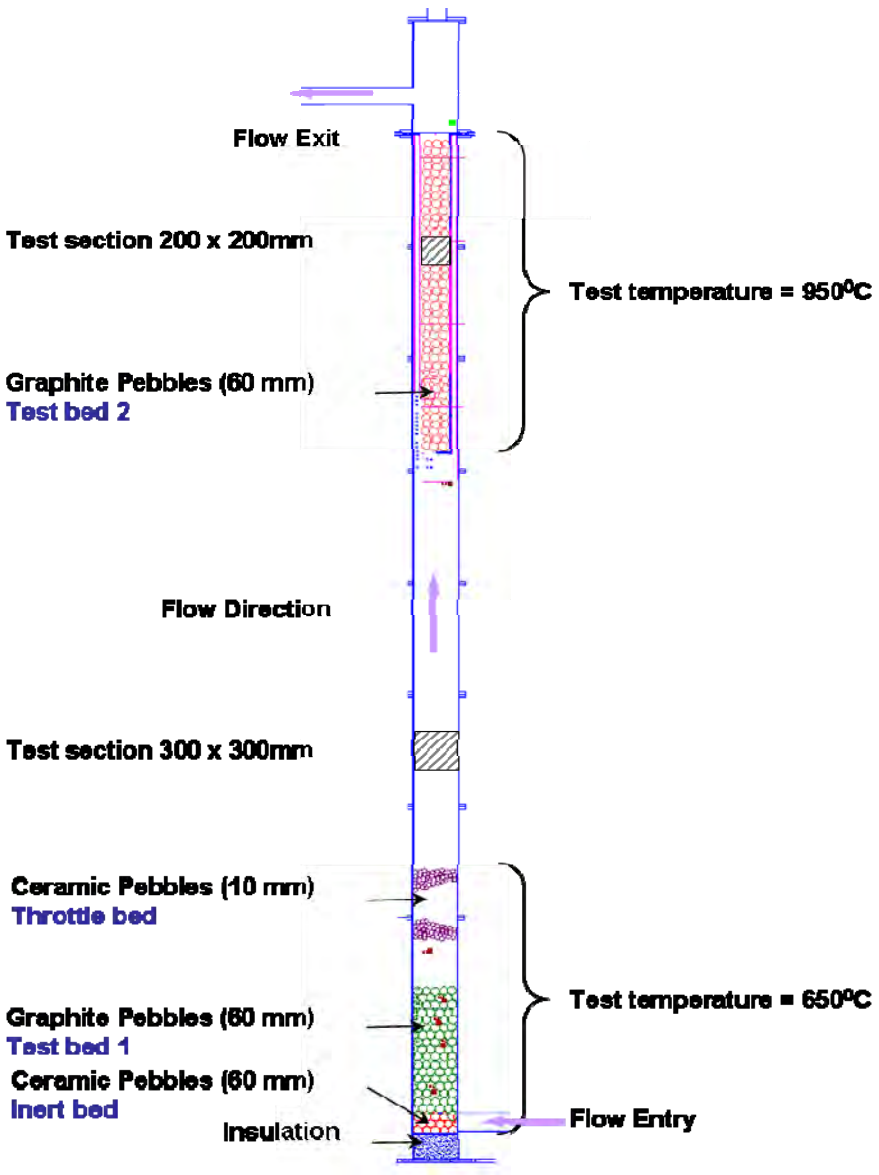

Figure 39: NACOK 2005 – Schematic Diagram

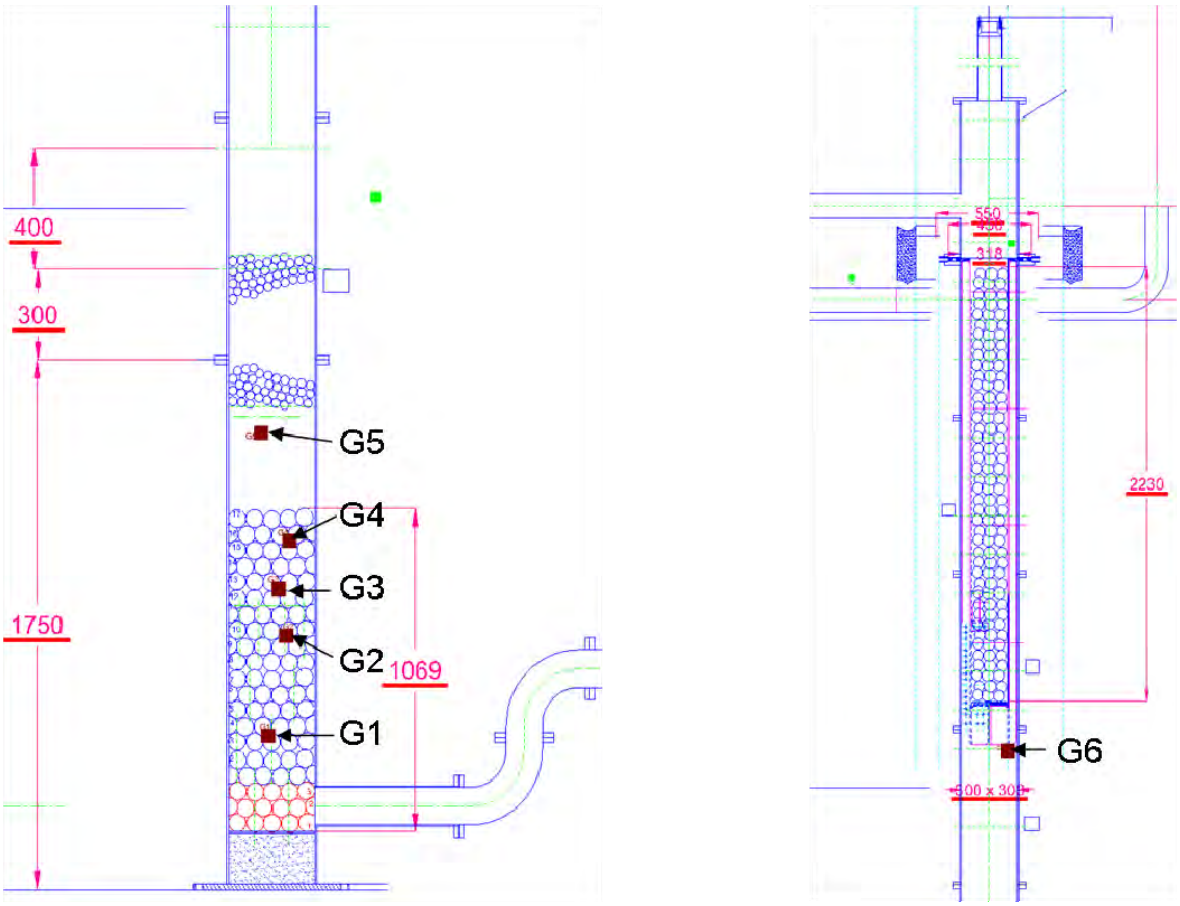

Figure 40: NACOK 2005 - Drawing

During the experiment, logs were taken of the essential parameters such as solid and gas temperatures, gas analysis at various levels, flow rates, etc. For this test a series of sixteen gas and sixteen solid temperatures were recorded. Gas analyses were conducted at eight different locations. Due to the upper bed being assembled in the horizontal position and then moved vertical, only solid temperatures were recorded in this zone.

Multiple tests were conducted, and the weights of samples were taken before and after the total test. Since the CFD simulation would consider only one specific test, the gas analysis data was considered. Gas analysis probes were located at various heights of the experimental channel. Their locations are detailed in Table 6. Note the zero datum was the centre of the inlet pipe.

Table 6: NACOK 2005 – Gas Analysis Locations

Name	Height (mm)	Description of Location
G1	290	3rd layer of spheres in lower graphite bed
G2	650	9th layer of spheres in lower graphite bed
G3	770	11th layer of spheres in lower graphite bed
G4	870	13th layer of spheres in lower graphite bed
G5	1160	Below 10mm ceramic bed
G6	4572	Below upper graphite bed
G7	7115	Above upper graphite bed
G8	n/a	Exit pipe

7.1.2 Experimental Procedure

Pebble fuel and structural graphite are manufactured to very specific tolerances and with due care. Experiments have to be conducted with diligence to ensure that the results are as accurate as possible and with minimal external interference. If the proper bake out procedure is neglected or air is allowed into the system before the configuration is ready for the actual test, premature oxidation would occur and the results will not be accurate.

The experimental procedure that was followed is discussed to place the process in perspective. The duration of this particular test was approximately 10 days. Each pebble was labeled, weighed and placed in position along with the instrumentation. A proper bake out process was followed and this was conducted with an inert gas, in this case nitrogen. The bake out ensured that all the moisture that resided within the structures was removed prior to the test. Moisture would influence the oxidation rate, and in a nuclear reactor under the rupture scenario, the graphite would be in operation and well dried out. The initial heating rate from the experiment log was approximately 1 °C per minute. With this rate it would take several hours to reach the required temperatures.

Once a set value of 300°C was reached a leak test was performed. The facility was refurbished around late 2003. Prior tests found that leakage was a problem and influenced the earlier tests. Once the scientists were satisfied that no leaks occurred on the configuration, heating proceeded to a set value of 550°C. At this temperature a two hour oxidation test was conducted

and this was repeated at 600°C. The main test was at 650°C. Air was allowed into the system. It took a further 3 hours before the upper bed reached 950°C. The total test duration was approximately 9 hours. The results showed a trend towards steady state after approximately 4 hours, and the system was stable till around 8.8 hours from the start of the main test. The criteria for the test duration were to obtain enough corrosion so that it could be measured, yet a low enough corrosion level so that the test specimens were not destroyed due to corrosion.

On completion of the test, the system was cooled. Each pebble was removed individually and weighed after the test.

7.1.3 Experimental Results

A data pack of this test was provided by FZJ in electronic form. The volumetric flow rate of the air entering the experiment was measured. Mass flow rate can be obtained by the use of the air density at the inlet temperature. Once mass flow rate is known, quantity of air in the system can be calculated with Equation (47).

$$Q_{air} = \dot{m} * t \Big/ M_{w,air} \tag{47}$$

In Equation (47) Q_{air} is the moles of air, $\dot{m}$ is the mass flow rate, t is time and $M_{w,air}$ is the molecular weight of air.

The experimental data for gas and solid temperatures are detailed in Figure 41 and Figure 42 which are extracts from the FZJ report [62]. Figure 41 details the measurements from the thermocouples located in the gas stream, the legend details the numbering reference used by FZJ and the height of the measurement location. Similarly, Figure 42 shows temperature measurements within solids. From these plots, it is seen that temperature remained steady from about the 4 hour mark till almost 9 hours. The conditions at the 8 hour mark are selected for use in a steady state CFD analysis.

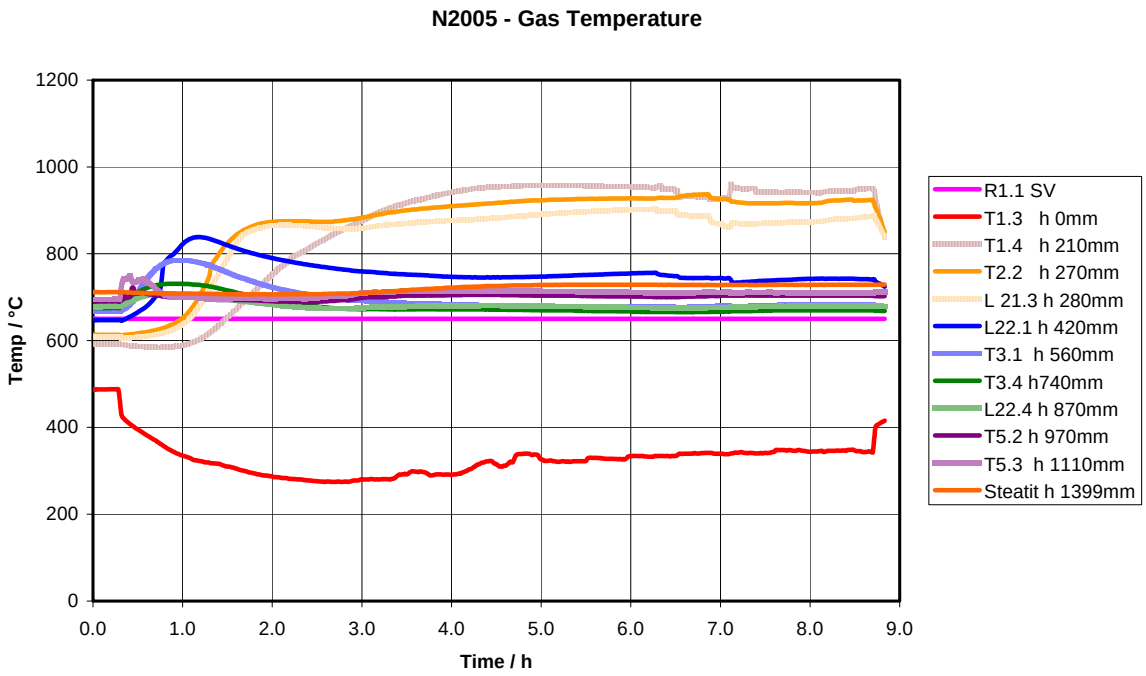

Figure 41: NACOK 2005 – Experimental Gas Temperature versus Time

(Extracted from Niessen et al. [62])

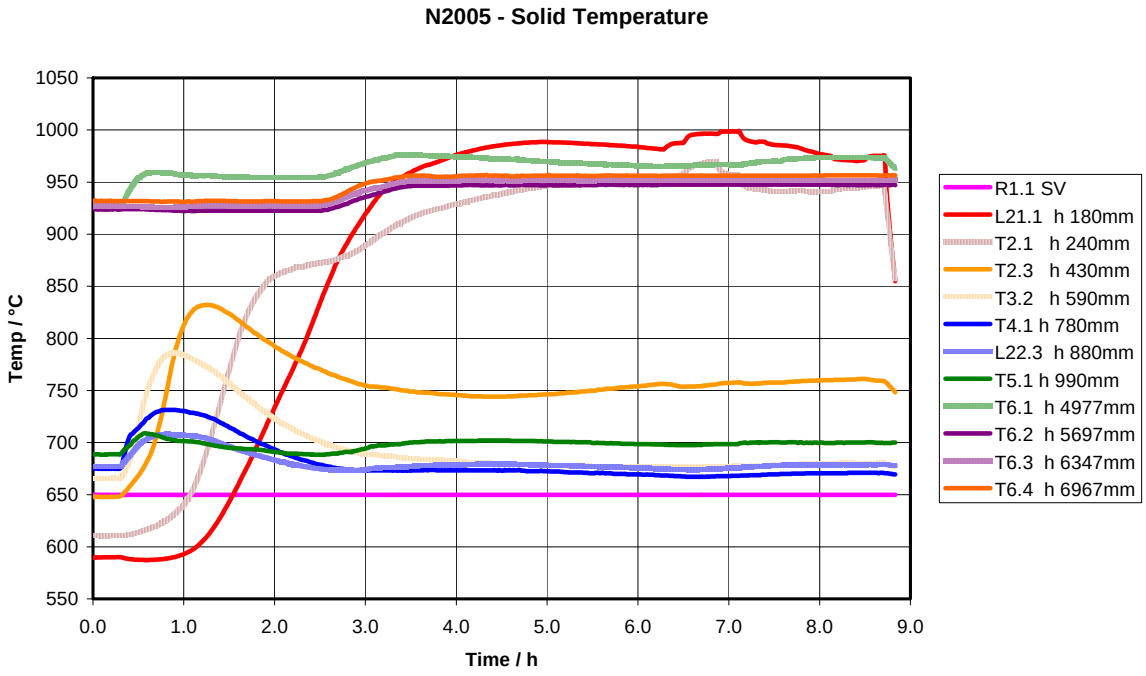

Figure 42: NACOK 2005 – Experimental Solid Temperature versus Time

(Extracted from Niessen et al. [62])

Data was analyzed at the 8.0 hour mark to determine the thermal distribution along the height. It should be noted that the upper pebble bed only had solid temperatures recorded. The solid and gas temperatures are shown in Figure 43. In this figure, temperature was plotted on the X axis and height on the Y axis. The zero location was in the centre of the inlet pipe. It was found that the temperature in the lower bed spikes over the set value of 650°C to over 970°C. This is probably due to the exothermic reaction with an oxygen rich inlet environment.

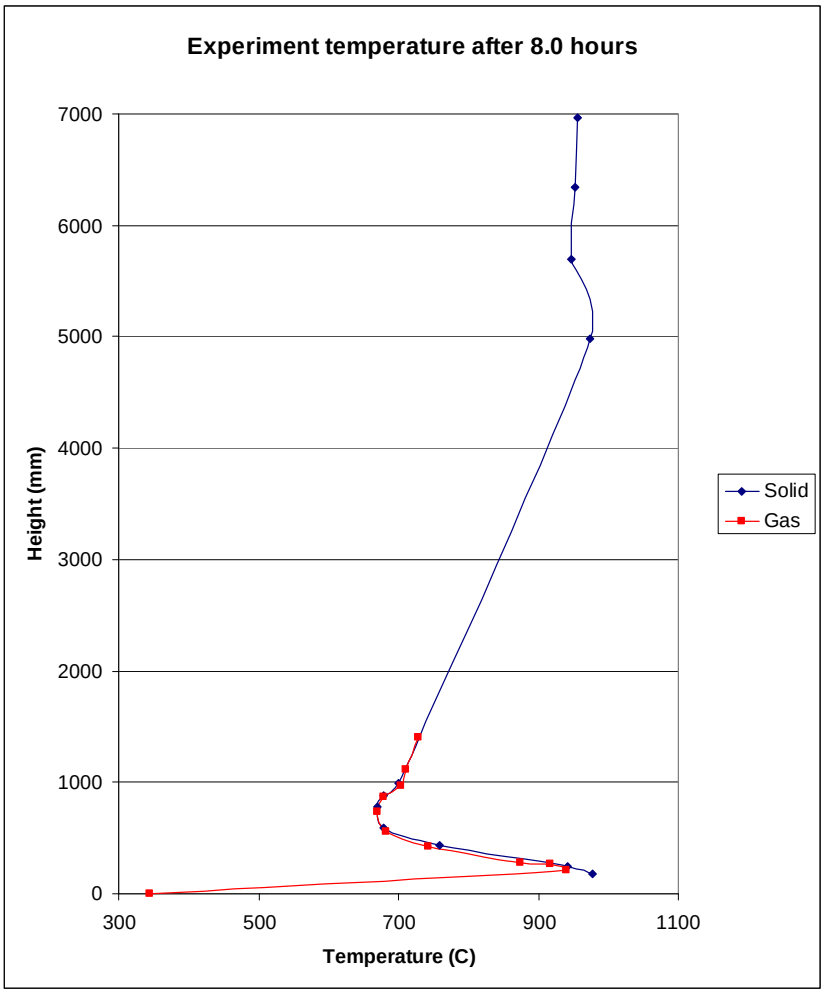

Figure 43: NACOK 2005 - Experimental Temperature After 8.0 Hours

Gas analysis data remained reasonably constant in the time frame preceding the 8.0hour mark; however variations occur at the different heights. Figure 44 details the gas analysis results at the different heights. The X axis is the gas analyzer number and the Y axis is the species mole fraction.

Gas meter - G4 was within the lower graphite bed (see Figure 40), G5 was below the small pebble ceramic bed, G6 was below the upper graphite bed and G7 was above the upper

graphite bed. An interesting trend was found when looking at the concentration data. First consider the oxygen data. At G4 and G5 there was virtually no oxygen, however G6 shows a mole fraction of approximately 5% oxygen. CO was below 1% at G4, it drops to zero at G6 and increases to approximately 1.8% at G7. CO_2 was approximately 21% at G5, it drops to 16% at G6 and up to 20.5% at G7.

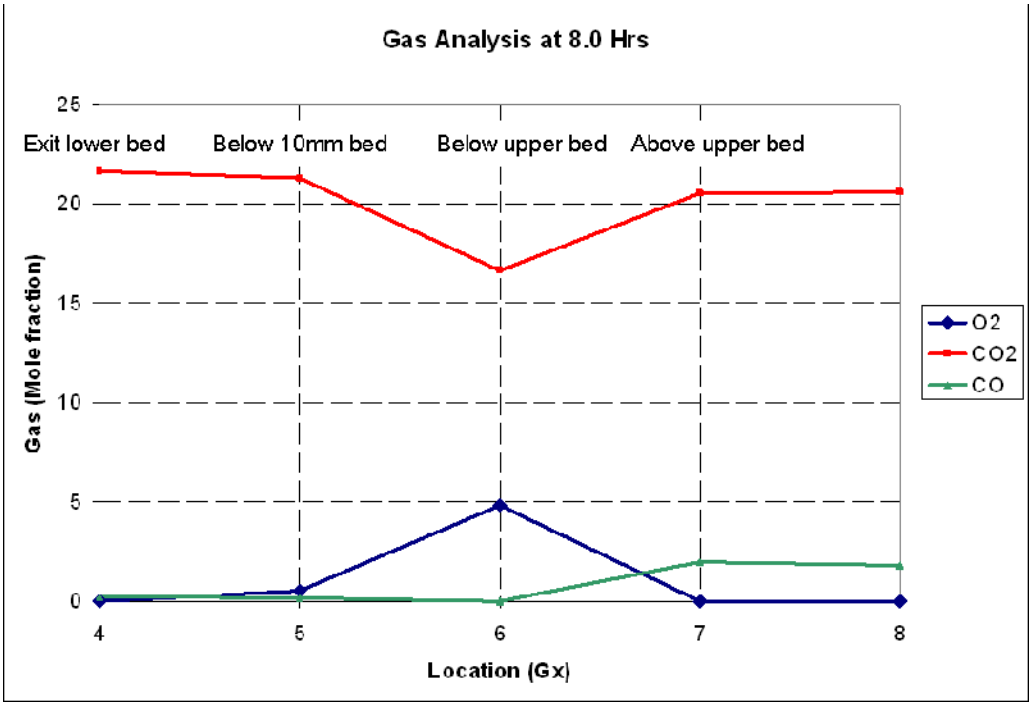

Figure 44: NACOK 2005 – Gas Analysis Data After 8.0 Hours

The report by FZJ confirms that oxygen would have been present on the upper bed, based on visual confirmation of the soot formation on the pebbles after the experiment. Based on this information and the knowledge that gas analysis probes were at set locations within the flow stream, it is possible that probes G4 and G5 which were located towards the centre of the bed did not detect the oxygen. They are not representative of the total oxygen passing the cross sections where the gas measurements were taken. Wall channeling could occur in the lower bed, as well as possible disturbances created by test instrumentation. Flow would be fairly uniformly distributed on exit from the small pebble ceramic bed, due to the high flow resistance and mixing that would occur in the bed (braiding effect). G6 would receive a better mix of flow; however the location of G6 was also not ideal since it resided just below the change in cross section from 300mm x 300mm to 200mm x 200mm in the experimental channel, where flow might have been stagnant or re-circulating. The location of G6 is shown in Figure 40.

In summation of the analysis of the gas data, it can be postulated that possible channeling occurred in the lower bed. This was despite the use of some half pebbles in the experimental configuration. One possible reason for this is wall channeling; the other is that corrosion could have formed a localized channel. A further possibility is interference of instrumentation. Figure 45 shows the matrix of thermocouples inserted in the lower bed.

For the upper bed both the Boudouard reaction and the oxygen reaction needs to be considered. The depletion of CO_2 and the increase in CO, along with no oxygen at G7 (exit from the upper bed), indicates that the Boudouard reaction would also occur in the upper bed. Figure 45 details some pictures (extracted from FZJ report [62]) of the state of pebbles before and after oxidation.

Figure 45: NACOK 2005 – Pebbles Before and After Oxidation

(Sourced from Niessen et al. [62])

From the data pack provided by FZJ it was found that the mass of graphite lost can be calculated by considering the gas analysis data. The quantity of air (Q_{air}) was established for a time interval of one minute as per the logged data. Graphite loss was calculated per minute and the sum for the duration of the test is then taken as detailed in Equation (48). Mole fraction data in this case was from the experimental log data and the molecular weight of carbon is known.

$$Q'_{graphite} = \sum_{time} \left\{ Q_{air} * (X_{CO_2} + 2X_{CO}) / 100 * M_{w,C} \right\} \quad (48)$$

Where $Q'_{graphite}$ is the quantity of graphite lost in kg. Note that the mole fractions were expressed as percentages out of 100 in this equation. Equation (48) can also be used for the CFD approach. The quantity of air can be calculated from the mass flow rate of the simulation, the time period is the duration of the test (this then voids the summation term) and species mole fractions are calculated outputs of the simulation. The modified version of Equation (48) is detailed in Equation (49).

$$Q'_{graphite} = \left(Q_{air-test\_duration} * (X_{CO_2} + 2X_{CO}) / 100 * M_{w,C} \right) \quad (49)$$

From the experimental mass balance, the lower bed consumption was 6.54kg, and the total including the upper bed was 9.77kg. The weight data differed a little from the gas analysis. The lower bed showed a weight loss of 7.48kg, and the upper bed 2.27kg. There was also 0.38kg of dust formed. For the total weight lost the loss in each bed is summed and the dust formation is subtracted. This gives a total weight loss due to corrosion of 9.37kg for this experiment.

7.2 CFD Simulation of NACOK 2005

The simulation of the test involved numerous steps. Each stage is discussed separately to explain how it was accomplished.

7.2.1 Numerical Grid Generation

With this geometry, there were four individual pebble bed regions. It was impractical to simulate each pebble along with its surface area; hence a porous media approach had to be used to simplify the pebble bed. It was found that mass flow rate remained stable for a long duration in the experiment; hence steady state analyses were conducted.

The porous medium approach enables the use of a conformal hexahedral mesh. This allows an economic computational grid, hence lower computational requirements and resources.

Figure 46 details the outline of the computational domain created for this case. The labels are the names used on the different cell zones for the simulation. The approach of a half model with a symmetry plane was used. The symmetry plane cuts through the centre of the inlet and outlet pipes. The final number of computational cells on this case was approximately 50 000 cells after grid sensitivity checks were conducted.

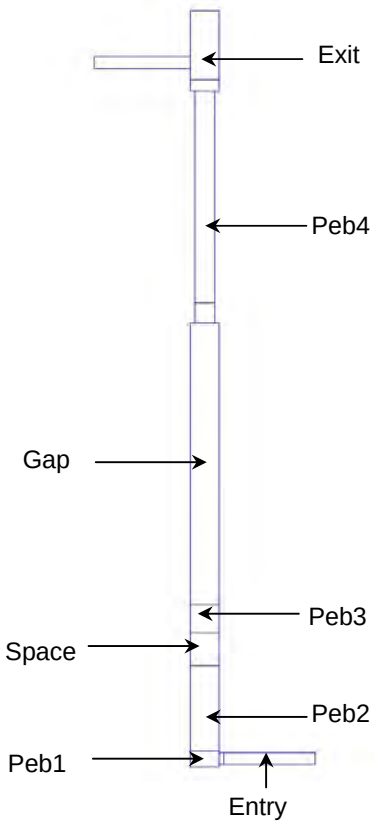

Figure 46: CFD Geometry for NACOK 2005

7.2.2 Model Setup

For the simulation a three dimensional model was created with a symmetry plane. The double precision, pressure based solver with physical velocity in the porous formulation was used.

7.2.3 Inlet and Outlet Boundaries

It is known from measurements that the mass flow rate remained stable for a long duration of the experiment; hence a mass flow rate boundary condition was used at the inlet boundary.

The measuring devices on the experiment consisted of a volumetric flow meter and a mass flow meter. From personal communication with the FZJ scientist [61], it was known that the volumetric flow rate should be used since the instrument measuring the mass flow rate was later found to have large measurement errors. The calculated mass flow rate from the volume flow rate for the test duration was 3.11g/s. With a half symmetry model only half the mass flow rate was applicable. The inlet air temperature was set to 296K or 23°C.

The inlet boundary data required input on the initial species mixture. In an air ingress event, the incoming air would be atmospheric air and would contain moisture; the same applies to the NACOK experiments. For this particular test the air moisture was not documented, hence sensitivity to moisture study was conducted on the lower bed. A psychrometric chart was used to source data for humidity levels of 30% and 90%. At 30% humidity the mass fraction of moisture was 0.5%, and oxygen was 22.5%, while at 90% humidity the moisture content was 1.6% and oxygen was 20.8%. A pressure boundary was used at the outlet of the domain.

7.2.4 Material Properties

Gas species material properties and diffusion coefficients are temperature dependent and were as used in earlier simulations.

For this experiment the solid materials in the porous zones needed to be included in the materials list. Properties of ceramics used for this study are detailed in Annexure C. The graphite thermal conductivity is discussed in more detail in the next section.

7.2.5 Turbulence

For this test the effect of turbulence was neglected. The expected velocities were low, hence so would be the Reynolds numbers. Calculations showed a Reynolds number around 200. Within the porous zones, the effect of the solids were not considered for turbulence, hence only the outer walls provided a frictional resistance. Due to the relatively high flow resistance, the porous zones produced a uniform velocity distribution.

7.2.6 Thermal Conductivity

Ceramic and graphite properties were added to the solid properties for participation in the porous media. The details of ceramic are included in Annexure C. The orthotropic input was used for the thermal conductivity of graphite. This allowed a different conductivity in each Cartesian direction. The axial direction was specified based on a calculation with the Zehner-Schlünder formulation as discussed in the Theory section. The values used in the axial direction on the lower bed are detailed in Table 7. A fixed value of 1.34 W/m.K was used in the radial direction.

Table 7: Effective Axial Thermal Conductivity for Packed Bed

Temperature (K)	Axial Effective Thermal Conductivity (W/m.K)
296	2.99
473	4.13
673	6.52
873	10.13
1073	14.58
1273	19.16

7.2.7 Reactions

As in the KAIST experiments, the default Fluent carbon monoxide air reaction was used as a starting point. The forward reaction is repeated below.

$$CO + \tfrac{1}{2} O_2 \longleftrightarrow CO_2 + 0H_2O \tag{4}$$

This reaction was detailed in the Theory section of this report, and the moisture term considers the concentration of moisture present and takes the form of $K[CO][O_2]^{1/4}[H_2O]^{1/2}$. This moisture component would now become important to the study of oxidation as it quickly converts CO to CO_2 in the presence of O_2. For this simulation Equation (4) was input as 'Reaction-1'.

The reverse equilibrium reaction was inserted into the reaction template by default as 'Reaction-2', but was not used as part of this study.

For the primary reaction of carbon and oxygen, the form expressed in Equation (32) was used once again.

$$C + xO_2 \rightarrow yCO + zCO_2 \tag{32}$$

From the Theory and Literature (works such as that by Nightingale [63] and Moormann [55]) it is known that fuel matrix graphite has different properties to that of the structural graphite. Up to this stage, the oxidation studies all pertained to structural graphite.

For fuel matrix graphite, the correlation from Contescu et al. [10] was used. Data from this paper was digitized and curve fitted. Analysis of the curve fit provided an activation energy of 169.29 kJ/mol and a pre-exponent factor of 15. The order of reaction from Contescu et al. [10] was taken as 1.0. This would be input as activation energy of 1.6929e8 and pre-exponent factor (K_o) of 9.59e6 (at a temperature of 650°C). The data for the stoichiometric values were determined by the correlation devised by Kim and No [41] and detailed in Equation (37). Equation (32) was taken as 'Reaction-3' and 'Reaction-4' for this simulation set. The reason for duplicating this reaction as 'Reaction-3' and 'Reaction-4' was to handle the different approach to surface reactions with porous cell zones and reacting surfaces. This is discussed further in the user defined functions.

It should be noted that the $C-O_2$ reaction is within the in-pore diffusion regime. Based on Figure 28 it is known that the mass transfer regime begins at 1100^0C. For the KAIST study it was found that a fine boundary layer was required to resolve a solution in this regime. The effects of using a porous media and the mass transfer regime are not quantified in this study since the range is out of bounds of the experiment. It is quite possible that another grade of graphite would have a different temperature where the change of slope occurs, meaning that the mass transfer regime temperature may change and the use of porous media in this regime would then require further quantification.

Moormann [57] conducted a series of high temperature experiments with fuel matrix graphite for FZJ and proposed an expression for the Boudouard reaction as shown in Equation (50).

$$R_{CO_2}(mg.cm^{-2}.s^{-1}) = \frac{14.5.\exp\left(-25000/T\right)P_{co_2}}{1+3.4e^{-5}.\exp\left(7000/T\right)\sqrt{P_{co_2}}} \tag{50}$$

With P_{co_2} in Pascal and T in Kelvin.

This is a Hinselwood Langmuir type of format. While being the most appropriate to describe the oxidation process, it is not in a form that can be readily used in the simulation with the chosen chemistry model.

As shown by the equation above it was not that evident how to obtain the activation energy as compared to previous equations used for oxidation. Hence the approach used was as follows. The model was set up with the lower bed reacting and tests were conducted to determine the best correlation. Once this was completed, the mass fraction of CO_2 that would enter the upper bed was obtained from the simulation. This value was used to determine the partial pressure of CO_2.

Microsoft Excel was used to calculate the reaction rate based on Equation (50). The data was converted to SI units and plotted in the form of an Arrhenius curve as shown in Figure 47. The CFD value for mass fraction of CO_2 at location G6 (0.269) was used to calculate the partial pressure of CO_2. This allowed the use of the conventional method for determining the activation energy and the pre-exponent factor. The activation energy used for this simulation was calculated to be 237kJ/mol and a K_o value of 7.012e6, with a temperature and rate exponent of CO_2 being equal to 0.9. This data provided input for 'Reaction-5', which is repeated below.

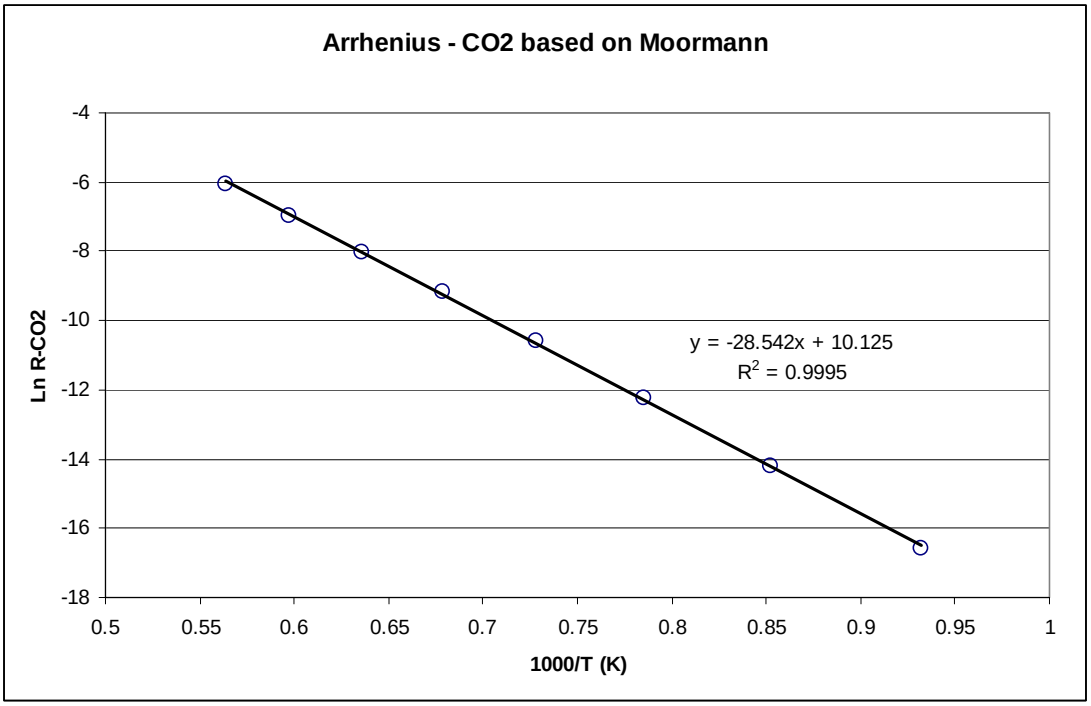

Figure 47: Arrhenius curve for the CO_2 reaction

$$C + CO_2 \longrightarrow 2CO \qquad (5)$$

7.2.8 Mechanism

The reaction mechanisms feature of Fluent allows the user to specify a reaction or group of reactions applicable to a surface or cell zone. For this simulation three mechanisms were specified and are as follows:

Mechanism-1 is the combination of 'Reaction-1' and 'Reaction-3'. This is applicable to porous cell zones with the primary reaction of carbon and oxygen.

Mechanism-2 is the combination of 'Reaction-3' and 'Reaction-5'. This is the mix of the primary carbon oxygen reaction and the Boudouard reaction.

Mechanism 3 is 'Reaction-1' which is the secondary reaction of carbon monoxide and oxygen.

7.2.9 User Defined Function

The UDF originally developed for the KAIST experiment was evolved to include surface reactions within porous cell zones. The UDF is included in Annexure E.

Some of the features of the UDF are discussed. It uses the KAIST ratio of CO/CO_2 as expressed in Equation (37) to calculate the stoichiometric values of Equation (32), based on the surface temperature for face data and cell temperature for porous zones. Concentration data was sourced from the solver. 'Reaction-3' was applicable to porous cell zones with surface reactions and passes cell data to the UDF. 'Reaction-4' was a duplicate reaction but was called when face data was required for a reacting surface. Based on the data passed to the UDF, the appropriate source was returned for the solver. The UDF was also written for use on a parallel solver machine.

7.2.10 Wall Conditions

In this case no reacting walls were present, since all of the reactions occurred in porous cell zones. The walls did require the temperature distribution as controlled by the heaters in the experiment. This was achieved via the define_profile UDF. This appears at the end of Annexure E. Based on the grid coordinate system the region below 84mm was given a temperature of 334°C. The region between 84mm and 900mm form the first reacting bed and this region had a wall temperature of 650°C. The region above 4500mm was set to 950°C. The region between 900mm and 4500mm was given a temperature gradient from 650°C to 950°C.

7.2.11 Cell Zone Conditions

Porous cell zones require input for porosity. As explained in the Theory section, wall channeling in a packed bed has to be accounted for. The viscous and inertial coefficients were calculated with Equations (30) and (31) and were based on the Ergun formulation. The grid was created with a space of one pebble diameter from the wall defined as a separate zone on regions of pebble beds 1 to 3. The average porosity of the cell zones was 0.395.

In previous chapters the simulation of the KAIST experiments used an explicit method when reacting surfaces were considered. In this case when a porous medium is used, the pebbles and hence the surface reactions need to be considered implicitly with a factor for the reacting surface area to the volume ratio.

Within a porous zone, the software requires additional data input to define the available surface area for reactions within a porous media. For this experiment, the number of pebbles per zone was documented. Based on the known number of spheres, the available surface area of the spheres per zone can be calculated. The available surface area per zone is then divided by the volume of the relevant porous zone to obtain the surface to volume ratio. The available surface to volume ratios are kept constant across the porous media.

The solid material of pebble beds one and three are ceramic. The pebble diameter was 60mm for pebble beds one, two and four, while for pebble bed three it was 10mm. Details of the porosity, viscous resistance, inertial resistance, surface to volume ratio and the reaction mechanisms applied to each of the porous zones are documented in Table 8.

Table 8: Porous Zone Input Data

	Porosity (ε)	Viscous Resistance ($1/\alpha$)	Inertial Resistance (ϕ)	Surface to volume ratio	Reaction mechanism
Peb1-Bulk	0.38	291891	659	-	-
Peb1-Wall	0.48	101876	274	-	-
Peb2-Bulk	0.38	291891	659	65	1
Peb2-Wall	0.48	101876	274	65	1
Peb3-Bulk	0.38	10508092	3955	-	-
Peb3-Wall	0.48	3667535	1646	-	-
Peb4	0.395	247462	573	53.25	2

7.2.12 Solution Control

The PISO method was used for pressure-velocity coupling. The discretization method for pressure was specified as body force weighted, to account for buoyancy. The rest of the parameters used the second order upwind scheme. The under relaxation factors needed to be lowered, pressure was set to 0.1, species, body forces and density were set to 0.9, while momentum was set to 0.5 and energy to 0.7. Species and energy were set to a convergence tolerance of 1e-6, and the other parameters to a convergence tolerance of 1e-3. Mole fractions were monitored at multiple locations to ensure solution stability and convergence.

7.2.13 Solution Strategy

Should all of the solution parameters be activated at the same time, the chance of the solution being too stiff and diverging was very possible. Hence a staged approach had to be used. First the flow solver was activated, then energy and species were activated with the exception of moisture. Once the solution settled, moisture was activated; once stable, the heat and mass feedback were switched on.

An approach of solving the lower bed first and then activating the upper bed was used. After this, the Boudouard reaction was included in the upper bed.

7.2.14 CFD Results NACOK 2005

Once a converged solution was obtained the results were analyzed. Figure 48 details the input wall temperature distribution on the left. The image on the right is the temperature of the gas on the symmetry plane.

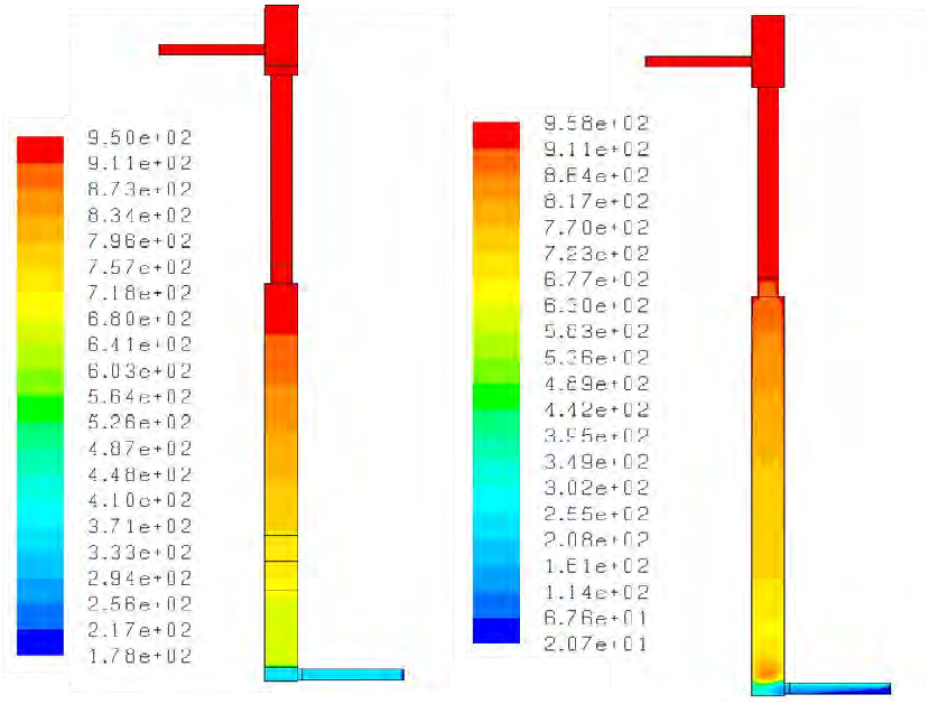

Figure 48: NACOK 2005 – Temperature on Wall and Symmetry Plane

The temperature distribution on the symmetry plane is considered in more detail in Figure 49. The image on the left is the lower bed. The input wall temperature was 650°C.

The feedback from the exothermic reaction raises the temperature to 840°C. This is approximately 100°C less that that found in the experiment in a similar region. The upper bed is at 958°C, which is similar to the experimental values.

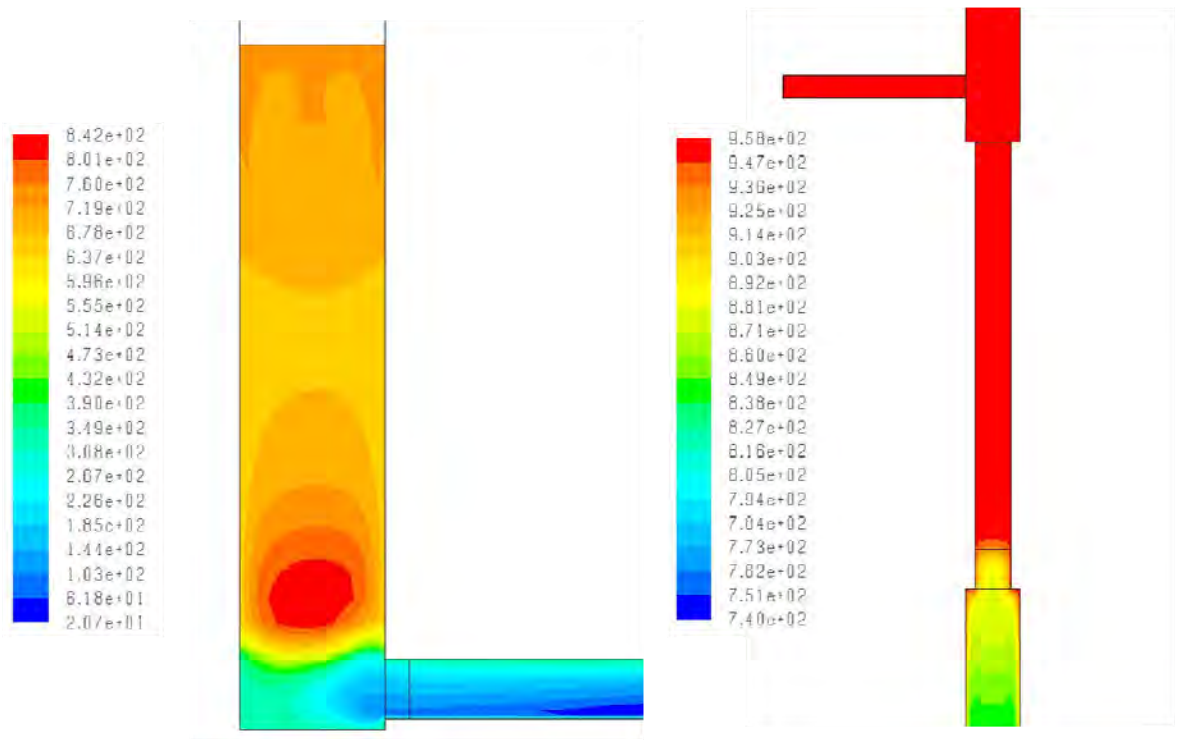

Figure 49: NACOK 2005 – Temperature on Symmetry Plane

Figure 43 showed the experimental temperature on the solids and gases. The data range was modified since the lower bed was of concern. The height was reduced to 1.4m and the CFD gas results from the centre line were included in this plot of temperature versus height as shown in Figure 50. From this figure the variation of the CFD peak temperature and the experimental peak temperature are illustrated. The variation in temperature could possibly be attributed to a host of different factors including, the pre-exponent factor used for the simulation or the surface area to volume ratio.

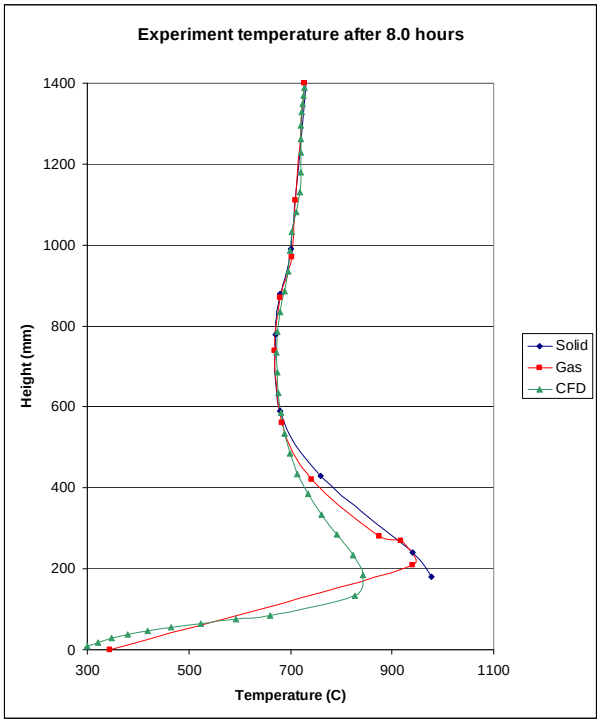

Figure 50: Comparison of Temperature versus Height – Experiment and CFD

The lower bed was simulated with wall channeling; this effect is evident in Figure 51, where higher velocities are seen around the wall. The low velocity region seen above the bed was created in the 'space' region before flow enters the densely packed small bed.

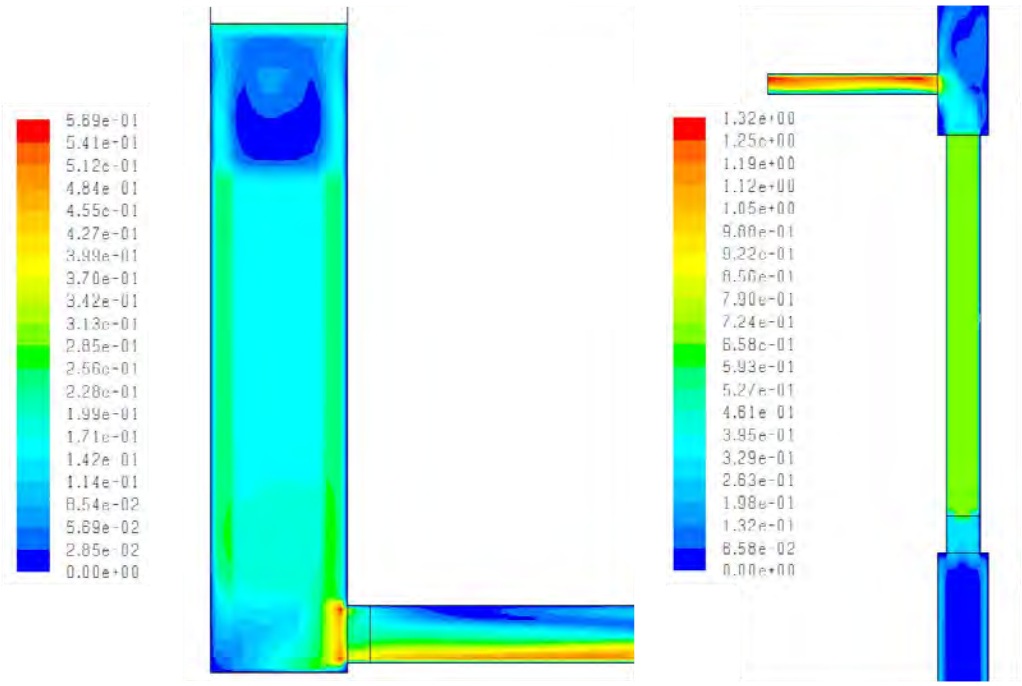

Figure 51: NACOK 2005 – Velocity

The mole fraction of oxygen is detailed in Figure 52. Approximately 2.4% oxygen enters the upper bed.

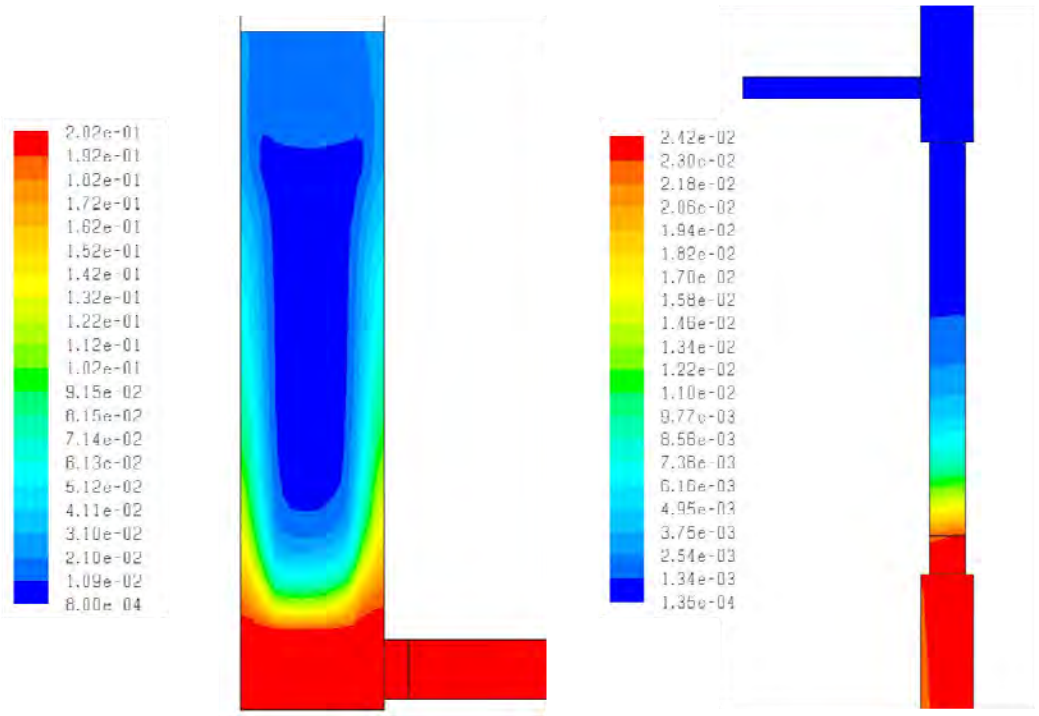

Figure 52: NACOK 2005 – Mole Fraction of O_2

Figure 53 shows the generation of CO_2. The main region of generation is the centre of the lower bed. The plots shown are purely the distribution on the symmetry plane. Since all the oxygen was not consumed in the lower bed, the upper bed has the reaction of $C-O_2$ combined with the $C-CO_2$ reaction. The amount of CO_2 consumed by the Boudouard reaction was relatively low when compared with the generation of CO_2 by the carbon oxygen reaction.

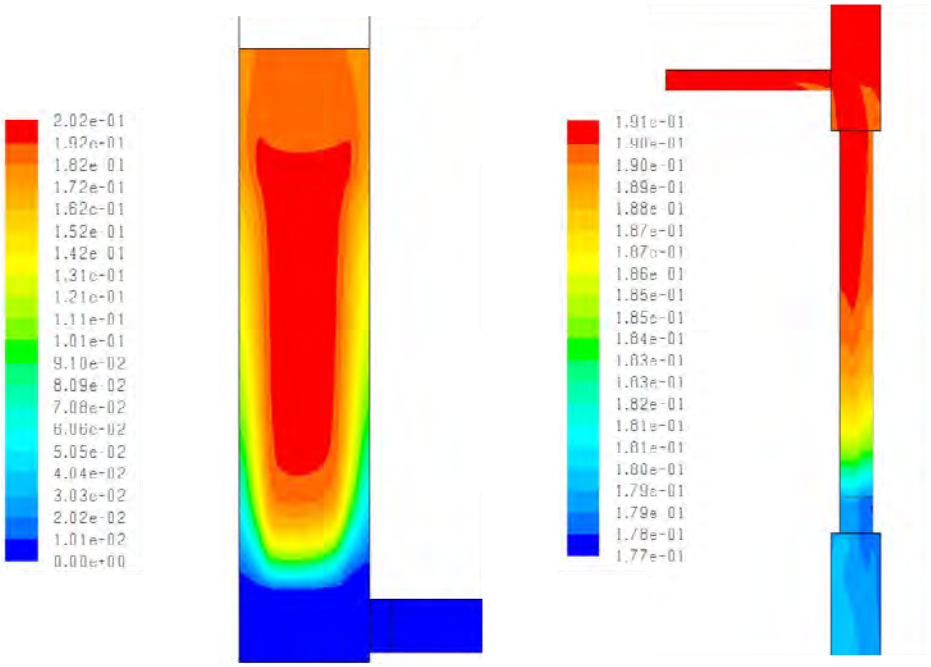

Figure 53: NACOK 2005 – Mole Fraction of CO_2

The generation of CO is shown in Figure 54. The lower bed shows generation of CO close to the outer walls. The upper bed has a combination of the oxygen and CO_2 reaction. If considered in conjunction with Figure 52, it is noticed that the Boudouard reaction occurs, as expected, at approximately the location where the oxygen is depleted.

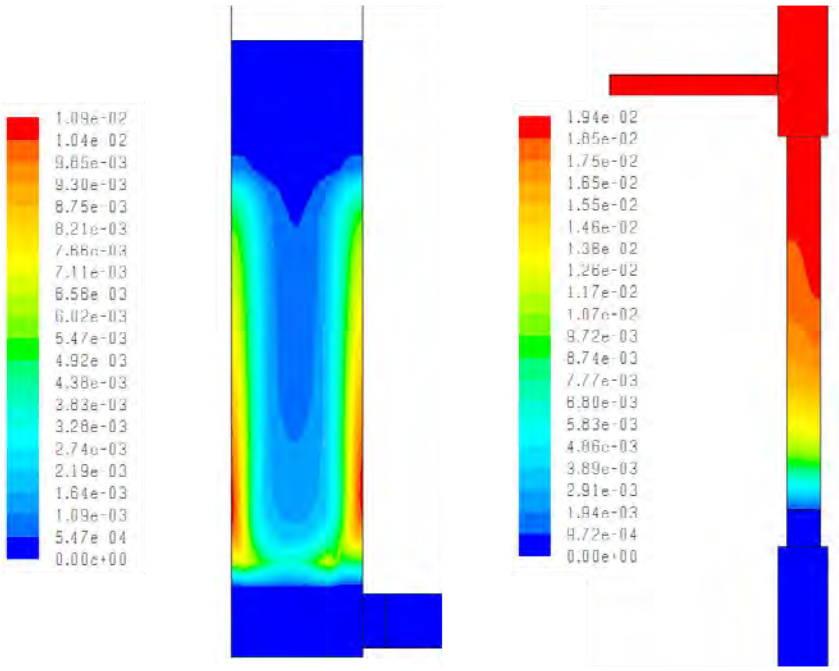

Figure 54: NACOK 2005 – Mole Fraction of CO

For the oxidation calculations, cross sectional planes were created and the area weighted averages across the entire surfaces were considered. The steady state results are in terms of rates, i.e.: quantity per second. Multiplying this with the duration of the test leads to a quantity for a given period of time. The time considered for the CFD simulation is 8.8hours, which is 515minutes or 28 800seconds. The mass flow rate from the CFD simulation needs to be doubled for the mass flow rate calculation. Since a symmetric half model was simulated, only half the mass flow rate was used for the simulation. This gives a total of 3.3137 kmol of air which is comparable to the experimental quantity of air which was 3.3197kmol.

With a 30% humidity, the lower bed shows a graphite loss of 7.065kg. The experimental value for this region was 6.54kg. The Boudouard reaction was included in the upper bed; this produced a total weight loss of 9.100kg or 2.036kg in the upper bed. The experiment showed a total weight loss of 9.77kg. Graphite lost was calculated with a similar approach to that used by FZJ and detailed in Equation (49). Results from the experimental data and the CFD prediction are summarized in Table 9, which represents the graphite lost per zone.

The sensitivity case with 90% humidity produced a weight loss of 6.357kg in the lower bed and a total weight loss of 8.479kg or 2.121kg in the upper bed. The peak temperature on the symmetry plane increased from 958°C to 962°C.

Table 9: NACOK 2005 – Summary of Results

		Lower bed	Upper bed	Total
Experiment Gas analysis	kg	6.54	3.23	9.77
Experiment Mass analysis	kg	7.10	2.27	9.37
CFD 30% humidity	kg	7.07	2.04	9.10
CFD 90% humidity	kg	6.36	2.12	8.48

From the predicted results it can be seen that quantitative results may be obtained. The predictions in the upper bed region at high temperatures are not very accurate yet. The accuracy of the results may improve if better experimental correlations are available. It should also be noted that the simulation was a steady state approximation of a transient event. Hence the initial developments of the oxidation process and the effect that it may have on the various parameters are neglected. As oxidation takes place particles would dislodge from surfaces and possibly accumulate and influence parameters such as the surface area to volume ratios used in a porous medium approach.

7.3 NACOK 2004 Experiment

This test was conducted in 2004 [25]. It consisted of multiple blocks of structural graphite and a small pebble bed. Figure 55 shows a schematic of the experiment, while Figure 56 shows a few photographs of the setup. This experiment was an open chimney configuration with the experimental channel heated to a temperature of 650°C.

7.3.1 Experimental Configuration

The experiment had an inlet pipe of diameter 125mm and the experimental channel had a cross section of 300mm x 300mm. The lowest plenum had four stills each of diameter 50mm. The second plenum chamber consisted of two blocks; each had six holes of diameter 40mm cut out of them. Above this were blocks that represented the reflector of a reactor. They consisted of two blocks each. Each had 48 holes of diameter 16mm. The first set of blocks had a height of 160mm, and the second layer a height of 200mm. The second set of reflector blocks were rotated 90 degrees with respect to the first, hence creating a staggered hole arrangement. Above the second reflector block were layers of pebbles of 60mm diameter for a height of 350mm. This was followed by an open space and then a pebble bed of 10mm pebbles for a height of 600mm.

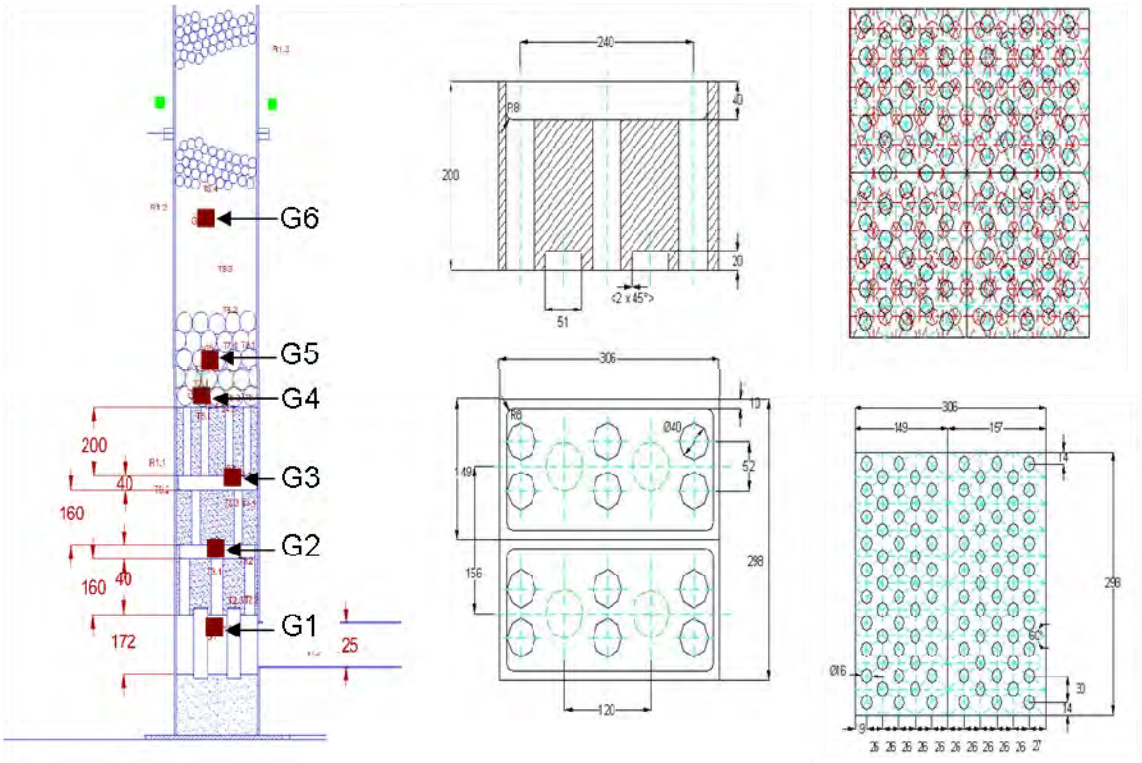

Figure 55: Schematic of NACOK 2004 Experiment

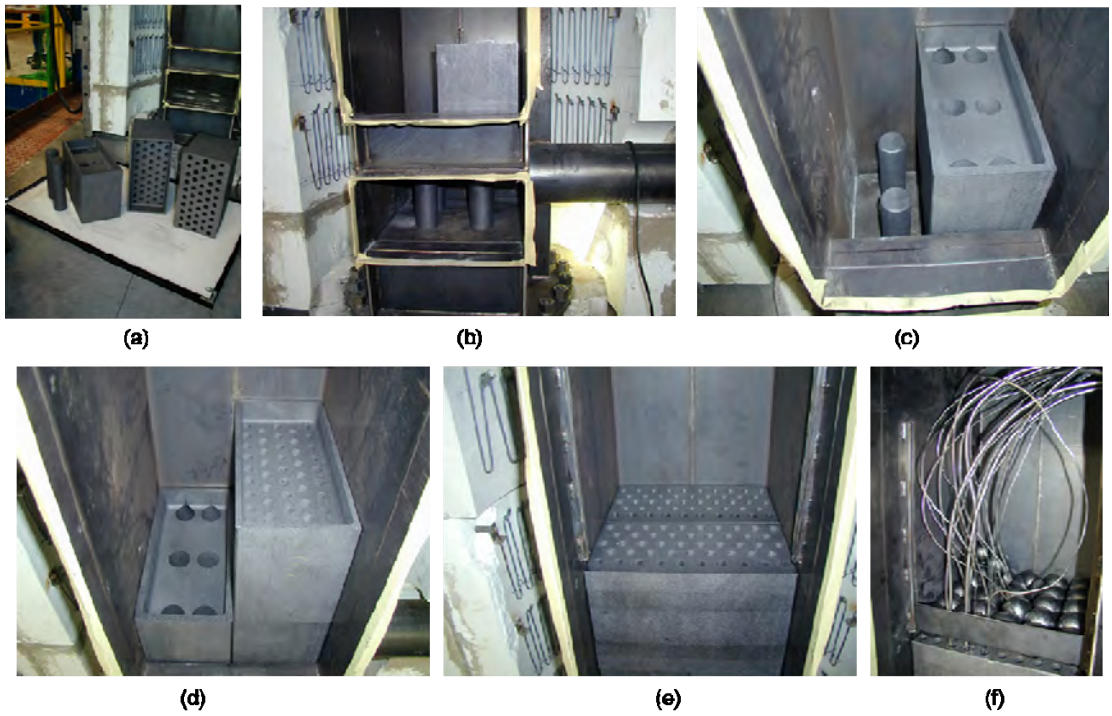

Figure 56: Photograph of NACOK 2004 Experiment

(Sourced from Hinssen et al. [25])

As with the previous experiment there were multiple gas and solid temperature measurements. With the different configuration, the locations of the gas analysis probes were different. The locations are detailed in Table 10. PBMR is in possession of the raw data for this experiment but since it was not conducted specifically for PBMR, a report was not issued. For this reason details such as the pebble composition were unknown.

Table 10: NACOK 2004 – Gas Analysis Locations

Name	Height (mm)	Description of Location
G1	0	In plenum 1
G2	268	Between plenum 2 and reflector 1
G3	468	Between reflector 1 and reflector 2
G4	700	1st layer of pebble bed 1
G5	760	In pebble bed 1
G6	1200	Exit of pebble bed 1 and just before 10mm bed.

7.3.2 Experimental Results

During the experiment the gas and solid temperatures were logged at multiple locations. Figure 57 details the gas temperature, while Figure 58 shows the solid temperatures. It can be seen that temperatures remained fairly stable from the 6th hour (360min) to the 8th hour (480min) range. For the CFD analysis the temperature after 480 minutes was analyzed and plotted as a function of height in Figure 59.

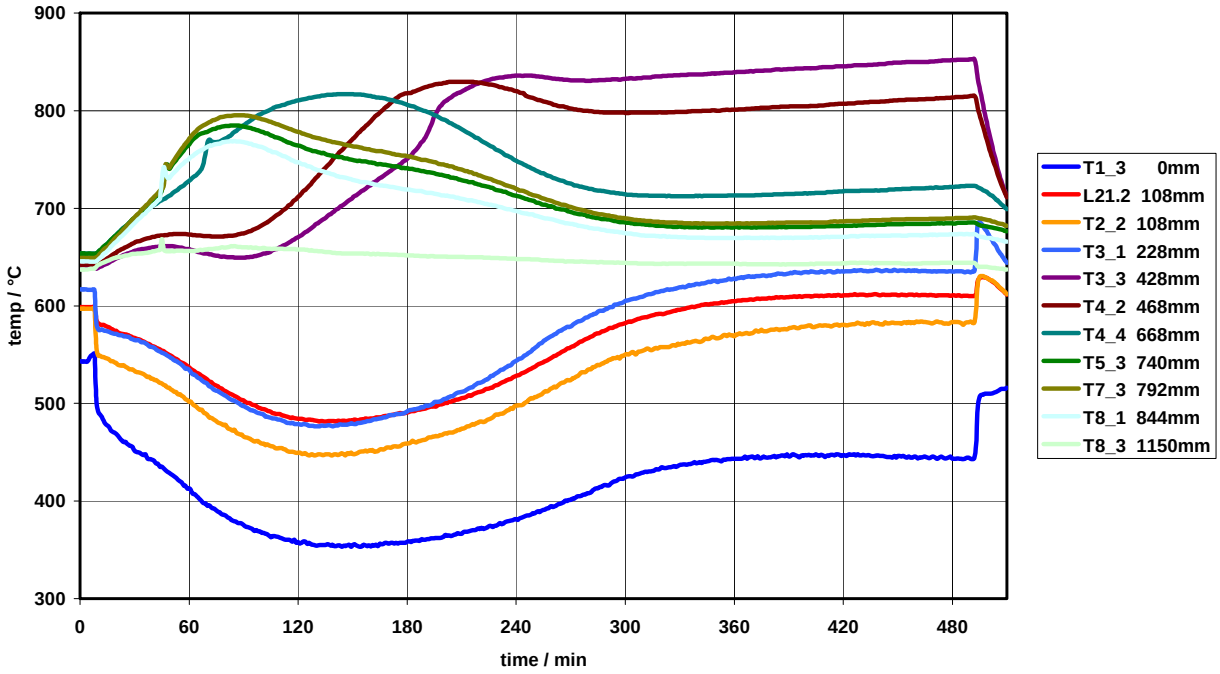

Figure 57: NACOK 2004 – Experiment Gas Temperature versus Time

(Extracted from Hinssen et al. [25])

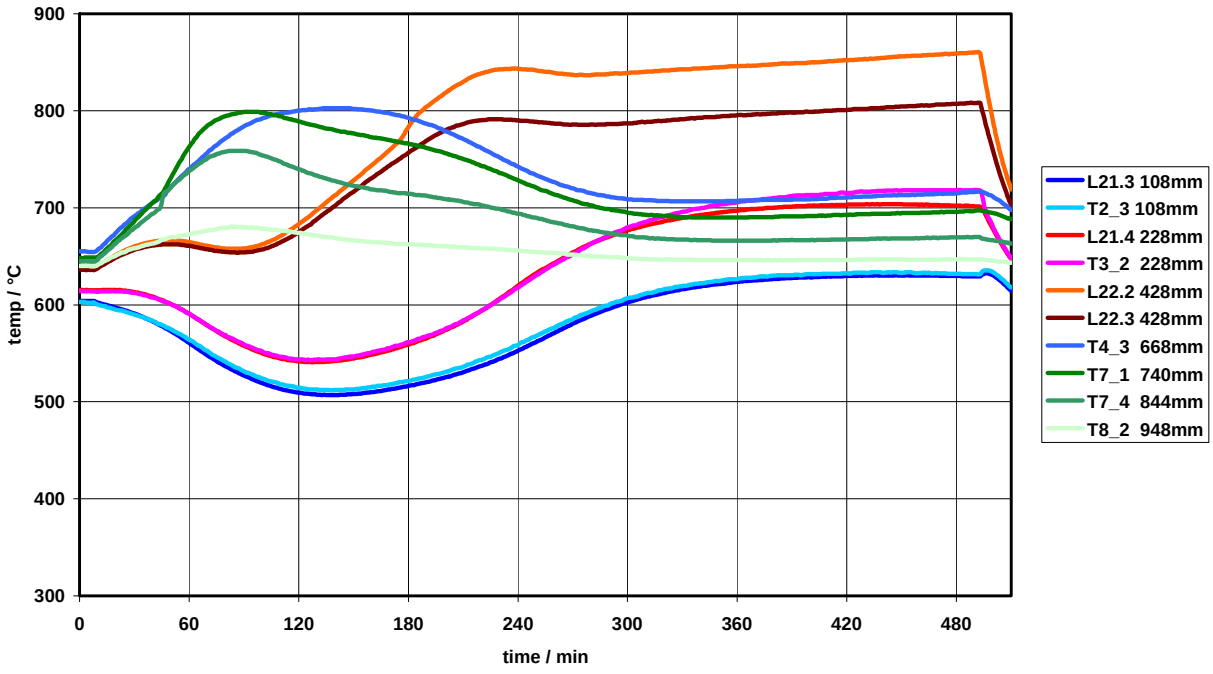

Figure 58: NACOK 2004 – Experiment Solid Temperature versus Time

(Extracted from Hinssen et al. [25])

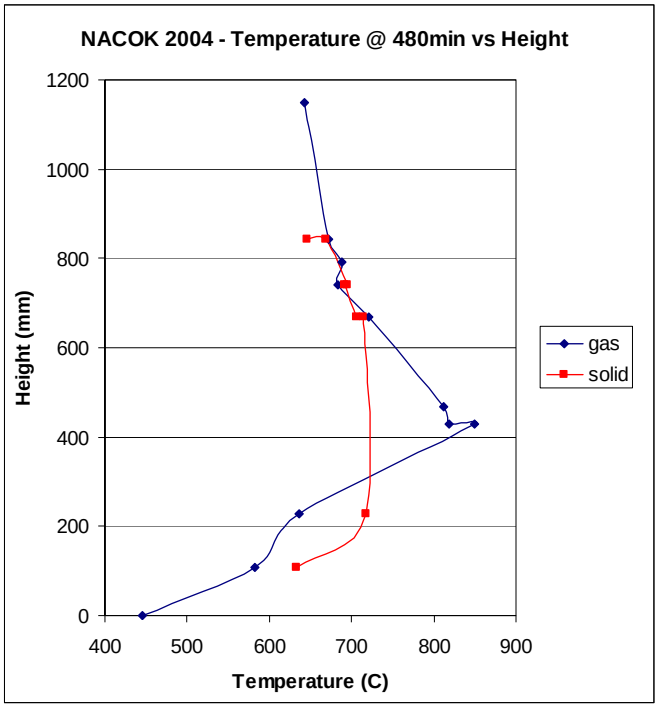

Figure 59: NACOK 2004 – Temperature versus Height

Graphite lost per zone after 8 hours at 650°C is shown in Table 11, and was calculated with Equation (49). The gas analysis data was used for comparison with the CFD simulations. The gas analysis data at G6 is documented as Figure 60. Photographs of the experiment before and after oxidation are shown in Figure 61 and Figure 62.

Table 11: NACOK 2004 – Graphite Loss

Location	**Graphite loss by gas analysis (kg)**
Plenum 1	0.07
Above plenum 2	1.24
Exit reflector 1	4.76
Exit reflector 2	1.30
Exit bed 1	1.40
Total	8.77

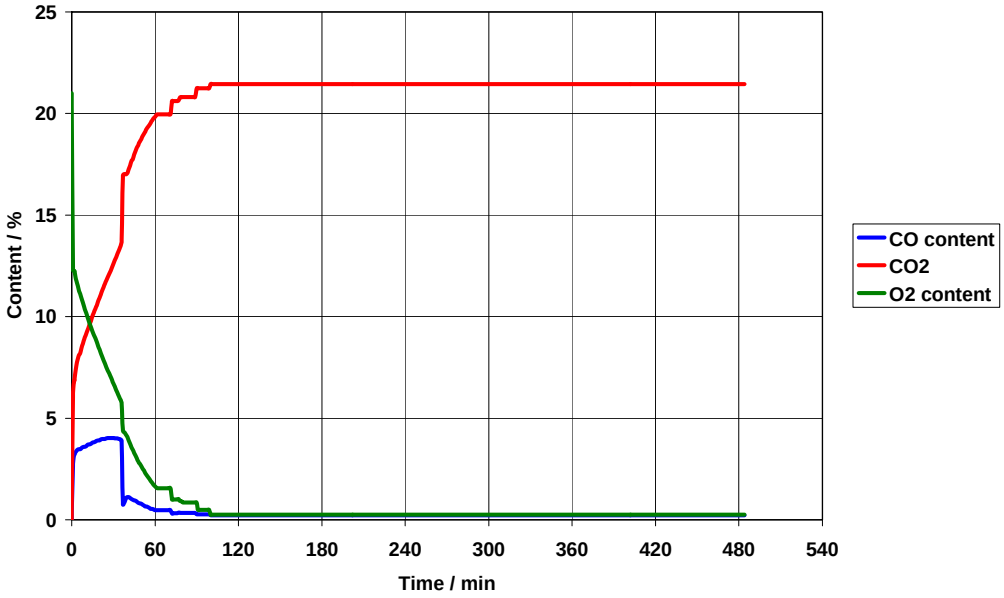

Figure 60: NACOK 2004 – Experiment Gas Analysis

(Extracted from Hinssen et al. [25])

Figure 61: NACOK 2004 – Photographs

(Sourced from Hinssen et al. [25])

Plenum 2 & Reflector 1 Before Oxidation

Plenum 2 After Oxidation

Top of Pebble Bed Before Oxidation

Pebbles After Oxidation

Figure 62: NACOK 2004 – Photographs (2)

(Sourced from Hinssen et al. [25])

7.4 CFD Simulation of NACOK 2004

The simulation of this detail geometry was approached in two stages. The first stage involved the simplification of the detailed reflector blocks to a porous medium, and the second stage included the actual geometry of the detailed blocks. The porous approach includes the implicit treatment of the detailed reflector blocks and reaction chemistry with the lumping of the surface area to volume ratio within the porous medium. The detailed model included surface reactions on the reacting walls. The combination of the two approaches allowed a more efficient manner of testing sensitivities to different oxidation correlations before a large geometry with a detailed computational mesh was simulated and to establish the feasibility of each approach.

7.4.1 Porous Model

For the porous model plenum 1 and 2 were modeled in detail. Reflector blocks 1 and 2 consisted of 96 holes. Each flow path required a proper boundary layer to do justice to the surface modeling approach, and these blocks were simplified and simulated as porous media in

the first approach. The overall computational mesh for this study was approximately 152 000 cells.

One of the limitations of the approach was that pressure drop data across the reflector blocks was not available. To ascertain the pressure drop across the reflector blocks, a sub study was conducted using CFD. The geometry was modeled in detail with the reflector blocks. Computational grid sensitivities were conducted with adaptive grid methods around the reflector blocks. The pressure gradient was considered, this was used to mark cells with high pressure gradients and conduct localized adaptive grid refinement, until the pressure drop did not change due to computational mesh changes. Inlet velocities were varied from 0.2m/s to 2.5m/s. The high inlet velocity was taken since the approach velocity across the sectional area of the experimental channel would be much lower. Calculations of the Reynolds number in the experimental channel were well within the laminar region and ranged from 29 to 363. The inlet section has a Reynolds number up to 3000. This could be in the transitional range from laminar to turbulent flow. For this portion of the study, the approach velocity to the detailed reflector is essential. With this flow being well within the laminar range, turbulence is neglected in the characterization study

Results of pressure were analyzed across the blocks. A polynomial curve was fitted through the range of data and this was used to calculate the inertial and viscous resistance factors through the reflector blocks.

Figure 63 details the approach velocity in the test channel cross section versus the pressure drop across the detailed reflector blocks. The blocks were of different heights, hence the slight difference in results. The hollow points are CFD results from the simulations with the detailed reflector blocks, while the solid lines are the results from the porous media simulation with the curve fitted resistances. In excess of seventy simulations were conducted to characterize the reflector block and generate these curves.

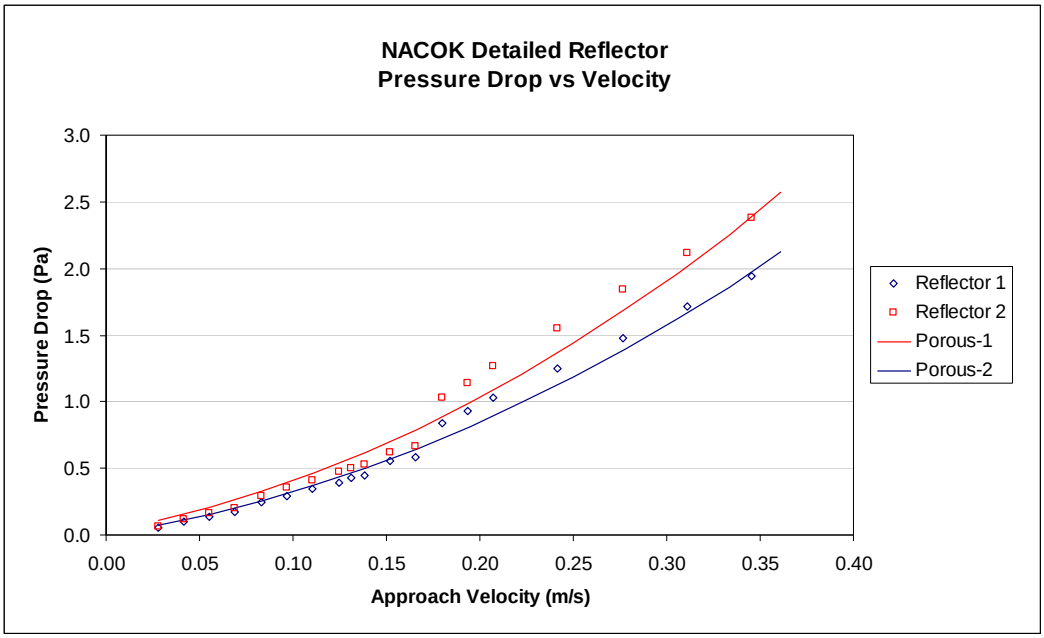

Figure 63: NACOK 2004 – Pressure Drop across Detailed Reflector Blocks

For the oxidation model the works of Roes [71] and Fuller and Okoh [19] were selected as correlations. The work conducted by Roes was on the NACOK facility, and some correlations included flow effects. Burn-off of graphite will have to be included in the oxidation correlation.

Fuller conducted work with burn-off. However, the grade of graphite was IG-110 which is not the same as the German graphite used in NACOK. The work of Fuller and Okoh [19] detailed a pre-exponent factor of 538 and activation energy of 188kJ/mol. The Roes [71] activation energy was 194.88kJ/mol. Conversion on the pre-exponent factor from the report gave a value of 236. The equation was populated with data for the maximum oxygen concentration and the pre-exponent factor (K) varied vastly to 5382891. This changes the K_o factor from 1.51e8 to 3.44e12. With this large variation, some sensitivity analysis needed to be conducted to determine the influence of this change.

The pebbles were assumed to be graphite pebbles and not fuel matrix pebbles. The mass flow rate inlet boundary was used with a specification of 1.7066 g/s for the model. This was half the actual flow rate since a half symmetry model was simulated. Wall temperatures were specified as per the experiment. Input temperatures were from the 8.0hour point in the experiment. The same time was taken as the test duration. For this time, the quantity of air entering the experiment was 8.3897 kmol from the CFD simulation, which compares favorably with the 8.390 kmol of air measured during the experiment. The simulation included the formulation as in the

previous simulations for diffusivity, material properties, convergence criteria and updated monitors for solution stability.

7.4.2 Results Porous Model

The results from the various simulations are summarized in Table 12. The results consider the graphite loss per zone and the overall graphite loss, percentage difference of the overall graphite loss compared to the experiment, along with the maximum gas temperature and exit species mole fraction.

Table 12: NACOK 2004 – Summary of Results (Porous Models)

		Experimental	**Fuller & Okoh**	**Roes K =236**	**Roes K =768**	**Roes K =1300**	**Roes K =5e6**
Plenum 1	kg	0.07	0.14	0.03	*0.06*	0.14	1.16
Above plenum 2	kg	1.24	4.53	2.32	*1.48*	4.53	5.94
Exit reflector 1	kg	4.76	2.84	3.99	*5.23*	2.84	1.12
Exit reflector 2	kg	1.30	0.82	1.29	*1.35*	0.85	0.34
Exit bed 1	kg	1.40	0.02	0.02	*0.29*	0.06	0.0
Total	kg	8.77	8.42	7.72	*8.42*	8.54	8.77
% variation to experiment	%	n/a	3.98	11.98	*4.03*	2.58	2.28
Max Temperature (Gas)	°C	850	882	922	*913*	882	843
X_{CO_2} - Exit bed 1		21.8	20.1	18.6	*20.1*	20.3	20.5
X_{CO} - Exit bed 1		0.17	0.28	0.20	*0.32*	0.35	0.27
X_{O_2} - Exit bed 1		0.00	0.45	2.04	*0.51*	0.84	0.06

Initially the Fuller and Okoh correlations and the Roes correlations with K at 236, 1300 and 5e6 were tested. Neither of the oxidation correlations were able to predict the correct regions of oxidation accurately when compared with the experimental data. The results obtained using the Fuller and Okoh correlation were similar to the results obtained using Roes correlation at

K=1300. The results obtained using the Roes correlation with K=236 showed a better comparison with the experimental results in the reflector region. However, the predicted total amount of graphite consumed was too low, the predicted peak temperature is too high and the predicted mole fractions (to show the overall consumption ratio) do not compare well with the experimental results. Notable in the predicted gas analysis was that the CO_2 levels were too low and there was still oxygen present in the exit stream meaning incomplete oxidation.

The results of the simulation using the Roes correlation with K=5e6 produced too much oxidation in the lower region of the geometry, and no oxidation in the upper bed. In light of the results it was decided to create a point between the K values of 1300 and 236, namely K=768. These predicted results compared better with the experimental results with the exception of the pebble region. The results illustrated that the correct oxidation may be obtained in the various regions if more accurate experimental data was available. Using lower pre-exponent factors would slow the reaction in the second plenum and allow oxygen to travel further up the geometry. This will increase the reaction in the pebble bed region. Even though the simulation was not accurate enough, the correct trend of regions with maximum oxidation was achieved.

The most promising result still requires further development in the pebble bed region. However, in light of the knowledge that the proper kinetic data for oxidation was not available nor was the proper grade of graphite known, it can be said that the results were reasonable and may be improved upon should better experimental data of the oxidation kinetics be available.

A possible area that can be investigated for further development is the splitting of the user defined function in Fluent to accommodate different activation energies based on the reaction that is being called. At the moment the activation energy is defined at the beginning of the user defined function in Fluent and the same activation energy applies to all reactions. It is known that the activation energies of the fuel matrix and structural graphite differ. For this study, it was assumed that the pebbles were of the same material as the structure due to lack of further information.

The lumped surface to volume ratio in a porous medium employed in this investigation is a limitation. The reactions on, and the deformation of the individual surfaces were therefore not modeled. In the actual experiment, the crumbled pieces would obstruct the flow path and as graphite is eroded away, the shape of the reflector blocks would change along with the reacting surface.

It can be concluded that if the appropriate correlation data can be obtained from experimental data, the process could be simulated satisfactorily with a porous medium approach. The user coding developed as part of this study, would require further work to be applied to surface and porous reactions with different grades of graphite.

7.4.3 Detailed Reflector Model

To quantify the porous medium approach and the surface reaction approach, the appropriate Roes correlation was used in a detailed CFD model of the reflector.

A computational grid was generated in Gambit and was approximately 2.2 million tetrahedral and hexahedral cells. The tetrahedral cells were converted to polyhedral cells. This reduced the overall cell count to approximately 1.4 million cells. The complete domain is detailed in Figure 64. The zoomed region shows the detail around the plenum and reflector geometry, along with labels corresponding to the naming used for this simulation.

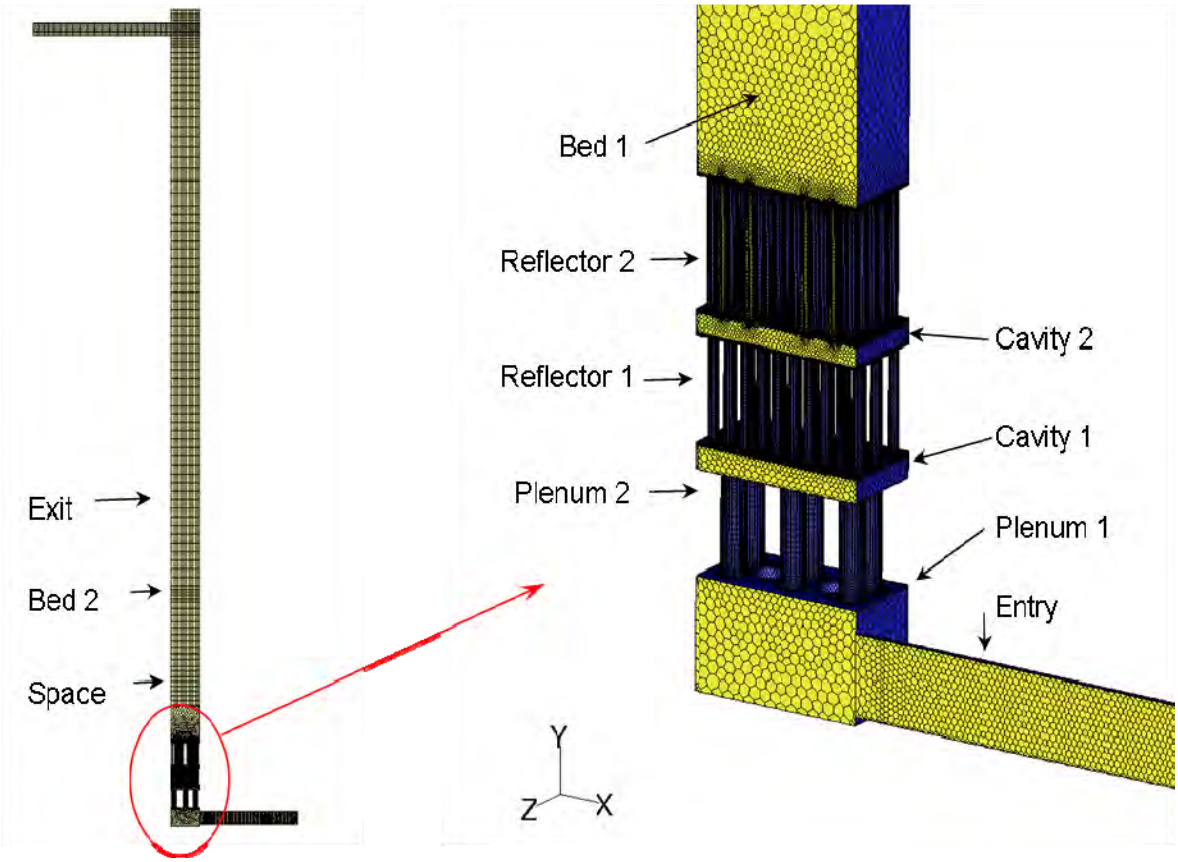

Figure 64: NACOK 2004 – Detailed Model

The geometry of plenums one and two are shown by Figure 65 and Figure 66 respectively. The zoom shows the detailed boundary layers in plenum 1. Plenum 2 was meshed with a fine grid density to capture as much detail as possible and allow a fine boundary layer for surface reactions. The reflectors shown in Figure 67 also included fine boundary layer cells as required for surface reactions.

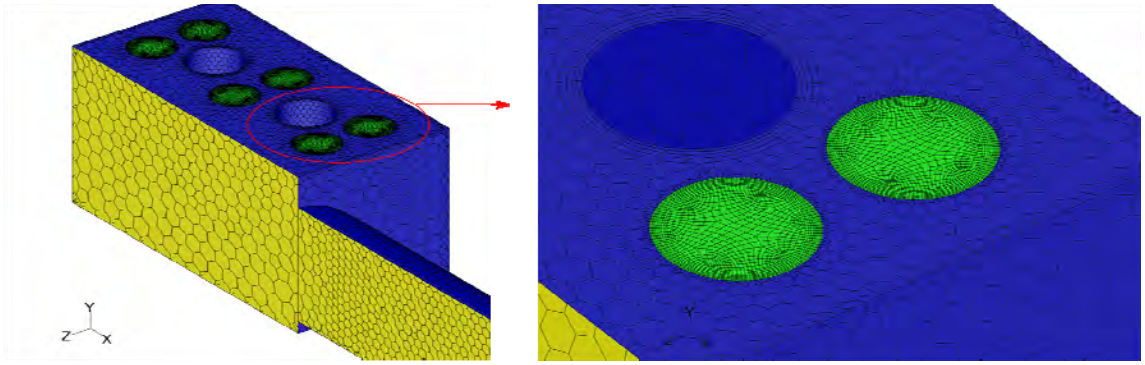

Figure 65: NACOK 2004 – Plenum 1

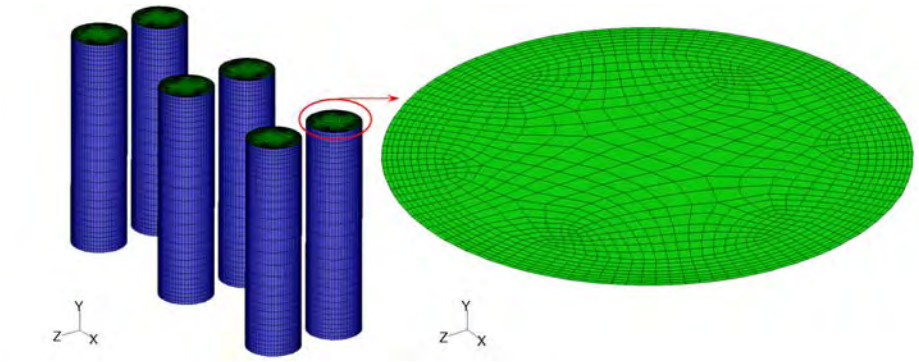

Figure 66: NACOK 2004 – Plenum 2

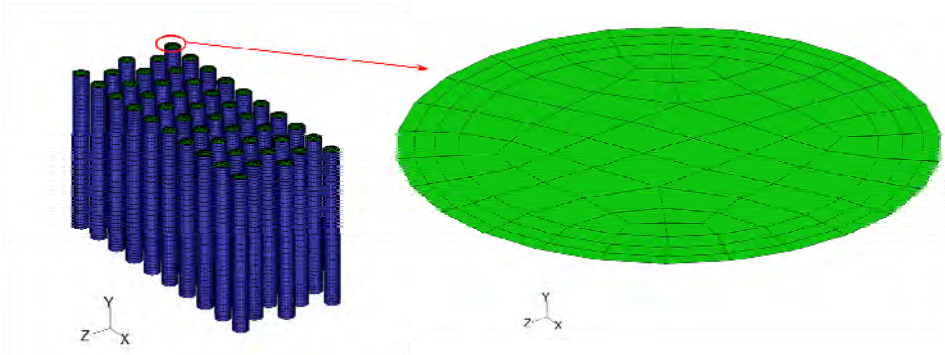

Figure 67: NACOK 2004 – Reflectors

Figure 68 shows the cavity regions surrounding the reflector blocks. The upper and lower surfaces included chemical reactions and were modeled with boundary layers and size functions to enable smooth transition between different cell sizes.

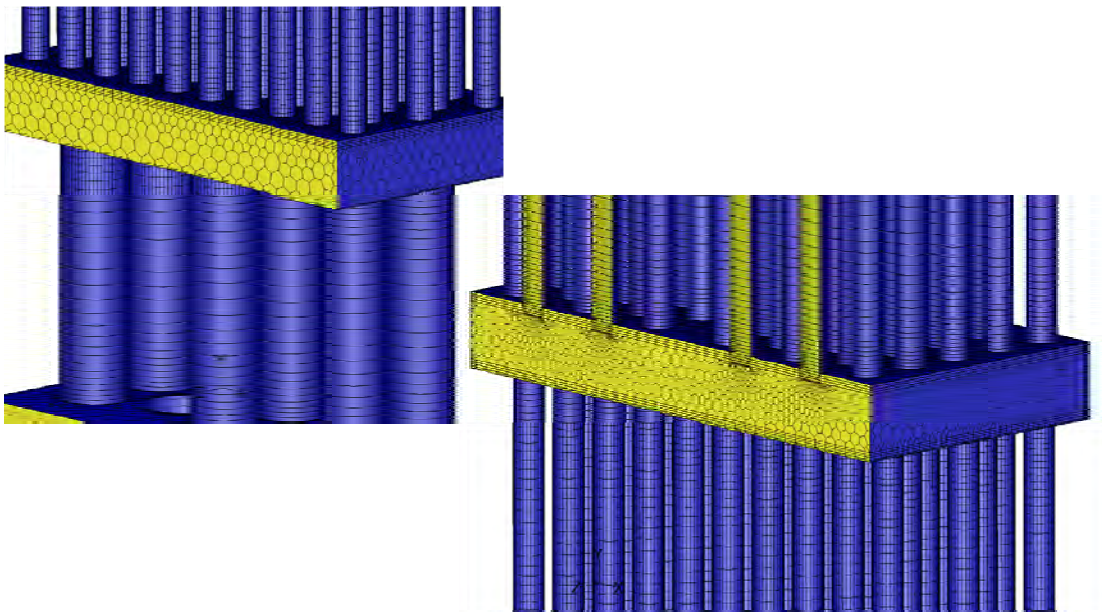

Figure 68: NACOK 2004 – Transition Zones

Figure 69 shows more detail of the size function and cell growth at the exit from the second reflector.

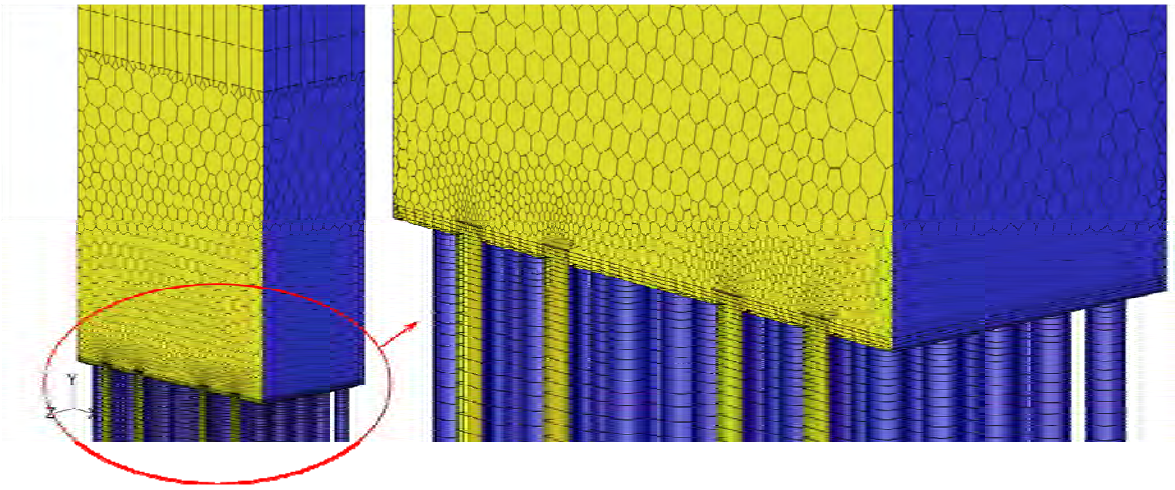

Figure 69: NACOK 2004 – Transition with Size Functions

The setup of this case was similar to the porous model. Earlier calculations of the Reynolds number showed that flow would possible be in the transition region of laminar and turbulent flow on the inlet channel with a Reynolds number in the range of 3000. It is expected that the

geometry would impart some swirl to the flow as it changes direction to enter the experimental channel. Swirl would possibly redistribute the oxygen concentration in the flower geometry. For this reason it was decided to include a flow turbulence model. The renormalized group (RNG) k-epsilon model was selected with enhanced wall treatment. The Fluent manual [17] recommends this model with enhanced wall treatment for applications with low Reynolds numbers, swirl and buoyancy effects all of which are present in the study considered. The effects of different turbulence models were not quantified in this study as it was beyond the scope of the study.

The boundary of this case stipulated an inlet mole fraction of oxygen of 20.9% and moisture of 0.9%. The best oxidation of the porous model was used for the oxidation parameters, which was the Roes correlation with K equal to 768.

7.4.4 Results Detailed Model

The wall temperature profile provided the input boundary data and was sourced from the experimental data. Plenum one was simulated with a temperature of 500°C. The regions of plenum 2 till the exit of reflector 2 were simulated with a wall temperature of 720°C, while the rest of the domain was at 650°C. The inlet had most of the wall set as an adiabatic wall. Hence the temperature gradient is seen on the inlet wall of Figure 70. The image on the right of Figure 70 is the temperature profile of the gas on the symmetry plane. From this image, it is seen that the maximum temperature appears in cavity 1 and is 830°C. The experimental peak temperature was approximately 850°C.

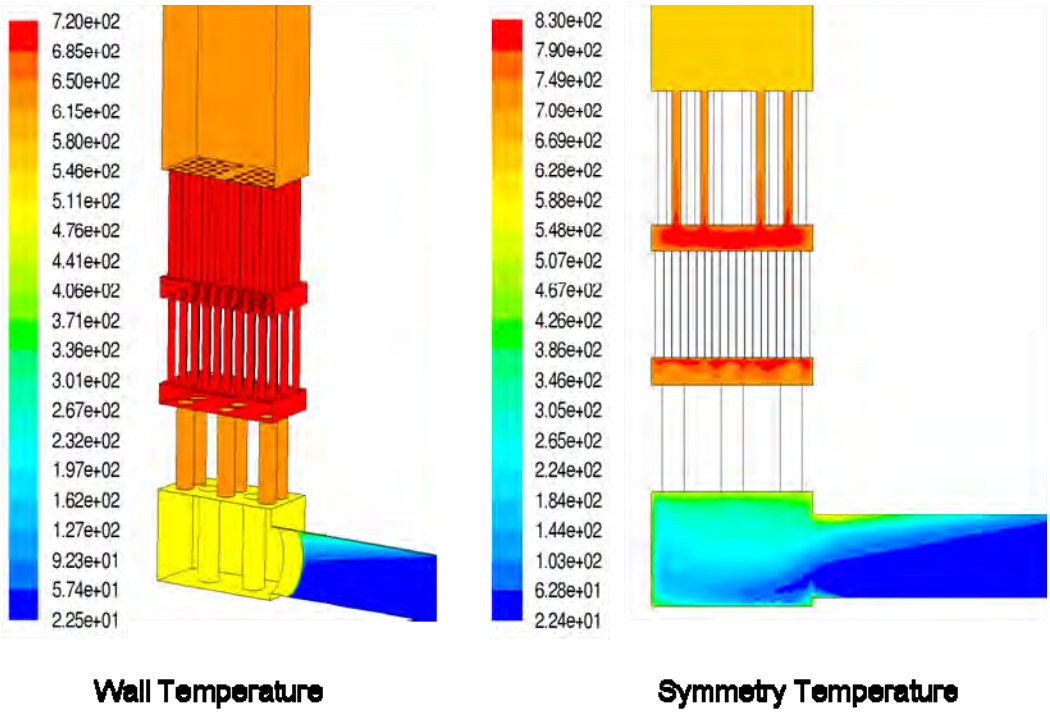

Figure 70: NACOK 2004 – Temperature

Further investigations were conducted to find the source of the high temperature. Sectional plots were taken through the domain, at locations that cut both the reflector geometries and plenum 2. These locations correspond to a Z coordinate of -0.075m and -0.105m. The temperature distributions through these sections are shown in Figure 71. The images in the centre are zoomed locations where the peak temperatures were located. The peak temperatures were found within reflector 1, in the fine reflector holes. The maximum temperature shown by the simulation was approximately 970°C. The peak temperature shown by the experiment was 850°C. It has to be remembered that experimental readings are singular point measurements. Figure 70 shows an average of 870°C in an equivalent region to where the temperature probe would be located. However, the temperature does range from approximately 850°C to 890°C in this region. Based on this, it is quite possible that the peak temperatures within reflector 1 are true and were not captured by the experiment.

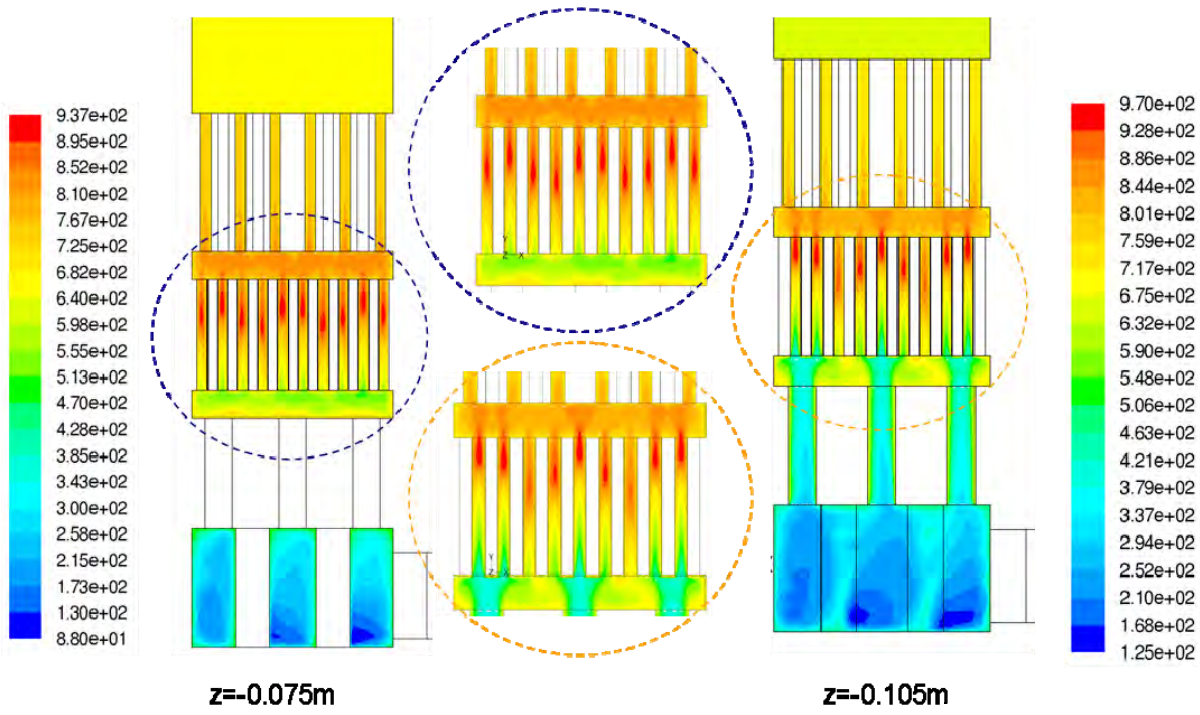

Figure 71: NACOK 2004 – Temperature on Sectional Planes

The velocity profile through the domain and a path line plot colored by temperature are shown in Figure 72. As expected, high velocity jets are created at the exit from the detailed reflector blocks and impinge onto adjacent geometry.

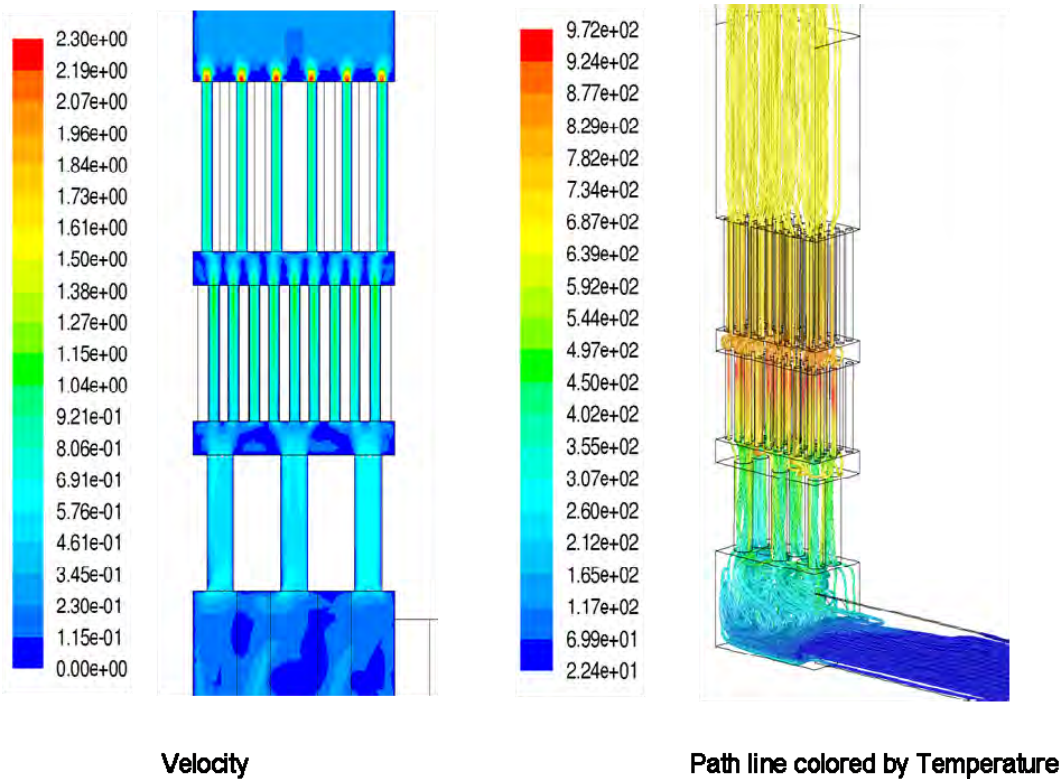

Figure 72: NACOK 2004 - Velocity Contour and Temperature Path-lines

Figure 73 shows the species concentration at the cross section at a location of z=-0.105m.

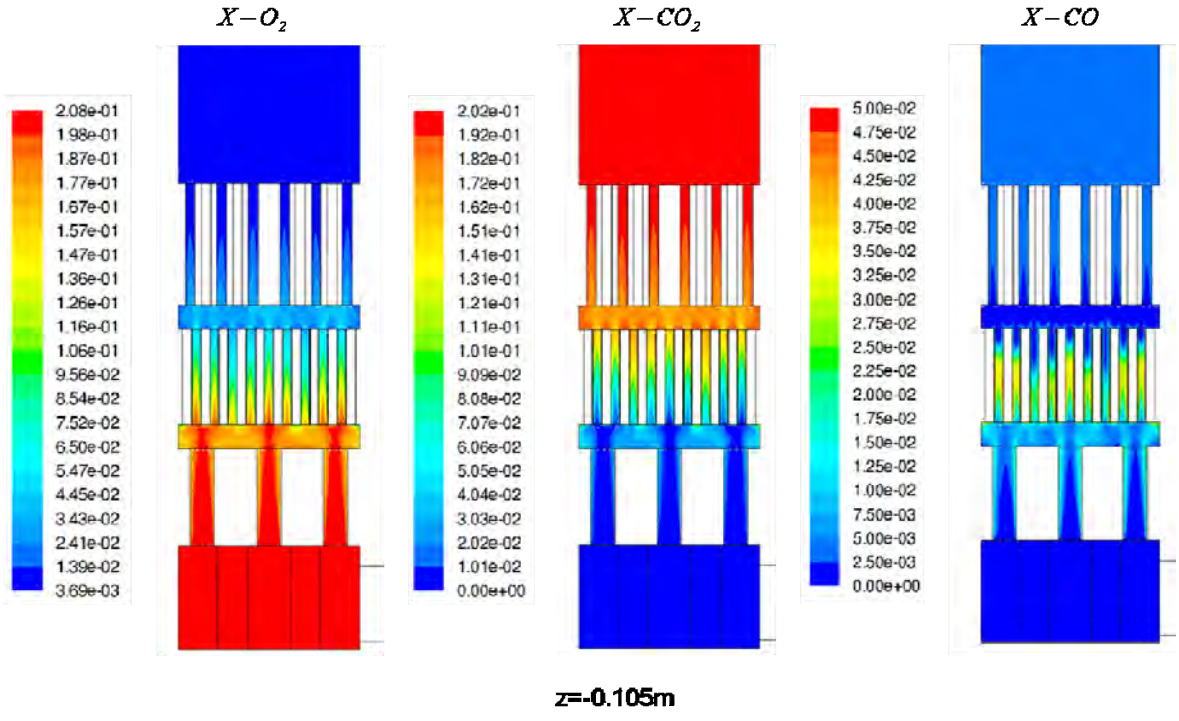

Figure 73: NACOK 2004 – Species Concentration

Based on the species concentration the graphite lost was calculated using Equation (49). For a period of 8 hours the graphite lost was 8.55kg. The total experimental value was 8.77kg and the initial porous model showed a result of 8.42kg. The results of the simulation were in reasonable agreement with the overall graphite loss. The porous model and detail model produced virtually the same overall graphite loss despite being vastly different in cell count.

When comparing the graphite loss per zone, there are still differences (especially in the pebble zone) between the experimental results and the results of the CFD simulation as shown in Table 13. This was explained in the porous model section as being due to the depletion of oxygen in the CFD model, and better comparison may be obtained with a better experimental correlation and a lower pre-exponent factor. It was also assumed that the pebble material was the same as the structural material for this test due to the lack of information.

The trend between the porous model and the detailed model remains similar. Although the accuracy of the predicted results is not good, the regions of maximum oxidation are correctly shown as the region of 'reflector 1'. The photograph of the experiment (Figure 61) also shows the degradation of the reflector block.

Table 13: NACOK 2004 – Graphite Loss (Detailed model)

Location	**Graphite loss - Experiment (kg)**	**Graphite loss – Porous model (kg)**	**Graphite loss – Detailed model (kg)**
Plenum 1	0.07	0.06	0.05
Above plenum 2	1.24	1.48	1.52
Exit reflector 1	4.76	5.23	5.76
Exit reflector 2	1.30	1.35	1.15
Exit bed 1	1.40	0.29	0.07
Total	8.77	8.42	8.55

7.5 Summary

This chapter considered two sets of experiments conducted at the NACOK facility in Germany. Both tests were of the open chimney configuration.

The 2005 experiments were two pebble beds at different temperatures. The lower bed included the reaction of $C-O_2$. The second bed was at a high temperature and the reaction of $C-CO_2$ was included. The oxidation characteristics for fuel matrix used on the fuel spheres and structural graphite were different due to their respective manufacturing processes. The packed bed required an approach that employed a porous medium with reaction chemistry. The experiment was studied and data interpreted. Results show that the experimental processes were also subject to pitfalls and interpretation. It was found that bed effective thermal conductivity in the axial direction was important along with inclusion of effects of wall channeling. Air humidity was found to influence the results. Experimental results were assessed by weight and gas analysis. The gas analysis method is more convenient for the comparison of results with the CFD predictions and the calculation of carbon loss. The oxidation correlation sourced from Contsecu [10] was used as for the $C-O_2$ reaction while data from Moorman [57] was used for the Boudouard reaction. Reasonable comparison was obtained between the CFD results and experimental results with the porous approach considering that the experimental data was not for the exact same grade of graphite.

The 2004 NACOK experiment used structural graphite closest to the inlet and a small pebble bed region. The structural graphite was of multiple block configuration and different sizes of holes. This represented the bottom reflector region of a high temperature reactor. For this test PBMR only had the final results and not the full report. As a first estimate the two detailed reflector blocks were simulated as porous media. This required a CFD to CFD comparison to characterize the block pressure drop. Various correlations for oxidation parameters were tested. It was found that the overall calculated graphite loss was within a good tolerance. A detailed model was developed to quantify the porous approach used on the reflector geometry. A larger model was constructed with detailed reflector blocks. A detailed mixed mesh of polyhedral and hexahedral cells was constructed and used for the simulations. Localized hot zones were identified in the detailed reflector region. It was found that the overall calculated graphite loss in the system was within good tolerance. In the CFD model the oxygen was consumed at a faster rate than in the experiment. This might be improved should better experimental data be available of the oxidation kinetics.

Although the accuracy may be improved upon, both the CFD approaches produced consistent results and showed the correct region where maximum oxidation would occur. It has to be noted that the simulations were conducted as steady state approximation of a transient event. Hence the initial developments of the oxidation process and the effect that it may have on the various parameters are not captured.

The limitations of the approach are that the oxidation process changes the shape of the graphite blocks as observed from the experimental data and this has a significant influence on the flow field. This effect was beyond the scope of this study and not modeled.

As the holes widen more exposed area is available for oxidation, changing the surface area to volume ratio of the blocks, hence changing the amount of oxidation that may occur. The particles that dislodge from the parent surfaces eventually accumulate in the structures and may influence the flow field. This effect was not simulated with the current CFD model.

Based on the above discussion, it can be concluded that a porous medium approach to oxidation yields representative results. The surface reaction would also yield good results. However, by nature of oxidation, the shape of the blocks would change and this would influence the surface area to volume ratio. No data was available on this aspect. The change in shape and particle accumulation would also influence the flow field. These effects were not modeled in the current CFD model due to the intense nature of adaptive mesh generation per iteration.

CHAPTER 8: CONCLUSIONS AND FUTURE WORK

8.1 Introduction

In Chapter 1, this study provided a brief background to the nuclear industry and previous developments on high temperature reactors. The PBMR was introduced and explained in the context of the 400 MWt demonstration plant with the Brayton cycle. Previous designs were developed using experimental testing and empirical correlations. With the development of computational capacity, computer aided design is used extensively in modern design. However, for use in a nuclear environment the software needs validation and verification.

Events that may pose safety risks to the plant and public were analyzed even if the probability that such events occur are extremely low. One such event is the ingress of air into the reactor. The oxygen content of air will react with hot graphite to produce carbon monoxide and carbon dioxide. Besides the formation of toxic gases, oxidation would change the density of graphite and influence the strength of the graphite blocks. The heat from chemical reactions could change the fuel temperature. Numerical analysis may be used to determine the change in fuel temperature and determine if the fuel remains in a safe temperature band. This study aimed at developing an approach using commercial CFD software to simulate nuclear graphite oxidation by benchmarking the CFD predicted results against experimental data. The experiments are relatively small scale to test the effects of physics. Each are explained in more detail along with the results obtained.

Chapter 2 provided a Literature survey of previous work. It identified that the theory of oxidation pertaining to temperature dependence, reactions, regimes and mechanism were reasonably well documented and can be studied to obtain an understanding on the subject of nuclear graphite oxidation. The KAIST experiment provided controlled experiments where oxidation parameters were studied and the results published. Previous CFD work conducted by MIT identified the need for experimental data to adequately study oxidation. It was also identified that the user coding used by MIT was not optimized for graphite oxidation and that this could be improved. This study begins with the simulation of diffusion and natural convection to show the codes ability to predict these phenomena. The KAIST experiments were simulated to obtain a basic understanding of the implementation of reaction chemistry and to improve on user coding of surface reactions in Fluent. Two experiments of NACOK were simulated. The first investigated the feasibility of using a porous medium with reaction chemistry to simulate the

reactor pebble bed. The second test used a porous and surface approach to model detailed reflector blocks to compare the two methods. The work was conducted with the main stakeholder being PBMR and with the intention of further developing the present capability to simulate air ingress with the commercial CFD code Fluent.

The theory pertaining to this study was discussed in Chapter 3. It explored molecular diffusion in a little more detail since it is relevant to air ingress. The focus was then shifted to oxidation. Initially, the graphite manufacturing process for structural and fuel matrix graphite was explored to aid in understanding the oxidation thereof. Oxidation mechanisms and regimes were explored. The main equations and change in enthalpy for reactions of graphite were detailed. The effect of burn-off was also studied. For this study some theory relating to packed pebble beds needed to be used and was briefly explained. The aspects of pressure drop, effective thermal conductivity and porosity variation with near wall effects were introduced.

The methodology chapter (Chapter 4) explored the process followed to conduct a generic CFD simulation. The basic conservation equations of mass, momentum and energy were introduced. The reaction chemistry features of CFD were investigated by species conservation. Aspects of diffusion and molecular reactions were explored. Analysis within a nuclear environment is extremely controlled. The CFD process at PBMR was introduced in the Chapter 4.7 on Validation and Verification.

This study considered oxidation in the context of air ingress. The processes preceding oxidation are molecular diffusion and natural convection. In Chapter 5 each of these processes were considered independently to show that the CFD code used in this study is capable of simulating the relevant phenomena. The simulation of diffusion was benchmarked by comparing the predicted results with the results obtained from an independent analytical solution. A long tube was filled with helium and nitrogen and the gases were allowed to mix purely by diffusion. The simulation of this basic experiment aided in understanding the parameters of diffusion and the correct simulation thereof. Transient analyses were conducted to test the influences of computational time step size and grid sensitivity. Three different temperatures were considered for the diffusion test. The results of the analytical solution and the CFD compared well.

A 2002 test at the NACOK facility considered the return duct experiment to determine mass flow rates under conditions of natural convection. This was basically an inverse U tube with a temperature gradient on each leg. The temperature gradient gave rise to a density variation which resulted in a difference in buoyancy forces and lead to natural convection flow. The results predicted by the simulation were benchmarked against the results of this experiment.

The aspects of pressure drop in a packed bed were also explored in this section. Multiple simulations were conducted with varying temperature gradients. Reasonable comparison was obtained between the results of the experiment and the results predicted by the CFD simulations. Some variations occurred at low mass flow rates and possible causes were explored. However, the correct trend between the simulations and the experiment were observed.

In Chapter 6, the results predicted by the CFD simulation were benchmarked against the results of the KAIST oxidation experiments. The published data presented two sets of experiments. The first was the oxidation of graphite and oxygen and the second set was the reaction of carbon with carbon dioxide. The simulation of these basic experiments allowed the understanding of graphite oxidation. The different reactions and the inputs for the CFD simulations were explored. The partial and complete reactions of carbon and oxygen were expressed as one equation with the ratio of CO/CO_2 taken into account as a function of temperature. This reaction was used to begin the development of a user defined function to define the surface reaction rate in Fluent. The stoichiometric values of the CFD simulations were determined by the user coding and varied with temperature. From the results, it was found that the in-pore reaction regime and the mass transfer controlled regimes were distinguished. It was found that a fine computational grid was required for the mass transfer regime. The reactions with carbon dioxide were implemented successfully. These experiments did not consider the effects of graphite burn-off.

In Chapter 7, the results of the CFD simulations were benchmarked against the results of two sets of tests conducted at the NACOK facility for oxidation. Both tests were of the open chimney configuration. The tests of 2005 considered two pebble beds at different temperatures. The lower bed would have the reaction of carbon and oxygen at a temperature of 650°C. The second bed was at a higher temperature of 950°C where the reaction of carbon with carbon dioxide was expected. The oxidation characteristics of fuel matrix used for the fuel spheres and the characteristics of the structural graphite were different due to their respective manufacturing processes (this was detailed in Chapter 3 – Manufacture of Graphite). The packed bed required an approach that employs reaction chemistry within a porous medium. The experiment was studied and the data interpreted. Results showed that the experimental processes were also subject to pitfalls and interpretation. It was found that the bed effective thermal conductivity in the axial direction is important along with the inclusion of the effects of wall channeling. Air humidity was found to influence the results. The experimental results were assessed by weight and gas analysis. The oxidation data used for this simulation set was sourced from Literature and it is known that the graphite burn-off would change with time and that this would influence

the reaction rate. The gas analysis provided a more convenient manner of comparing the results and carbon loss to the CFD simulations. Reasonable agreement was obtained between the results predicted by the CFD simulations using the porous approach and experimental results. The accuracy of the prediction may be improved if better experimental data for oxidation of the specific grade of graphite used on the NACOK facility were available.

The NACOK test of 2004 used structural graphite and a pebble bed region. The structural graphite was of multiple block configuration with different sizes of holes. This best represented the bottom reflector region of a high temperature reactor. For this test PBMR only had the final results and not the full report. As a first estimate the two detailed reflector blocks were simulated as porous media. This required a CFD to CFD comparison to characterize the pressure drop across the reflector blocks. Once the porous characteristics of the blocks were obtained, a model was built to test various oxidation correlations. The experimental data had large variations in the pre-exponent factors. Some points along the expected range were tested. It was found that the experimental results and the results predicted by the CFD simulations were comparable. Better comparison might be obtained should more appropriate experimental data be available with the effects of graphite burn-off. The trend of the areas with maximum oxidation was observed.

The porous medium approach enables the use of a relatively economical sized computational mesh. The surface reaction approach requires detailed grids, but the two approaches needed to be investigated to quantify the differences with an approach of reaction chemistry in a porous medium and surface reaction chemistry. A detailed mixed mesh of polyhedral and hexahedral cells were constructed and used for simulations. Localized hot zones were identified in the detailed reflector region. Again it was found that the overall graphite loss in the system was within good tolerance. The porous approach and the surface reaction approach produced virtually the same end result for the considered experiments. The accuracy per zone of the experimental result and the CFD prediction needs improvement, however the two methods are comparable in the sense that the areas of maximum oxidation were predicted correctly.

The accuracy of the simulation may be taken as being acceptable for an engineering application considering that the steady state simulations are an approximation of a transient test and that some of the initial phenomena and their effects on the various parameters are not considered. Other considerations are that the oxidation process changes the shape of the graphite blocks as observed from the experimental data and this would influence the flow field. This effect was not modeled.

As the holes widens more exposed area is available for oxidation, changing the surface area to volume ratio of the blocks, hence changing the amount of oxidation that may occur.

The particles that dislodge from the parent surfaces eventually accumulate in the structures and may influence the flow field. Simulation of these effects was beyond the scope of the current study.

8.2 Conclusions

The objective of this study was to develop a simulation approach for nuclear graphite oxidation with the use of commercial CFD software.

This was achieved by using a staggered and modular approach to the problem with a focus on understanding the underlying physics that drive the problem. Research was conducted in areas of molecular diffusion, since it is part of the air ingress process to which oxidation would apply. A brief summary of graphite manufacture was conducted to aid in understanding oxidation. The theory of oxidation, relevant equations for air reactions, reaction regimes and mechanism and issues relating to graphite burn-off were detailed. With reaction chemistry in CFD the Arrhenius reaction with the finite rate chemistry model was identified as the most applicable model. A detailed understanding of the interpretation of the curve was obtained from literature.

Before simulating the chemistry, the effects of molecular diffusion and natural convection driven flow were explored. CFD simulations were compared with analytical solutions and experimental data respectively to show the ability of the code to predict these phenomena.

The KAIST experiments were identified from literature and used as a starting point to understand oxidation on a small and controlled experiment. The simulation of this experiment provided valuable knowledge on the implementation of the simulation process and the required data for such simulations. The partial and complete reactions of carbon with oxygen were expressed as one equation with varying stoichiometric values with a dependence on temperature. The ratio of CO/CO_2 was used to formulate the stoichiometric values. Temperature dependent gas properties were sourced. Molecular diffusion coefficients were calculated and the correct implementation in CFD was established. For reaction chemistry the order of reaction was used from literature and partial pressure reformulation was considered. Activation energies were sourced from literature. The information was used to manipulate the base form of the reaction rate expressions in the species conservation equation and formulate the pre-exponent factors required for the Arrhenius reaction rate equations. The knowledge

gained was used to develop a user defined function for the surface reaction rate, with a dependence on surface temperature and varying stoichiometric coefficients. The numerical aspects of grid density were explored. The importance of good wall boundary cells was identified in the mass transfer regime. Solution control and the interpretation of data were also formulated.

The expansion of the study to the NACOK experiments also provided valuable insight. Two experiments were used as benchmarks. The first experiment, conducted in 2005, was with two pebble beds at different temperatures. This meant the reaction with oxygen would dominate in the lower bed while the reaction with carbon dioxide would occur in the upper bed. For the simulation of the bed regions a porous medium approach was used. The surface reaction rate, user defined function was evolved to work in a porous media. The interpretation of the experimental data was a large learning point. Data revealed the importance of test instrument location within the experimental facility. It was also established that the scatter of the experimental data was relatively large when different techniques were used to analyze the data. For the simulation of the experiment the following areas were identified as being essential; the pressure drop in the bed, the axial thermal conductivity and the effect of wall channeling. The effect of air moisture was also demonstrated with these simulations. Fuel matrix data was sourced from literature and reasonably good comparisons were obtained between the simulations and experimental data using the porous media approach.

The NACOK tests of 2004 were multiple sized blocks combined with pebble bed regions. The block geometry represented the lower reflector region of the reactor. Some blocks were with small diameter holes. With the knowledge that very fine computational grids are required for adequate resolution of chemistry, the first approach was to characterize the blocks with small diameter holes and use a combined surface and porous approach to simulate the reflector region. Without further detail of the reflector blocks a CFD to CFD comparison was conducted, the pressure drop across the blocks was obtained and the results used in a porous model.

With the knowledge that graphite burn-off would influence the reaction rate and knowing that the NACOK tests were relatively long (with respect to time duration), oxidation correlations were from tests that considered the effects of burn-off. Results showed that the overall graphite loss compared favorably. With better experimental data on the kinetic of oxidation and the effects of burn-off on the reaction rate, it might be possible to get better agreement between the results predicted with CFD and the experimental results without the use of trial and error. The data from literature showed large variations in the pre-exponent factors. Due to the nature of oxidation and the limitations of the simulation technique the results obtained can be considered to be a good engineering estimate.

A detailed model inclusive of a detailed reflector region was developed to quantify the porous medium approach and the approach of surface reactions. This resulted in a much larger computational mesh. The detailed mesh revealed that peak temperature regions occurred within the fine holes of the reflectors; this also means that most oxidation occurred in these regions. The overall results of the porous model and the detailed reflector models are comparable; however, quantitative comparisons per region have low accuracy. The oxygen in the CFD simulations was consumed too quickly. This can be fixed by using better experimental correlations. The prediction of regions with maximum oxidation was however successful.

It can therefore be concluded that the porous approach is more economical and works reasonably well. It has to be remembered that these simulations were conducted in steady state, but in reality, they are transient, hence some of the initiating events and the influence on oxidation parameters are neglected. The limitations of CFD simulation of oxidation is that it does not account for the change in geometric shape due to oxidation. As oxidation occurs the holes become wider and the lower surfaces of the blocks disintegrate, this changes the surface area to volume ratio of the blocks (with the porous approach), resulting in a different oxidation profile than that of the original geometry. The effects of change in geometric size of the blocks due to oxidation were not accounted for in this study. The other possible reason for differences in weight of graphite lost is that as the surfaces disintegrate, accumulation of particles occurs and this may bias the flow distribution.

8.3 Importance and Applicability of the Work

This work is applicable to high temperature reactors in general. The developments of this study will aid PBMR in furthering the air ingress simulations with CFD to account for graphite oxidation.

The air ingress studies provide valuable information for onset times to natural convection based on specific break locations and sizes. Knowing the allowable time brings the opportunity to take mitigating action such as inert gas injection.

This study will enable the design team to determine the temperature that the fuel maybe exposed to; hence establish the integrity of the fuel.

After oxidation, the quantity of carbon monoxide and carbon dioxide may be calculated in a known period. This will aid in determining the accumulation of the gases in the reactor and the risk thereof.

Although the accuracy of the CFD simulations requires further improvement, this may be achieved with better experimental data. The trend of correct region identification for maximum oxidation is important. The locations of oxidation will also assist designers in concentrating on areas of the reactor where graphite strength may change and aid better design to ensure structural integrity in the event of air entering the reactor.

8.4 Recommendations for Further Research

The need for experimental data for oxidation was already identified by PBMR. This study was conducted prior to these tests being conducted and therefore sourced information from the existing literature. More precise oxidation data from the chemical regime would be useful. Tests should be conducted in accordance to the ASTM method. This method standardizes sample size and flow rates to be used for experimental conditions. Details such as the activation energy, pre-exponent factor and the order of reaction are determined. Data pertaining to peak graphite burn-off and a curve of change in reaction rate versus burn-off would also be useful.

It is important to note that with the considered experiments the porous media approach was used within the in-pore diffusion regime for the $C-O_2$ reaction. Simulations of the KAIST experiment showed that a fine boundary layer is required to resolve the mass transfer regime. The effects of using a porous media with the reaction in the mass transfer regime were not quantified in this study since it falls beyond the temperature range considered. Further experimental data and the grade of graphite, may reveal a different change of slope and transition to the mass transfer regime. Should the mass transfer regime be applied to a porous media it is strongly recommended that further investigations be conducted.

PBMR conducted a propriety test at the NACOK facility. This test should also be simulated since the block geometry differs from that considered in this study and the grade of graphite is that which will be used in the PBMR reactor.

The user defined functions developed for this work can be expanded to accommodate multiple reactions with different activation energies per reaction.

The detailed reflector blocks were simulated with the original shape intact; methods of deforming meshes to account for change in shape can be explored. With the present computational requirements this can best be expressed as challenging, but may be possible in future considering the rapid developments in computational technology.

While still on an experimental scale the interface to structural analyses of the blocks should be explored. Fluent is now part of the Ansys suite of software. Ansys is traditionally a structural analysis code. This can be used to ascertain the change in mechanical strength of the graphite blocks.

By the conclusion of this study the PBMR design was in the stage of redesign and change. A steam generator would be used to include a Rankine cycle. This study also should be expanded to consider the influence of steam ingress into the reactor.

BIBLIOGRAPHY

[1] Achenbach E, 'Heat and flow characteristics of packed beds', Experimental Thermal and Fluid Science, vol. 10, pp. 17-27, 1995.

[2] Adams BR, Cremer MA and Wang DH, 'Modeling non-equilibrium CO oxidation in combustion systems', Presented at International Mechanical Engineering Congress & Exposition, Florida, USA, 2000.

[3] Balden M, Klages KU, Jacob W and Roth J, 'Oxidation erosion of graphite in air between 600 and 1000 K', Journal of Nuclear Materials, vol. 341, pp. 31 – 44, 2005.

[4] Ball S, Richards M and Shepelev S, 'Sensitivity studies of air ingress accidents in modular HTGRs', Nuclear Engineering and Design, vol. 238, pp. 2935 - 2942, 2008.

[5] Ball S, 'Sensitivity studies of modular high temperature gas cooled reactor postulated accidents', Nuclear Engineering and Design, vol. 236, pp. 454 – 462, 2006.

[6] Blanchard A, 'Appendix 2 – The thermal oxidation of graphite' in document 'Irradiation damage in graphite due to fast neutrons in fission and fusion systems', IAEA, Vienna, Austria, TECDOC-1154, pp. 207 – 213, 2000.

[7] Brudieu AM and Kadak AC, 'Blind benchmark predictions of NACOK air ingress tests using computational fluid dynamics', Proc. HTR2006, 3rd International Topical Meeting on High Temperature Reactor Technology, South Africa, 2006, Paper C00000201.

[8] Brudieu AM, 'Blind benchmark predictions of the NACOK air ingress tests using the CFD code Fluent', MS Dissertation, Dept. Nuclear Eng., MIT, USA, 2007.

[9] Chi SH and Kim GC, 'Comparison of the oxidation rate and degree of graphitization of elected IG and NBG nuclear graphite grades', Journal of Nuclear Materials, vol. 381, pp. 9 -14, 2008.

[10] Contescu CI, Azad S, Miller D, Lance MJ, Baker FS and Burchell TD, 'Practical aspects of characterizing air oxidation of graphite', Journal of Nuclear Materials, vol. 381, pp. 15 – 24, 2008.

[11] Contescu C, Strizak J and Burchell T, 'Test method for air oxidation of manufactured carbon and graphite', Oak Ridge National Laboratory, Presentation to ASTM Committee, Toronto, Canada, 2006.

[12] Corwin WR, 'US Generation IV reactor integrated material technology program', Nuclear Engineering and Technology, vol. 38, no. 7, pp. 591- 618, 2006.

[13] Du Toit CG, 'Radial variation in porosity in annular packed beds', Nuclear Engineering and Design, vol. 238, pp. 3017 – 3079, 2008.

[14] Ergun S, 'Fluid flow through packed columns', Chemical Engineering Progress, vol. 48, no. 2, pp. 89 – 94, 1952.

[15] Ferziger JH and Peric M, 'Computational methods for fluid dynamics', 3rd Edition, New York, Springer Verlag, 2002.

[16] Fleming KN, 'Initiating event frequencies for the PBMR helium pressure boundary leaks and breaks', PBMR (PTY) Ltd., Centurion, South Africa, PBMR document 062910/4, 2008. (PBMR Proprietary Document.)

[17] 'Fluent User Guide' – Fluent Version 6.3, Fluent Inc., 2006. (Electronic version supplied with the software)

[18] Fullarton JW, 'VDI Heat Atlas', Die Deutsche Bibliothek, Düsseldorf, Germany, 1993(Translated from German to English).

[19] Fuller EL and Okoh JM, 'Kinetics and mechanisms of the reaction of air with nuclear grade graphites:IG-110', Journal of Nuclear Materials, vol. 240, pp. 241 – 250, 1997.

[20] Gerwin H, Neuhaus I and Roes J, 'Modifikation und welterentwicklung von reakionratenbeziehungen zur berchung des graphitabbrands bei storfallen mit massiven lufteinbruchen in das core eines hochtemperaturreaktors', FZJ, Germany, 1995.

[21] Hahn JR, 'Kinetic study of graphite oxidation along two lattice directions', Carbon, vol. 43, pp. 1506 – 1511, 2005.

[22] Haque H, 'Consequences of delayed air ingress following a depressurization accident in a high temperature reactor', Nuclear Engineering and Design, vol. 238, pp. 3041 - 3046, 2008.

[23] Heintz EA and Parker WE, 'Catalytic effect of major impurities on graphite oxidation', Carbon, vol. 4, pp. 473 – 482, 1966.

[24] Hinssen HK, Kühn K, Moormann R, Schlogl B, Fechter M and Mitchell M, 'Oxidation experiments and theoretical examinations on graphite materials relevant for the PBMR', Nuclear Engineering and Design, vol. 238, pp. 3018 – 3025, 2008.

[25] Hinssen HK, Hohn H, Niessen HF and Wohlrab D, 'NACOK experiment 2004_1-March 2004', Power point presentation by FZJ at PBMR workshop, South Africa, 2004.

[26] Hishida M and Takeda T, 'Study on air ingress during an early stage of a primary-pipe rupture accident of a high temperature gas-cooled reactor', Nuclear Engineering and Design, vol. 126, pp. 175 – 187, 1991.

[27] Hoffmann JL, 'CFD Best practice guide', PBMR (PTY) Ltd., Centurion, South Africa, PBMR document 099441/1, 2007. (PBMR Proprietary Document.)

[28] Hoffmann JL, 'CFD Software verification and validation plan', PBMR (PTY) Ltd., Centurion, South Africa, PBMR document 015136/3, 2007. (PBMR Proprietary Document.)

[29] Hunt ML and Tien CL, 'Non-Darcian flow, heat and mass transfer in catalytic packed bed reactors', Chemical Engineering Science, vol. 45, no.1, pp. 55 – 63, 1990.

[30] Ide A, Hayakawa H, Yasuno T, Takenaka Y, Hayashi S, Kobayashi T, Maeda S, Tonogouchi M, Takeda M, Horie M, Handa K, Nakamura Y, Kaneko M, Masuda T, Ikehara m, Takase Y and Ishiwatari M, 'Study of a high temperature gas cooled reactor heat utilization plant', HTR Heat Utilization Core Group, Japan. (PBMR reference PBMR/6738). Accessed November 2009 on PBMR (PTY) Ltd., PDMS.

[31] Ishihara M, Sumita J, Shibata T, Iyoku T and Oku T, 'Principle design and data of graphite components', Nuclear Engineering and Design, vol. 233, pp. 251 – 260, 2004.

[32] Ita LE and Sonntag RE, 'Thermal diffusion: Separation of He-N_2 system with temperature gradient in two directions', Journal of Chemical and Engineering Data, vol. 21, no.2, pp. 162 – 165, 1976.

[33] Jansen, E, 'PBMR Demonstration power plant qualification process white paper', PBMR (PTY) Ltd., Centurion, South Africa, PBMR document 080389/3, 2009. (PBMR Proprietary Document.)

[34] Kadak AC, 'MIT Pebble bed reactor project', Nuclear Engineering and Technology, vol. 39 no.2, pp. 95 – 102, 2007.

[35] Kadak AC, Ballinger RG, Alvey T, Kang CW, Owen P, Smith A, Wright M and Yao X, 'A response to the environmental and economic challenge of global warming', MIT, USA, 1998.

[36] Kadak AC, 'Nuclear power: Made in China', Department of Nuclear Science and Engineering, MIT, USA, (year not published).

[37] Kendall JM, 'High temperature gas cooled reactor technology development', IAEA, Vienna, Austria, TECDOC-988, 1997.

[38] Kerkhof PJ and Geboers MA, 'Analysis and extension of the theory of multi-component fluid diffusion', Chemical Engineering Science, vol. 60, pp. 3129 – 3167, 2005.

[39] Kern Technischer Ausschuss (KTA) – German Nuclear Safety Standards Commission, Rule 3102.3, Part 3, 'Loss of pressure through friction in pebble bed cores', Germany, 1981.

[40] Kim ES and No HC, 'Analysis of geometrical effects on graphite oxidation through measurement of internal surface area', Journal of Nuclear Materials, vol. 348, pp. 174 – 180, 2006.

[41] Kim ES and No HC, 'Experimental study on the oxidation of nuclear graphite and development of an oxidation model', Journal of Nuclear Materials, vol. 349, pp. 182 – 194, 2006.

[42] Kim ES and No HC, 'Experimental study on the reaction between nuclear graphite IG-110 and carbon dioxide', Journal of Nuclear Materials, vol. 350, pp. 96 – 100, 2006.

[43] Kim ES and No HC; 'Estimation of graphite density and mechanical strength variation of VHTR during air-ingress accident', Nuclear Engineering and Design, vol. 238, pp. 837 – 847, 2008.

[44] Koster A, Matzner DH, and Nicholls DR, 'PBMR design for the future', Nuclear Engineering and Design, vol. 222, pp. 231-245, 2003.

[45] Kugeler K, Epping CH, Schmidtlein P and Schreiner P, 'Aerosol formation by graphite corrosion in case of water and air ingress to the core of a high temperature reactor', Energy, vol. 16, pp. 491 – 499, 1991.

[46] Kugeler K and Roes J, 'Aerosol particles formatted in the bottom reflector and in the pebble bed by graphite corrosion during air ingress into the core of a high temperature reactor', Journal of Aerosol Science, vol. 24, pp. S255 – S256, 1993.

[47] Kuhlmann MB, 'Experimente zu gastransport und graphitkorrosion bei lufteinbruch-storfallen im hochtemperatur reactor', FZJ, Germany, 2002.

[48] Laage R, 'Graphite oxidation phenomena identification', PBMR (PTY) Ltd., Centurion, South Africa, PBMR document 040992/1, 2007. (PBMR Proprietary Document.)

[49] Lim HS and No HC, 'Development and validation of 3d multi-component mixture analysis tool (Gamma) for air ingress in HTGR', Proc. HTR2004, 2nd International Topical meeting on high temperature reactor technology, China, 2004, Paper C03.

[50] Lim YS, Chi SH and Cho KY, 'Change of properties after oxidation of IG-11 graphite by air and CO2 gas', Journal of Nuclear Materials, vol. 374, pp. 123 – 128, 2008.

[51] Lourens P, 'Diffusion calculation for nitrogen and helium', PBMR (PTY) Ltd., Centurion, South Africa, PBMR document T000307/1, 2008. (PBMR Proprietary Document.)

[52] Marsden BJ, 'Nuclear graphite for high temperature reactors', IAEA, Vienna, Austria. Available at http://www-pub.iaea.org/MTCD/publications/publications.asp. Accessed January 2009.

[53] Menter F, 'CFD Best practice guidelines for CFD code validation for reactor-safety applications', European Commission, 5th Euratom Framework Programme, 2002.

[54] Moormann R and Hilpert K, 'Chemical behaviour of fission products in core heatup accidents in high temperature gas cooled reactors', Nuclear Technology, vol. 94, pp. 56 – 67, 1991.

[55] Moormann R, Katscher W and Hinssen HK, 'The dependence of the corrosion rate of the A3-matrix/oxygen reaction on oxygen partial pressure', FZJ, Germany, 1979.

[56] Moormann R, Hinssen HK and Kühn K, 'Oxidation behaviour of an HTR fuel element matrix graphite in oxygen compared to a standard nuclear graphite', Nuclear Engineering and Design, vol. 227, pp. 281 – 284, 2004.

[57] Moormann R, 'Effect of delays in afterheat removal on consequences of massive air ingress accidents in high temperature gas cooled reactors', Journal of Nuclear Science and Technology, vol. 21, pp. 824 – 835, 1984.

[58] Moormann R, 'Phenomenology of graphite burning in massive air ingress accidents', Proc. HTR2006, 3rd International Topical Meeting on High Temperature Reactor Technology, South Africa, 2006, Paper F00000032.

[59] Murthy KL and Charit I, 'Structural materials for Gen 4 nuclear reactors: Challenges and opportunities', Journal of Nuclear Material, vol. 383, pp. 189 – 195, 2008.

[60] Nicholls DR, 'Status of the pebble bed modular reactor', Nuclear Engineering, vol. 39, pp. 231 – 236, 2000.

[61] Niessen HF, Forschungszentrum Jülich, Germany, Scientist on the NACOK and SANA experiment, Personal communication, 2009.

[62] Niessen HF, Hinssen HK, Hohn H and Kühn K, 'NACOK experiment 2005_1 - Experimental set-up, execution of the test, experimental results', FZJ, Germany, 2005, Report number FZJ-ISR-RC-5097/2005. (PBMR Proprietary Document.)

[63] Nightingale RE, 'Nuclear graphite', New York, Academic Press Inc, 1962.

[64] No HC, Lim HS, Kim J, Oh C, Siefken L and Davis C, 'Multi-component diffusion analysis and assessment of GAMMA code and improved RELAP5 code', Nuclear Engineering and Design, vol. 237, pp. 997 – 1008, 2007.

[65] Oh C, Kim ES, Schulyz R and Petti D, 'Implications of air ingress induced by density difference driven stratified flow', Proc. of the ICAPP Conference, Anaheim, USA, 2008, Paper 8023.

[66] Parks BT, 'Using the Fluent computational fluid dynamics code to model the NACOK corrosion test', MS Dissertation, Dept. of Nuclear Eng., MIT, USA, 2004.

[67] PBMR web site for fuel diagram. Available at http://www.pbmr.co.za/index.asp?Content=224, Accessed October 2009.

[68] Perkins G and Sahajwalla V, 'Modelling of heat and mass transport phenomena and chemical reaction in underground coal gasification', Chemical Engineering Research and Design, vol. 85, pp. 329 – 343, 2007.

[69] Perry RH and Green D, 'Perry's chemical engineers handbook', 5th edition, New York, McGraw Hill, 1985.

[70] Reutler H and Lohnert GH, 'Advantages of going modular in HTRs', Nuclear Engineering and Design, vol. 78, no. 2, pp. 129 – 136, 1984.

[71] Roes J, 'Experimentelle untersuchungen zur graphitkorrosion und aerosolentstehung beim lufteinbruch in das core eines kugelhaufen-hochtemperaturreaktors', FZJ, Germany, 1994.

[72] Roesler JF, Yetter RA and Dryer FL., 'Effect of O2 concentration on moist CO oxidation', Presented at Eastern States Section Meeting of The Combustion Institute, Cornell University, USA, 1991.

[73] Schmitz W, 'CFD-Tinte benchmark calculations', PBMR (PTY) Ltd., Centurion, South Africa, PBMR document 020234, 2004. (PBMR Proprietary Document.)

[74] Schmitz W, 'NACOK Testing requirement specification', PBMR (PTY) Ltd., Centurion, South Africa, PBMR document 025215, 2004. (PBMR Proprietary Document.)

[75] Schmitz W, 'Air ingress calculation model plan', PBMR (PTY) Ltd., Centurion, South Africa, PBMR document 039198, 2007. (PBMR Proprietary Document.)

[76] Schmitz W, 'Air ingress simulations', PBMR (PTY) Ltd., Centurion, South Africa, PBMR document T000085, 2007. (PBMR Proprietary Document.)

[77] Schmitz W, 'Heat dispersion in a pebble bed, Comparison of CFD and experimental results', PBMR (PTY) Ltd., Centurion, South Africa, PBMR document 020333, 2004. (PBMR Proprietary Document.)

[78] Schmitz W, 'Quantification of nitrogen injection for the ANS calculation report', PBMR (PTY) Ltd., Centurion, South Africa, PBMR document T000957, 2008. (PBMR Proprietary Document.)

[79] Schmitz W, 'Effect of pipe break gap size', PBMR (PTY) Ltd., Centurion, South Africa, PBMR document T001202, 2009. (PBMR Proprietary Document.)

[80] Schmitz W, 'Large break in pressure boundary analysis report', PBMR (PTY) Ltd., Centurion, South Africa, PBMR document T0017550, 2009. (PBMR Proprietary Document.)

[81] Schmitz W and Koster A, 'Air ingress simulations using CFD', Proc. HTR2006, 3rd International Topical Meeting on High Temperature Reactor Technology, South Africa, 2006, Paper F00000203.

[82] Schmitz W, Hoffman J, Sithole H and Halley L , 'Validation and verification of CFD computer codes and the PBMR air ingress model', Proc. HTR2006, 3rd International Topical Meeting on High Temperature Reactor Technology, South Africa, 2006, Paper F00000251.

[83] Sikik EU, 'Simulation of air and water ingress transients for the PBMR by means of the TINTE code', Proc. HTR2008, 4th International Topical Meeting on High Temperature Reactor Technology, USA, 2008, HTR2008-58104.

[84] Slabber J, 'Technical description of the PBMR demonstration power plant', PBMR (PTY) Ltd., Centurion, South Africa, PBMR document 016956, 2006. (PBMR Proprietary Document.)

[85] Snead LL, Nozawa T, Katoh Y, Byun TS, Kondo A and Petti DA , 'Handbook of SiC properties for fuel performance modeling', Journal of Nuclear Materials, vol. 371, pp. 329 – 377, 2007.

[86] Stanmore BR, Brilhac JF and Gilot P, 'The oxidation of soot: A review of experiments, mechanisms and models', Carbon, vol. 39, pp. 2247 – 2268, 2001.

[87] Sun Y, Gerwin H and Scherer W, 'Voruntersuchungen zum experiment NACOK mit dem reacktordynamik programm TINTE', FZJ, Germany, 1993.

[88] Takeda T and Hishida M, 'Studies on diffusion and natural convection of two-component gases', Nuclear Engineering and Design, vol. 135, pp. 341 – 354, 1992.

[89] Takeda T and Hishida M, 'Studies on molecular diffusion and natural convection in a multi-component gas system', Int. J. Heat Mass Transfer, vol. 39 no. 3, pp. 527 – 536, 1996.

[90] Takeda T and Hishida M, 'Study on the passive safe technology for the prevention of air ingress during the primary rupture accident of HTGR', Nuclear Engineering and Design, vol. 200, pp. 251 – 259, 2000.

[91] Takeda T, 'Research and development on prevention of air ingress during the primary-pipe rupture accident in the HTTR', Nuclear Engineering and Design, vol. 233, pp. 197 – 209, 2004.

[92] Van Goethem, Manolatos P Hugon M, Bhatnagar V, Casalta S and Deffrennes M (editors), 'FISA 2006 – EU Research and training in reactor systems', European commission – Euratom framework programme 2002 – 2006, Belgium, 2006.

[93] Van Rensburg JJJ, 'An integrated and detailed multiphysics approach for the CFD analysis of a high temperature reactor', Doctorate thesis, Dept. of Mech. Eng., North West University, South Africa, 2010, (In Press).

[94] Versteeg HK and Malalasekera W, 'An introduction to computational fluid dynamics the finite volume method', Longman Group Ltd, Malaysia, 1995.

[95] Walker PL, ‘Gas reactions of carbon and graphite’, Proc. of the Conference on Carbon, University of Buffalo, USA, pp. 75 – 81, 1956.

[96] Walmsley J, ‘High temperature gas cooled reactor historical aspects’, NSD R95/07, Nuclear Safety Division, 1995.

[97] Xiaowei L, Jean-Charles R and Suyuan Y, ‘Effect of temperature on graphite oxidation behaviour’, Nuclear Engineering and Design, vol. 227, pp. 273 – 280, 2004.

[98] Zehner P and Schlunder EU, ‘Warmeleitfahigkeit von schuttungen bei mabigen temperaturen’, Chemie Ingenieur Technik, vol. 42, no. 14, pp. 933 – 941, 1970.

[99] Zhai T, ‘LOCA and air ingress accident analysis of a pebble bed reactor’, MS Dissertation, Dept. of Nuclear Eng., MIT, USA, 2003.

[100] Zhang Z, Gerwin H and Scherer, ‘Analysis of the gas diffusion process during a hypothetical air ingress accident in a modular high temperature gas cooled reactor’, FZJ, Germany, 1993.

[101] Zhu Q, Qui X and Ma C, ‘The oxidation resistance improvement of matrix graphite of spherical fuel elements by slip gelation process’, Journal of Nuclear Materials, vol. 254, pp. 221 – 225, 1998.

ANNEXURE A: TUBE DIFFUSION

This annexure presents a few images for the simulation of the tube diffusion case presented in the main text. Figures pertain to the case at 900°C. Figure 74 details the initial grid used for the tube diffusion case before adaptive refinement.

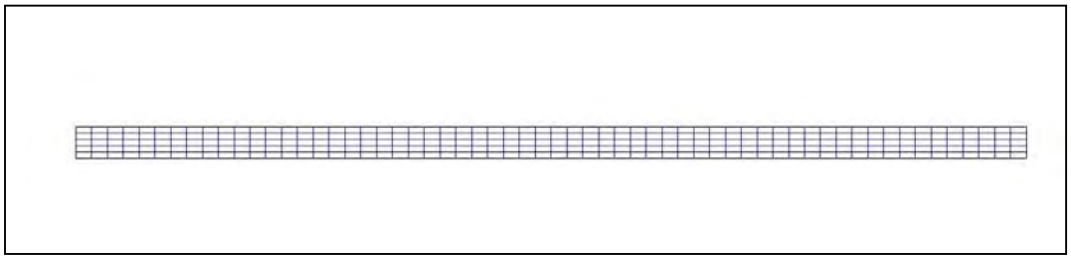

Figure 74: Tube Diffusion – Computational Grid

Figure 75 presents the initial species conditions (time equal to zero), the figure shows the mole fraction of helium as one and that of nitrogen as zero.

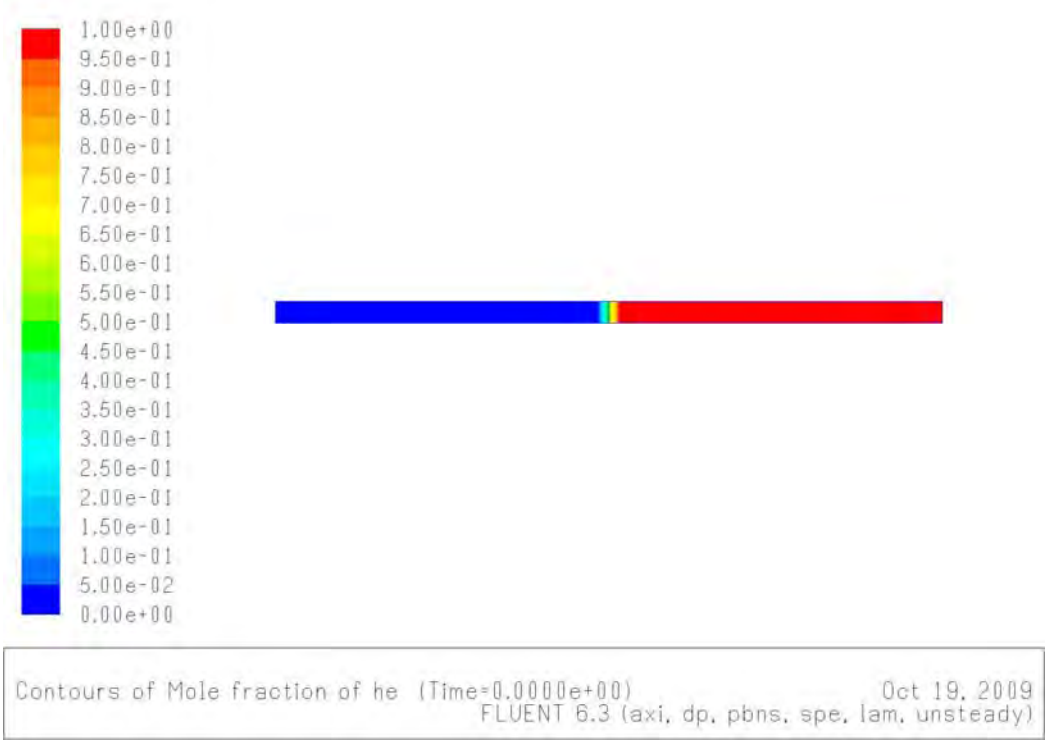

Figure 75: Tube Diffusion – Initial Species Condition

Figure 76 shows the mole fraction of helium after 500 seconds.

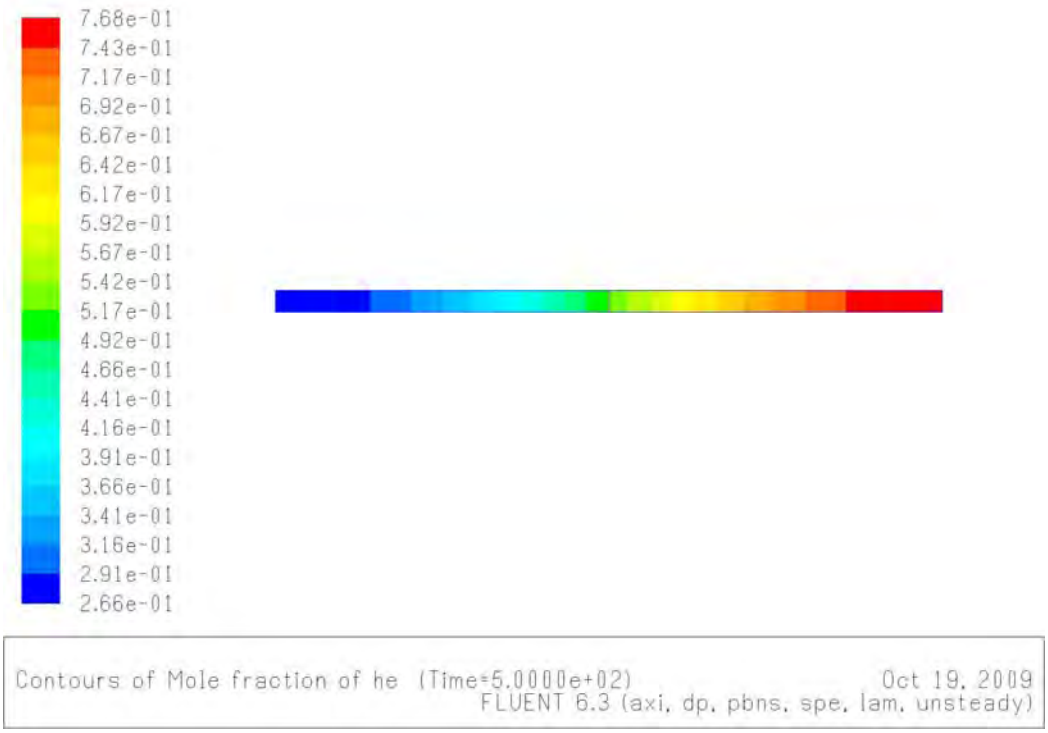

Figure 76: Tube Diffusion – Mole Fraction of Helium after 500 seconds.

ANNEXURE B: NACOK – MASS FLOW UNDER NATURAL CONVECTION

This section pertains to the simulation of the NACOK 2002 experiments conducted by Kuhlmann [47]. The configuration was that of the return duct as shown in Figure 23. This was basically an inverse U tube that represents the flow paths in a reactor under air ingress conditions. One leg was hot to represent the core outlet (under normal flow conditions) and the core region; the cold region would be normal flow inlet region. This test used different temperatures on the hot and cold legs with a 5m column of ceramic pebbles and measured the mass flow rate through the system.

Approximately thirty individual simulations were conducted to obtain the data presented in Figure 24. The data presented in Figure 77 was for one of the cases, i.e.: with a hot leg at 300 °C and a cold leg at 200 °C. The initial temperature distribution is shown in this figure.

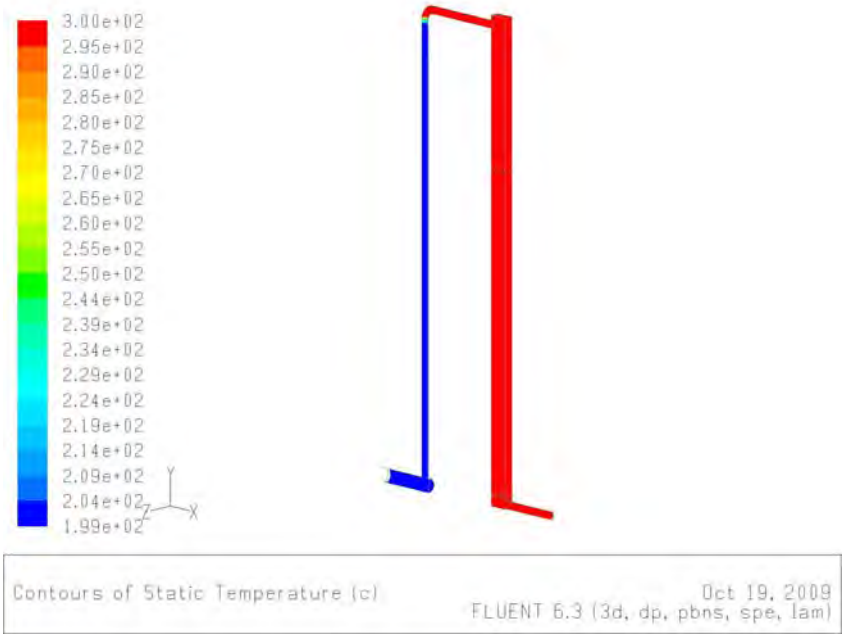

Figure 77: NACOK 2002 – Initial Temperature Distribution

The CFD results for the temperature and velocity distribution are shown in Figure 78 and Figure 79 respectively.

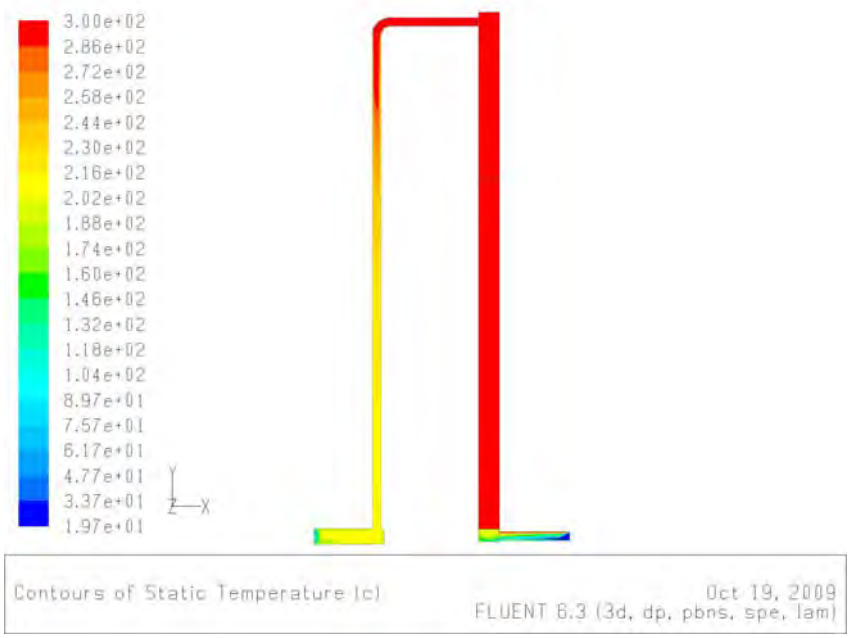

Figure 78: NACOK 2002 – Temperature Distribution

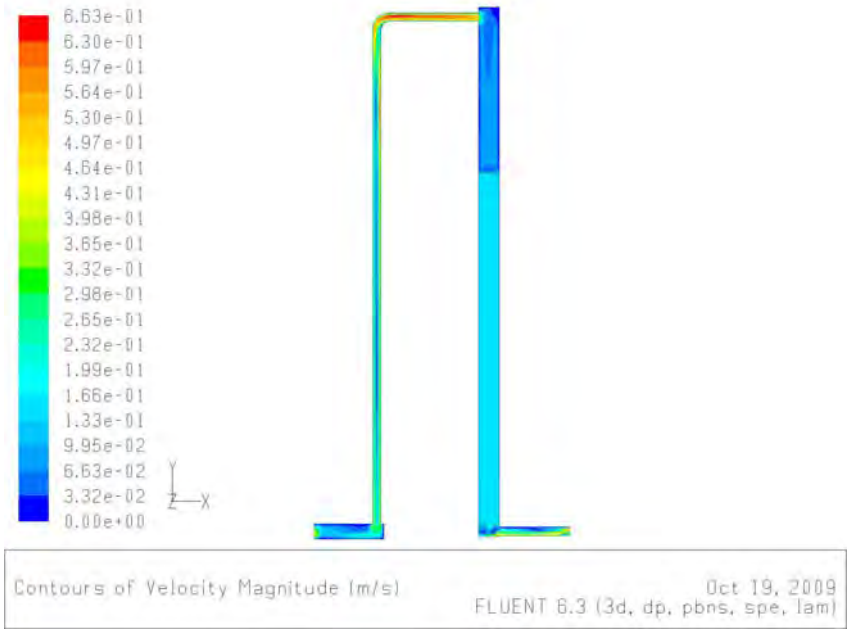

Figure 79: NACOK 2002 – Velocity Distribution

Figure 80 shows the pressure drop through the 5m ceramic pebble bed column.

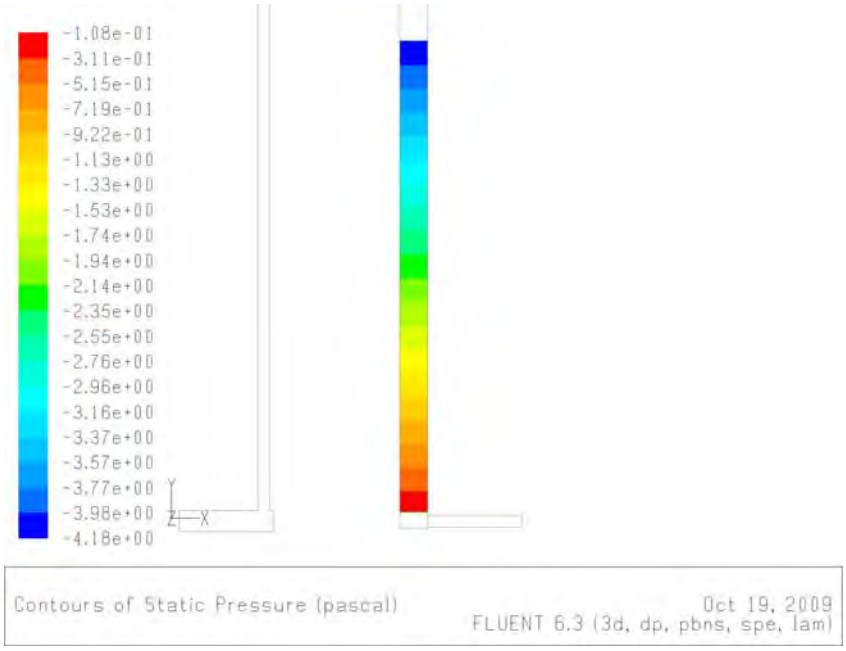

Figure 80: NACOK 2002 – Pressure Drop Through Pebble Bed

ANNEXURE C: MATERIAL PROPERTIES

This Annexure presents the material properties of species used in this study. The tables that follow present the coefficients for polynomial curve fits as a function of temperature (in Kelvin).

Table 14 presents the polynomial coefficients for species density. For example of density of helium (in $kg/m^3.s$) can be expressed as $\rho = eT^4 + dT^3 + cT^2 + bT + a$. The table shows the values of the coefficients.

All listed material properties were capped over a temperature range of 283K< T <1973K and at atmospheric pressure.

Table 14: Species Density ($kg/m^3.s$) – Polynomial Coefficients

	He	N_2	O_2	CO	CO_2
f	-	-	-7.56E-16	-	-1.04E-15
e	9.38E-14	6.57E-13	4.87E-12	5.37E-13	6.70E-12
d	-4.98E-10	-3.29E-09	-1.24E-08	-2.92E-09	-1.70E-08
c	7.90E-08	6.86E-06	1.56E-05	5.94E-06	2.15E-05
b	-8.77E-04	-6.14E-03	-1.03E-02	-5.56E-03	-1.41E-02
a	3.50E-01	2.45E+00	3.27E+00	2.35E+00	4.50E+00

Similarly the polynomial coefficients for species viscosity are presented in Table 15, Table 16 has the data for species specific heat capacity and Table 17 for species thermal conductivity.

Table 15: Species Viscosity ($kg/m.s$) – Polynomial Coefficients

	He	N_2	O_2	CO	CO_2
c	-5.14E-12	-5.82E-12	-9.26E-12	-7.83E-12	-7.48E-12
b	4.38E-08	4.04E-08	5.26E-08	4.66E-08	4.21E-08
a	7.59E-06	6.95E-06	5.97E-06	2.32E-06	5.98E-06

Table 16: Species Specific Heat Capacity ($J/kg.K$) – Polynomial Coefficients

	He	N_2	O_2	CO	CO_2
c	-1.229E-06	-3.374E-04	-8.998E-05	-5.985E-05	-2.412E-04
b	3.590E-03	7.094E-01	3.519E-01	2.970E-01	8.280E-01
a	5.192E+03	8.157E+02	8.235E+02	9.436E+02	6.437E+02

Table 17: Species Thermal Conductivity ($W/m.K$) – Polynomial Coefficients

	He	N_2	O_2	CO	CO_2
c	-3.980E-08	-7.680E-09	-4.210E-09	-6.910E-09	4.370E-09
b	3.450E-04	6.800E-05	7.840E-05	5.810E-05	6.650E-05
a	5.670E-02	6.740E-03	4.200E-03	1.030E-02	-2.710E-03

As explained in the Chapter 3.2, the diffusion coefficients for Fluent were input per possible binary mixture of gases to allow the multi-component diffusion formulation. Table 18 presents the polynomial coefficients for the calculation of diffusion coefficients as a function of temperature. The data was capped over the range 293K< T <1473K for the NACOK simulations.

Table 18: Species Diffusion Coefficients (m^2/s) – Polynomial Coefficients

	c	b	a
$N_2 - O_2$	1.167E-10	6.228E-08	-9.213E-06
$N_2 - CO$	1.154E-10	6.160E-08	-9.113E-06
$N_2 - CO_2$	9.241E-11	4.931E-08	-7.295E-06
$N_2 - He$	3.945E-10	2.105E-07	-3.115E-05
$N_2 - H_2O$	1.485E-10	7.925E-08	-1.172E-05
$H_2O - O_2$	1.487E-10	7.935E-08	-1.174E-05
$H_2O - CO$	1.457E-10	7.774E-08	-1.150E-05
$H_2O - CO_2$	1.186E-10	6.329E-08	-9.362E-06
$H_2O - He$	4.718E-10	2.518E-07	-3.724E-05
$He - O_2$	4.044E-10	2.158E-07	-3.192E-05
$He - CO$	3.854E-10	2.056E-07	-3.042E-05
$He - CO_2$	3.220E-10	1.718E-07	-2.542E-05
$CO_2 - O_2$	9.090E-11	4.851E-08	-7.176E-06
$CO_2 - CO$	9.085E-11	4.848E-08	-7.172E-06
$CO - O_2$	1.146E-10	6.114E-08	-9.044E-06

Table 19 presents the thermal conductivity of the ceramics.

Table 19: Thermal Conductivity of Ceramic

Temperature (K)	Thermal Conductivity (W/m.K)
293	1.37
473	1.59
673	1.86
873	2.41
1073	3.2
1273	4.6

ANNEXURE D: SIMULATION OF THE KAIST BOUDOUARD REACTION

The following plots are from the simulation of the reaction of carbon and CO_2 to form CO. This reaction is called the 'Boudouard' reaction. Multiple simulations of the KAIST experiment were conducted to obtain Figure 38. This section shows the results from the case with a surface temperature of 1300°C and a CO_2 mole fraction of 10%. Figure 81 shows the temperature distribution for this simulation. Incoming CO_2 was at an ambient temperature of approximately 20°C, and the heated surface was at 1300°C.

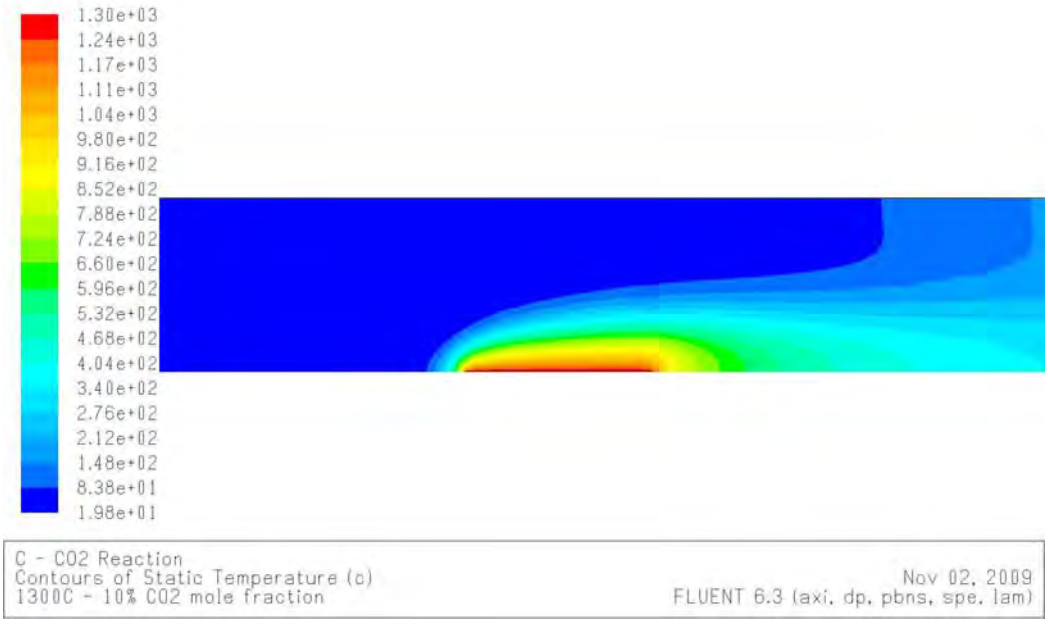

Figure 81: $C - CO_2$ Simulation – Temperature Distribution

Figure 82 shows the depletion of CO_2 on the heated surface.

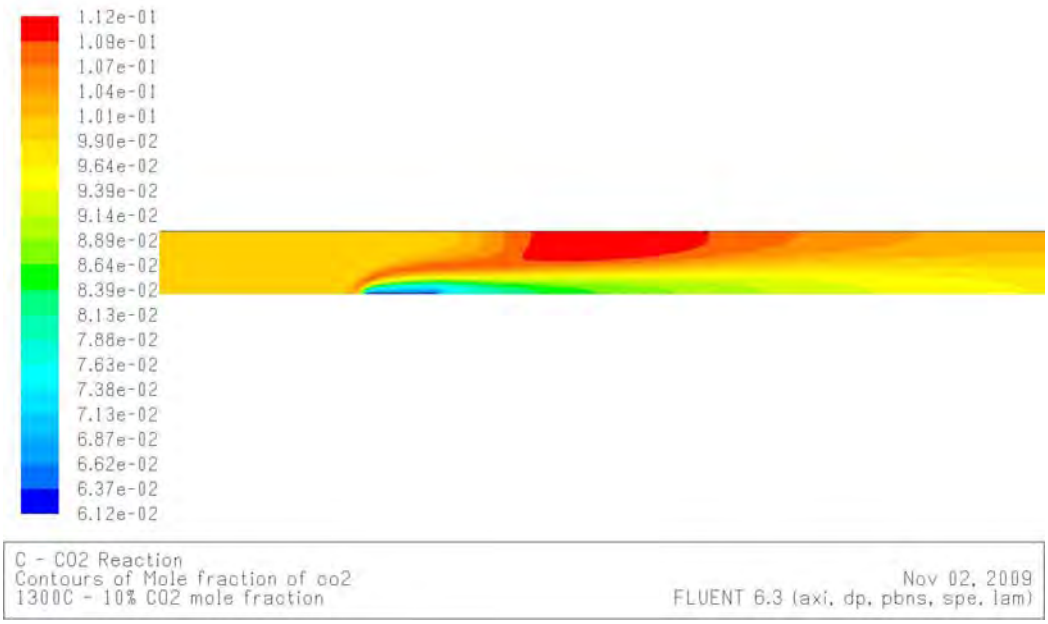

Figure 82: $C - CO_2$ **Simulation – Mole Fraction of** CO_2

Figure 83 details the generation of CO on the reacting surface.

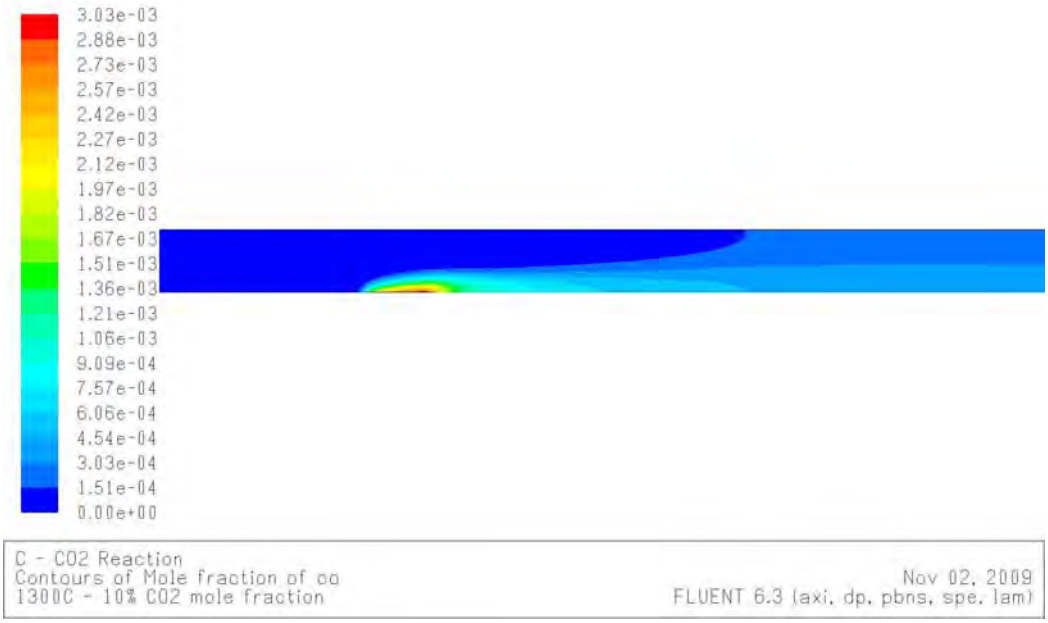

Figure 83: $C - CO_2$ **Simulation – Mole Fraction of** CO

The reacting surface influences the velocity profile in the region around the reaction, this is shown in Figure 84.

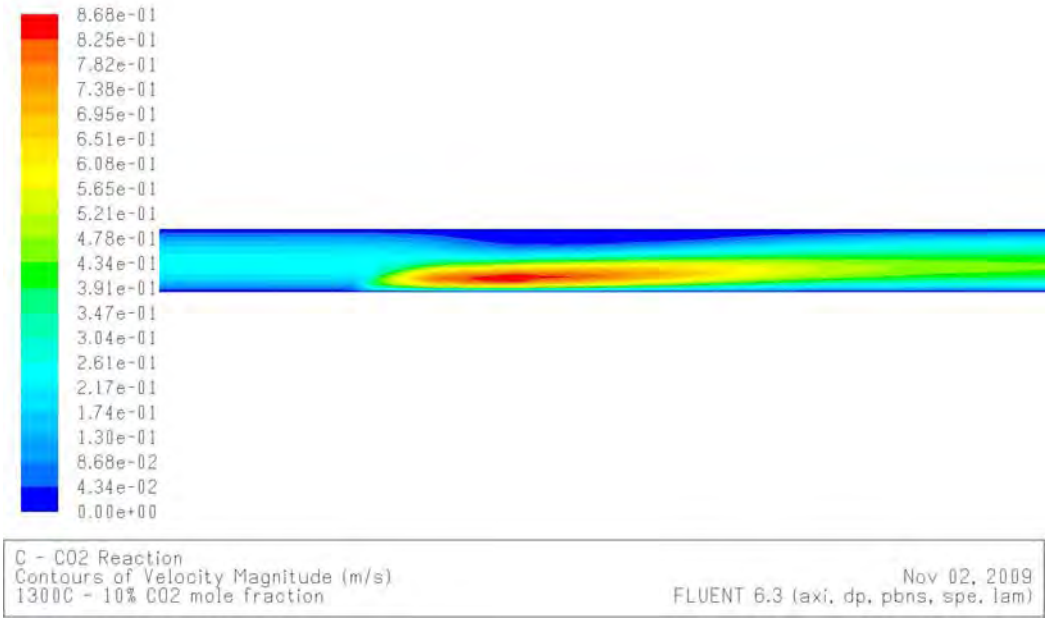

Figure 84: $C - CO_2$ **Simulation – Velocity**

The change in temperature results in a change in gas density, Figure 85 shows the density profile for this simulation.

Figure 85: $C - CO_2$ **Simulation – Density**

ANNEXURE E: REACTION RATE USER CODING

This Annexure presents the user coding in C++ for the 'Define_sr_rate' UDF in Fluent.

User defined surface reaction rate for use on wall surfaces and porous media.
Note Reaction-3 is the cell data in the case of porous media.
Reaction-4 is the wall surface reaction

```
/************************************************************************
 Custom surface reaction rate UDF
Define SR_Rate
Varying Stoichiometric co-efficient and Pre-exponent factor in Carbon Oxygen Reaction
 ************************************************************************/
#include "udf.h"
/* ARRHENIUS CONSTANTS */
#define ACTIVE 1.6929e+08
#define BETA 0.0
real arrhenius_rate(real Ttemp)
{
/*Based on Contescu     Note n=1.0*/
static real PRE_EXP;
if (Ttemp > 773.0)
        PRE_EXP = (1.0*(15/12)*pow((UNIVERSAL_GAS_CONSTANT*Ttemp),1.0));
        else
        PRE_EXP=0.0;
return
PRE_EXP*pow(Ttemp,BETA)*exp(-ACTIVE/(UNIVERSAL_GAS_CONSTANT*Ttemp));
}

/* Species numbers. Must match order in Fluent panel */
#define o2  0
#define co2 1
#define co 2
#define h20 3
#define n2 4
#define NUM_SPECS 5
#define c_s 6

/* Reaction Exponents */
#define o2_EXP  1.0
#define co2_EXP 0.0
#define co_EXP 0.0
#define c_s_EXP 0.0
#define MW_c_s 12.0
#define MW_o2 32
```

```
/* Reaction Rate Routine */

real reaction_rate(real temp, real dens,real mw[],real yi[])

/* Note that all arguments in the reaction_rate function call in your .c source file MUST be on the
same line or a compilation error will occur */
{
real conceno2 = dens*yi[o2]/mw[o2];
return arrhenius_rate(temp)*pow(conceno2,o2_EXP);
}
/* For Stoichiometric calc */
#define ko 7396.0
#define k1 -69604.0
#define k2 8.31434

DEFINE_SR_RATE(sr_por,num,thread,r,mw,yi,rr)
{
/* For Muli-processor, calculation on Host only, not on all Nodes */
#if !RP_HOST
real A, B, C, Fx;
real temp, dens;

/*Operate on Cell Level */
if (STREQ(r->name, "reaction-3"))
{
        temp = C_T(num,thread);
        dens = C_R(num,thread);
        if (temp > 723.0)
        {
        Fx = (ko*exp(k1/(k2*temp)));
        A = (Fx+2.0)/((2.0*Fx)+2.0);
        B = Fx/(Fx+1.0);
        C = 1.0/(Fx+1.0);
        }
        else
        {
        A = 0.0;
        B = 0.0;
        C = 0.0;
        }
/*Message0("in Reaction3: C-T %g;Stoich_o2 %g; Stoich_co %g; Stoich_co2 %g\n",temp,A,B,C);*/
}
/*Operate on Facel Level */
if (STREQ(r->name, "reaction-4"))
{
        temp = F_T(num,thread);
        dens = C_R(F_C0(num,thread),THREAD_T0(thread));
        if (temp > 723.0)
        {
        Fx = (ko*exp(k1/(k2*temp)));
        A = (Fx+2.0)/((2.0*Fx)+2.0);
        B = Fx/(Fx+1.0);
        C = 1.0/(Fx+1.0);
```

```
        }
        else
        {
        A = 0.0;
        B = 0.0;
        C = 0.0;
        }
/*Message0("in Reaction4: faceT %g;Stoich_o2 %g; Stoich_co %g; Stoich_co2
%g\n",temp,A,B,C);*/
}

#define STOIC_o2 A
#define STOIC_co B
#define STOIC_co2 C

*rr =
reaction_rate(temp,dens,mw,yi);

#endif
}

/*Define temperature profile on some wall – sample*/

DEFINE_PROFILE(walltemp, thread, position)

{

        real y[ND_ND];
        face_t f;

        begin_f_loop(f,thread)
        {
                F_CENTROID(y,f,thread);
        if (y[1] <= 0.084)
        F_PROFILE(f, thread, position) = 607;
        else if ((y[1] > 0.084) && y[1] <= 0.9)
                F_PROFILE(f, thread, position) = 923;
        else if ((y[1] > 0.9) && (y[1] <= 4.5))
                F_PROFILE(f, thread, position) = ((67.081*y[1])+916.41);
        else
                F_PROFILE(f, thread, position) = 1223;
                }

                end_f_loop(f, thread)

}
```